

**CHARACTERIZATION OF THE GERMANIA SPRABERRY UNIT FROM  
ANALOG STUDIES AND CASED-HOLE NEUTRON LOG DATA**

A Thesis

by

**BABAJIDE ADELEKAN OLUMIDE**

Submitted to the Office of Graduate Studies of  
Texas A&M University  
in partial fulfillment of the requirements for the degree of  
**MASTER OF SCIENCE**

August 2004

Major Subject: Petroleum Engineering

**CHARACTERIZATION OF THE GERMANIA SPRABERRY UNIT FROM  
ANALOG STUDIES AND CASED-HOLE NEUTRON LOG DATA**

A Thesis

by

**BABAJIDE ADELEKAN OLUMIDE**

Submitted to Texas A&M University  
in partial fulfillment of the requirements  
for the degree of

**MASTER OF SCIENCE**

Approved as to style and content by:

---

David S. Schechter  
(Chair of Committee)

---

Jerry L. Jensen  
(Member)

---

Robert R. Berg  
(Member)

---

Stephen A. Holditch  
(Head of Department)

August 2004

Major Subject: Petroleum Engineering

## ABSTRACT

Characterization of the Spraberry Unit from Analog Studies and Cased-Hole Neutron  
Log Data.

(August 2004)

Babajide Adelekan Olumide, B.Sc., University of Ibadan, Ibadan  
Chair of Advisory Committee: Dr. David S. Schechter

The need for characterization of the Germania unit has emerged as a first step in the review, understanding and enhancement of the production practices applicable within the unit and the trend area in general.

Petrophysical characterization of the Germania Spraberry units requires a unique approach for a number of reasons – limited core data, lack of modern log data and absence of directed studies within the unit.

In the absence of the afore mentioned resources, an approach that will rely heavily on previous petrophysical work carried out in the neighboring ET O’Daniel unit (6.2 miles away), and normalization of the old log data prior to conventional interpretation techniques will be used.

A log-based rock model has been able to guide successfully the prediction of pay and non-pay intervals within the ET O’Daniel unit, and will be useful if found applicable within the Germania unit. A novel multiple regression technique utilizing non-parametric transformations to achieve better correlations in predicting a dependent variable (permeability) from multiple independent variables (rock type, shale volume and porosity) will also be investigated in this study.

A log data base includes digitized formats of gamma ray, cased hole neutron, limited resistivity and neutron/density/sonic porosity logs over a considerable wide area.

## **DEDICATION**

I dedicate this work to God Almighty, who has shown me mercy and showered upon me abundant blessings that have made it possible to be who I am and where I am today, and guide who I will become tomorrow.

To my father and mother for being loving, caring and supportive parents, and a formative influence in my life. To my brothers and sisters who shared my joys and bore my pains and still loved me after it all.

To my wife and 9 month old daughter, Isi and Oluwateniola, for being my support and joy ever since they came into my life.

To my cousin Jide and his wife Tola, for their good will, support and encouragement through the challenges I faced during this period.

Finally, to my late brother, Adebowale, who I wish could be here to share all my joys.

## ACKNOWLEDGMENTS

My sincere gratitude goes to my advisory committee chair, Dr. D.S. Schechter, who has been patient and supportive all through my indecision to the completion of this thesis. I am thankful for his open demeanor and being a subtle taskmaster. Also, I thank Dr. Jensen for his constructive criticism and input towards improving the quality of this work.

Thanks also to Dr. Erwinsyah Putra for his invaluable support to the Naturally Fractured Group as a whole, as well as his role as a mentor and resource base for me during the course of my program at A&M.

The US Department of Energy (DOE) and Pioneer Natural Resources (PNR) for funding and providing useful data towards the successful completion of this project.

To Dr. Tom Blasingame for his encouragement and making things possible for me during my period at Texas A&M.

To the friends from all backgrounds that I have made while I have been at A&M.

## TABLE OF CONTENTS

	Page
ABSTRACT.....	iii
DEDICATION.....	iv
ACKNOWLEDGMENTS .....	v
LIST OF TABLES.....	viii
LIST OF FIGURES .....	ix
CHAPTER I INTRODUCTION.....	1
Project overview .....	1
Area of interest.....	2
Rock-log model.....	4
Lithofacies based model .....	6
Non-depositional model.....	6
Permeability estimation techniques .....	9
Explicit probabilistic techniques.....	9
Implicit probabilistic techniques.....	10
Porosity estimation.....	11
Gamma ray.....	11
Clay content .....	12
Log normalization.....	13
Histogram.....	16
Crossplots.....	16
Overlays .....	16
CHAPTER II DATA REVIEW (E.T. O'DANIEL) .....	17
Core sampling .....	17
Depth matched core-log playback .....	18
Lithology.....	22
CHAPTER III DATA ANALYSIS .....	25
Log conversions and normalization .....	25
Gamma ray.....	25
Gamma ray maps .....	25
Gamma ray normalization.....	28
Neutron logs.....	31
Standardization of neutron log units .....	31
Conversion from neutron units to linear porosity units .....	32
Porosity .....	33
Corrections for porosity .....	34

	Page
ET O’Daniel log-core model .....	35
Log porosity – core porosity x-plots.....	35
Variables influencing permeability.....	39
Regression analysis.....	39
Shale effects on porosity and permeability.....	40
Data conditioning (‘ACE’) .....	44
The ‘ACE’ transformations.....	45
Water saturation.....	46
CHAPTER IV ET O’DANIEL AND GERMANIA ANALOGY .....	51
Shale volume.....	51
Porosity .....	54
Kolmogorov – Smirnov test for porosity and shale volume.....	56
Litho- stratigraphic section .....	58
CHAPTER V MODEL APPLICATION IN GERMANIA UNIT.....	61
Germania.....	61
Picks and interval properties.....	61
Uncertainties .....	65
Porosity .....	65
Permeability .....	65
Water saturation.....	66
Net pay .....	66
CHAPTER VI CONCLUSIONS.....	67
Conclusions.....	67
REFERENCES .....	69
APPENDIX A BACKGROUND GEOLOGY AND STRATIGRAPHY .....	76
APPENDIX B MAPS FOR ET O’DANIEL AND GERMANIA .....	89
VITA.....	100

## LIST OF TABLES

TABLE		Page
1.1	Criteria for pay identification in the ET O'Daniel unit.....	4
2.1	Summary of rock properties and saturations for ET O'Daniel wells.....	18
3.1	Regression from crossplots of core – log porosity for cored ET O'Daniel wells.....	38
3.2	Archie parameters used in determining saturation in the upper Spraberry.....	47
3.3	Interval averaged water saturations for well with resistivity curves.....	48
4.1	Kolmogorov-Smirnov test for porosity and shale volume.....	58



## LIST OF FIGURES

FIGURE	Page
1.1 Unit locations within the Spraberry trend area.....	3
1.2 Crossplot of shale volume and porosity for well ET 47, 1U sand.....	5
1.3 Porosity - permeability crossplot for the primary rock types identified.....	7
1.4 Identification of pay based on shale volume and effective porosity cutoffs.....	8
1.5 Non-linearity of the different models for estimating clay content using gamma ray.....	13
1.6 The log analysis process.....	14
2.1 Map of cored well locations in the ET O’Daniel pilot area.....	17
2.2 Typical core - log playback in the 1U interval.....	19
2.3 Crossplot of shale volume and porosity for well ET 37, 1U sand.....	20
2.4 Typical core – log playback in the 5U interval.....	21
2.5 Crossplot of shale volume and porosity for well ET 37, 5U sand.....	22
2.6a Crossplot for lithology identification in 1U sand for well ET 37.....	23
2.6b Crossplot for lithology identification in 5U sand for well ET 37.....	23
3.1 Minimum gamma ray values for ET O’Daniel unit in the 1U sand interval.....	26
3.2 Maximum gamma ray values for ET O’Daniel unit in the 1U sand interval.....	27
3.3 Variations in response from the gamma ray curves in ET O’Daniel.....	28
3.4 Histogram and CDF for wells 36, before and after normalizing against well 26.....	29
3.5 Corrected gamma ray distribution for ET O’Daniel wells.....	30
3.6 Normalized gamma ray values in 1U and 5U regions of upper Spraberry, ET O’Daniel unit.....	31
3.7 Effects on quality of porosity data from density and neutron porosity tools.....	34
3.8 Crossplot of core porosity and log porosity for ET 39, 1U sand.....	36

FIGURE	Page
3.9	Crossplot of core porosity and log porosity for ET 39, 5U sand..... 37
3.10	Playback of log and core porosity for ET 39, 1U sand..... 38
3.11	Playback of log and core porosity for ET 39, 5U sand..... 38
3.12a	ET 39 crossplot for shale volume and permeability..... 40
3.12b	ET 47 crossplot for shale volume and permeability..... 40
3.13a	ET 39 crossplot for log porosity and permeability..... 41
3.13b	ET 47 crossplot for log porosity and permeability..... 42
3.14a	ET 39 crossplot for shale corrected porosity and permeability..... 43
3.14b	ET 47 crossplot for shale corrected porosity and permeability..... 43
3.15	Playback of results from conventional regression and ACE regression.... 46
3.16	Saturation profile matched for ET 38, 1U using $R_w$ 0.035 ohm-m and $m$ 1.7..... 49
3.17	Saturation profile matched for ET 40, 1U using $R_w$ 0.035 ohm-m and $m$ 1.7..... 50
4.1	Statistics of $V_{sh}$ values for ET O'Daniel, 1U sand..... 51
4.2	Statistics of $V_{sh}$ values for ET O'Daniel, 5U sand..... 52
4.3	Statistics of $V_{sh}$ values for Germania, 1U sand..... 52
4.4	Statistics of $V_{sh}$ values for Germania, 5U sand..... 53
4.5	IQR and mean values of shale volume and porosity for ET O'Daniel and Germania units..... 53
4.6	Statistics of porosity values for ET O'Daniel, 1U sand..... 54
4.7	Statistics of porosity values for ET O'Daniel, 5U sand..... 55
4.8	Statistics of porosity values for Germania, 1U sand..... 55
4.9	Statistics of porosity values for Germania, 5U sand..... 56
4.10	Kolmogorov - Smirnov test on porosity function, 1U sand..... 57
4.11	Gross thickness map of the 1U sand..... 59
4.12	Lithostratigraphic section A-A' with datum at top of 1U interval..... 60
5.1	Payzone prediction based on rock model for GSU 146A, 1U sand..... 61
5.2	Estimate of rock types in GSU146A, 1U sand from shale volume – porosity crossplot..... 62

FIGURE	Page
5.3 Payzone prediction based on rock model for GSU214A, 1U sand.....	62
5.4 Vshale crossplot for GSU 214A, 1U sand.....	63
5.5 Payzone prediction for GSU214A, 5U sand.....	63
5.6 Vshale crossplot for GSU 214A, 5U sand.....	64
A1 Structure contour data, top of Spraberry sandstone Midland Basin, west Texas.....	77
A2 Regional geologic setting of Permian Basin, west Texas.....	78
A3 West –east stratigraphic cross section BB’ .....	79
A4 Lithofacies map, four County area with Spraberry isopach contours.....	81
A5 Facies model of clastic and carbonate dominated shelf margin systems....	82
A6 Distribution of environments, geometry of deposits, and channel patterns.....	83
A7 Sections of onlapping clastics and downdip widening of channels.....	83
A8 Isopach map of upper Spraberry unit in Midland County.....	85
A9 Clastic ratio map of upper Spraberry unit in Midland County.....	86
A10 Operational units within the upper Spraberry formation.....	87
A11 Location of class A & B Spraberry reservoirs of west Texas.....	88
B1 Minimum gamma ray map of ET O’Daniel, 5U sand.....	89
B2 Maximum gamma ray map of ET O’Daniel, 5U sand.....	90
B3 Paleo-structure map of ET O’Daniel, 1U sand.....	91
B4 Paleo-structure map of ET O’Daniel, 5U sand.....	92
B5 Paleo-structure map of Germania, 1U sand.....	93
B6 Paleo-structure map of Germania, 5U sand.....	94
B7 Porosity distribution map of ET O’Daniel, 1U sand.....	95
B8 Porosity distribution map of ET O’Daniel, 5U sand.....	96
B9 Porosity distribution map of Germania, 1U sand.....	97
B10 Porosity distribution map of Germania, 5U sand.....	98
B11 Effect of sample sizes on Kolmogorov – Smirnov distribution tests.....	99

## CHAPTER I

### INTRODUCTION

#### **Project overview**

The Spraberry trend area is a unitized hydrocarbon production Basin in the heart of west Texas. The major production comes from fine grained, low permeability siltstones and sandstones, enhanced by an intricate network of natural fractures. Carbonate and siliclastic (submarine fans) depositional episodes during the Permian era make up the lithofacies of the Spraberry unit.

Up to date production from the Basin is estimated at about 800 million barrels of oil and 3 trillion cubic ft of gas from over 8000 active wells<sup>1</sup>, this figure could range between 8 – 12% of the projected OHIP.

Of particular interest is the ET O’Daniel and Germania Spraberry units, two of eleven units operated by Pioneer Natural Resources. Extensive reservoir characterization work has been carried out in the ET O’Daniel based on recent core and log data acquisition, production data and simulation studies. The Germania Spraberry unit on the other hand lacks core and modern log data, and has not been characterized beyond pulse and tracer tests to analyze fracture trends and performance.

A preliminary step in the implementation of an enhanced recovery process within the unit is the characterization of the reservoir (petrophysics and fracture properties and fracture network).

This study is concerned with the log based characterization of the Germania unit and will focus on the petrophysical evaluation of the upper Spraberry unit, particularly the productive 1U and 5U intervals.

---

This thesis follows the style of *SPE Reservoir Evaluation & Engineering*.

A database of 85 log suites, primarily consisting of gamma ray and old cased hole neutron logs are available for this study. Core based relationships developed in the ET O'Daniel unit are borrowed upon to aid the characterization of this field, and will generally suffice due to the similar depositional environment and proximity of the units from one another (6.2 miles).

Established criteria for predicting rock type and pay zones in the ET O'Daniel will be applied if found applicable to Germania and will guide subsequent characterization efforts in the unit.

### **Area of interest**

The Spraberry trend area spreads over an area of approximately half-a-million acres and is trapped by complex updip pinchouts and facies changes within the thick upper Spraberry producing interval. A few fields are simple anticlinal structures like Benedum and Pegasus. The regional fracture patterns are enhanced by anti-clinal folds producing a locally commercial reservoir at Pegasus<sup>2,3</sup> (see Fig. A11 in appendix A).

The E.T. O'Daniel unit and the Germania unit are adjacent units at the north end of the Spraberry trend area. These fields are 2 of 11 fields operated by the Pioneer Natural Resources (PNR) and are located in the Midland County area of west Texas.

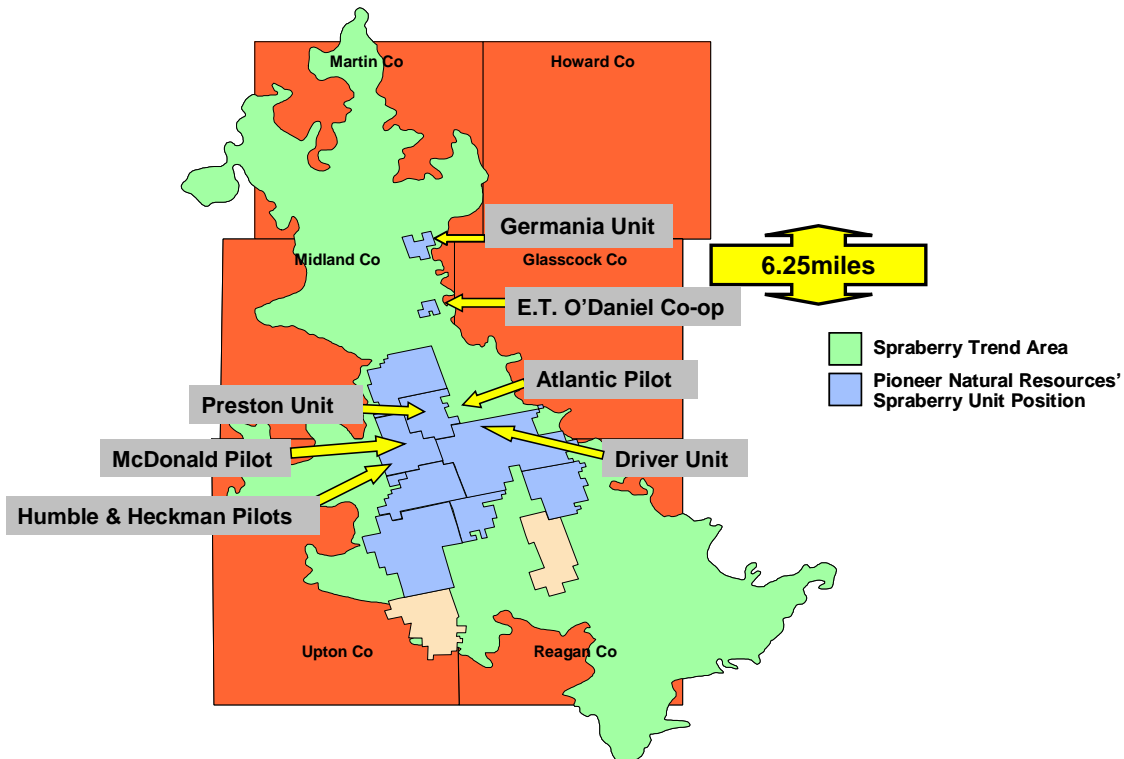


Fig. 1.1 – Unit locations within the Spraberry trend area.

The distance between the two fields is estimated to be about 6.2 miles based on inter-well distance measured from boundary wells (see Fig 1.1).

Whereas the ET O’Daniel has been the subject of major studies regarding fracture patterns<sup>4-6</sup>, log - core analysis<sup>7-11</sup> and waterflood and CO<sub>2</sub> injection pilot projects<sup>1,12-14</sup>, no major investigation of the lithofacies or fracture characteristics of the Germania unit has been performed. Fracture trends on a gross scale by way of pulse and tracer tests is the basis of predicting flow behavior within the Germania unit.

Due to the proximity of the ET O’Daniel unit to the Germania unit as well as the depositional environment within the four County area<sup>15, 16</sup> (Midland, Glasscock, Upton and Reagan) it becomes logical to superimpose the conclusions drawn from the petrophysical evaluation of the ET O’Daniel unit upon the Germania unit.

Bearing this in mind, further discussions on the characterization work regarding this area will be focused on the ET O’Daniel unit.

## Rock-log model

Gamma ray and old cased hole neutron logs form the bulk of the electric logging data available within the ET O'Daniel. More recently, array induction, density and neutron porosity data have been acquired in pilot areas within the unit. This acquisition is localized and hence the older neutron logs are an indispensable source for wide scale characterization of the field.

A log based rock model<sup>10,11</sup> was developed for the trend area using shale content (gamma ray) and porosity as discriminatory criteria for rock type. In this model, classification is made for 3 rock types – A, B and C.

Table 1.1 summarizes the identifiers for the rock model within the upper Spraberry operational units based on effective porosity and shale content<sup>17</sup>.

Table 1.1 - Criteria for pay identification in the ET O'Daniel unit.

Formation	Rock Type	Shale Volume	PHIE	Facies	Fluorescence	Pay	Unit
Upper Spraberry	A	< 15%	> 7%	SS	Strong	yes	1U, 5U
	B		< 7%	DS+SS	Weak	no	2U, 3U, 4U
	C	> 15%		SH+DS+SS	None		muddy zones

SS - Siltstone

SH - Shale

DS - Dolomite

More recently, 'Thin section' analysis of core samples within the upper Spraberry were point count analyzed to establish framework, cement mineralogy and diagenetic features of the rock<sup>8</sup>. Especially useful in identifying and classifying samples was x-ray diffraction (XRD) and scanning electron microscope (SEM) analysis to determine clay mineralogy and proportions of clay minerals within the various rock types. Prior to the results of the study, a direct relationship was assumed between porosity and gamma ray response and permeability and gamma ray response, which for the most part is true. What Schechter and Banik<sup>9</sup> also showed was that clay content is a significant factor in

predicting overall permeability. Sands with low clay content have a high overall permeability within the 1U.

Rock type A is the only reservoir quality rock identified within the upper Spraberry, types B and C are non-reservoir quality rock. A crossplot of the shale volume and the effective porosity provides an easy method of rock identification (Fig. 1.2).

Rock Type A – Massive, clean siltstone, low clay and dolomite content. Strongly fluorescent with low water saturation.

Rock Type B – Low clay, low dolomitic content with weak or no fluorescence and high water saturation.

Rock Type C – Muddy clay rich zones that do not fluoresce.

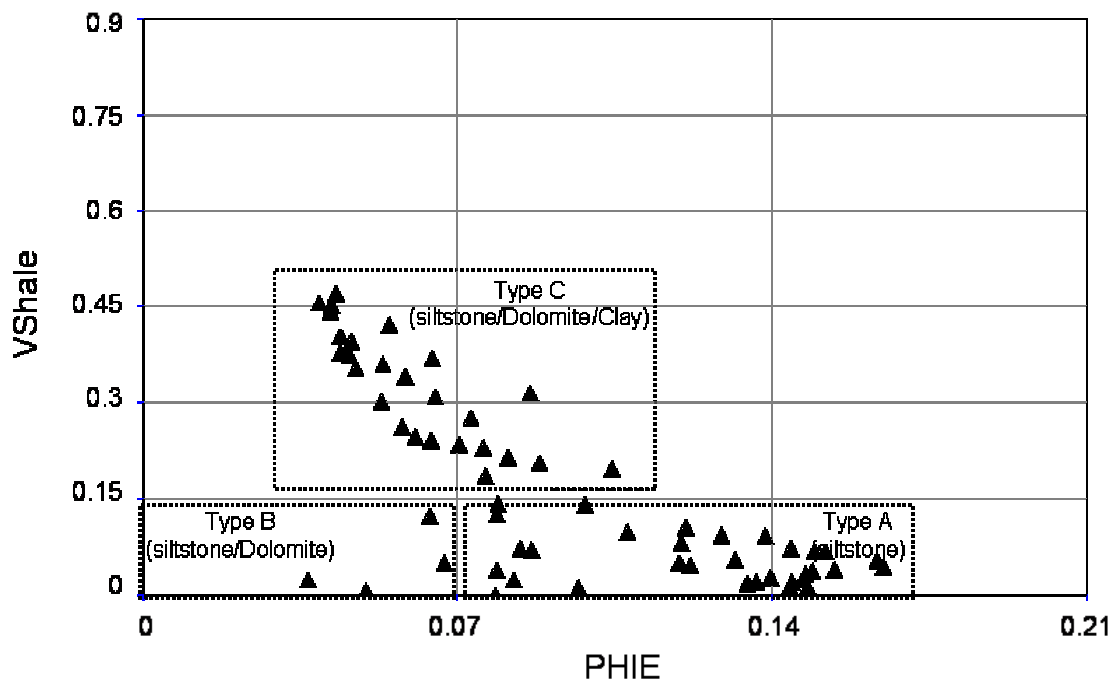


Fig. 1.2 – Crossplot of shale volume and porosity for well ET 47, 1U sand.



### **Lithofacies based model**

Eight separate lithofacies<sup>18</sup> are defined based on sedimentological, compositional and textural features of core samples. These are broadly divided into those with reservoir potential, and non-reservoir potential deposits.

Potential reservoir deposits consist of:

Type 1 – Massive siltstones and very fine grained sandstones

Type 2 – Thin bedded siltstones and very fine grained sandstones exhibiting basal intervals of massive sandstone grading vertically into parallel or cross laminated sandstone and siltstone.

Type 3 – Thin bedded, graded, cross laminated siltstones and very fine grained sandstones, interbedded with dark grey shales

Non-reservoir lithofacies consist of:

Type 1 – Massive silty dolostone and dolomite-cemented siltstone

Type 2 – Black shales containing phosphatic nodules and abundant pyrite

Type 3 – Thin bedded argillaceous siltstone showing abundant soft sediment deformation

Type 4 – Bioturbated argillaceous siltstone in which scattered silt-size grains of quartz and feldspar float in a groundmass of detrital clays

Type 5 – Parallel and finely laminated siltstone and silty shale.

### **Non-depositional model**

A more generic classification of the rock types of the upper Spraberry that relate better with rock quality based on non-depositional factors is developed using petrographic analysis, petrophysical analysis and compositional information<sup>18</sup>.

To avoid confusion, the log based rock model will be referred to as the secondary classification, and the generic model as primary.

The core based primary model shows that the upper Spraberry can be divided into six distinct rock types:

Type 1 – Coarse siltstones and very fine grained sandstones (A)

Type 2 – Laminated or patchy siltstones and very fine grained sandstones (B)

Type 3 – Silty dolomite mudstones (C)

Type 4 – Very patchy dolomitic siltstones (D)

Type 5 – Shale and silty shale(E)

Type 6 – Highly laminated siltstones (F)

Type 1 is the only rock type with reservoir potential.

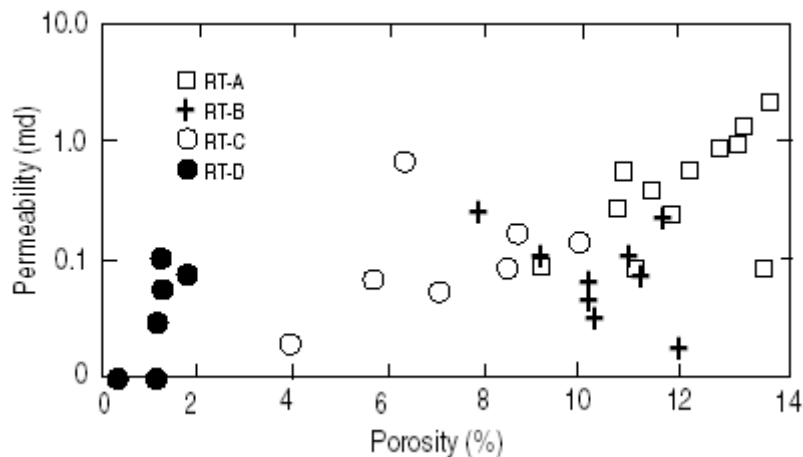


Fig. 1.3 – Porosity - permeability crossplot for the primary rock types identified<sup>18</sup>.

The rock log model has proved consistent in the preliminary identification of pay and non-pay reservoirs. Deflections from gamma ray corresponding to lower values were used to define probable reservoir quality sandstones in the past, with typical cutoffs ranging from 45 – 50 API units. With these cutoffs, individual zones within the 1U, 2U, 3U, 4U and 5U intervals were thought to be possible pay zones in the ET O’Daniel wells. Core data has however shown that only the 1U and 5U exhibit any fluorescence, moreover, the intermediate intervals 2U to 4U, despite showing gamma ray values in the

30 – 50 API range, had porosities under 7% and much higher concentrations of dolomite cement<sup>9</sup>. Core data indicate that shale volume can be determined from the gamma ray log, effective porosity from the density neutron log crossplots or from bulk density log data or from sonic transit time.

A typical playback using these criteria is shown in Fig. 1.4, in track 1 gamma ray and calculated shale volume using the Larionov non-linear model<sup>19</sup>, track 2 shows the shallow-medium-deep induction log, track 3 shows the effective porosity (shale volume corrected) and the core derived porosity values, track 4 shows the core derived permeability values and the calculated permeability values from log data using conventional regression techniques, track 5 shows pay and non – pay intervals using the log based rock model.

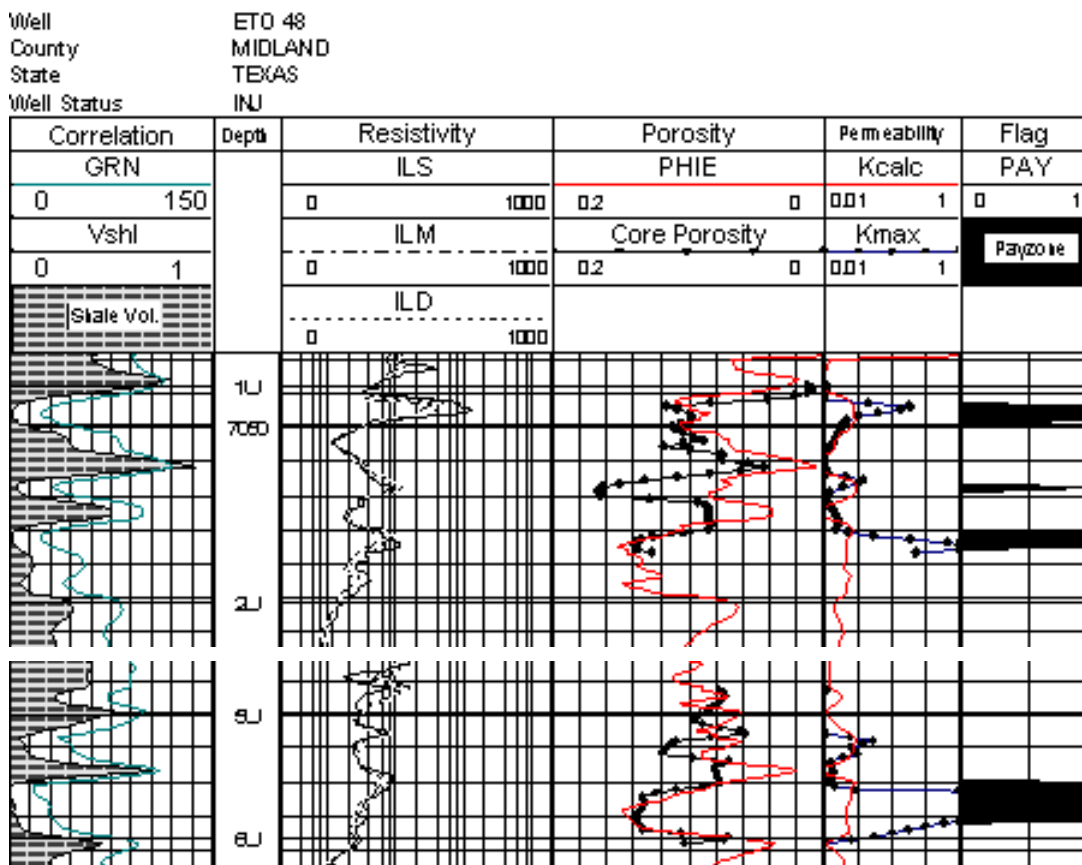


Fig. 1.4 – Identification of pay based on shale volume and effective porosity cutoffs.

## **Permeability estimation techniques**

An important parameter which is key to the rock model is the estimation of permeability from log data. Conventional methods estimate  $k$  from e-logs and consist of building models between regularly spaced core plug measurements and logs, without paying much attention to the various scales of core plug sampling<sup>20</sup>.

In uncored intervals  $k$  are usually estimated from well test, production or log data. Early attempts used porosity (unsatisfactorily), which is not unexpected as the permeability is related to pore throat size rather than pore volume. More recently, a host of relationships have been investigated between permeability and other rock attributes. Permeability as a function of porosity and irreducible water saturation<sup>21</sup>, or bulk density, neutron porosity, interval transit time and gamma ray<sup>22</sup>. A multi-dimensional histogram approach, deriving permeability based on bulk density, interval transit time and gamma ray was investigated successfully by Schlumberger. Some other functional relationships investigated are related to formation resistivity, normalized spontaneous potential and borehole Stoneley waves<sup>22,23, 24, 25</sup>.

In analyzing permeability dependency on single or multiple variable, regression as well as discriminant analysis are the most widely used techniques of evaluation.

These techniques can be classified into two broad groups: Explicit probabilistic methods and implicit irobabilistic methods.

### ***Explicit probabilistic techniques***

Regression Analysis – This is a crossplot of 2 dimensions, used to predict values in intervals without core data and wells without core data. This method assumes the functional form of the relationship between the prediction and response variable is unknown. The drawbacks of this method is that it over-simplifies reality and tends to smooth out real variations or trends in the data, because more often than not, other independent factors influence the prediction, therefore making a two dimensional

prediction inadequate for reliability. Sub-dividing the data into logically coherent groups in geologically correlated zones often improves the overall correlation.

Multiple Regression analysis includes additional variables or non-linear regression techniques.

The ‘ACE’ algorithm originally proposed by Friedman and Breiman<sup>26</sup> provides a method for estimating optimal transformations for multiple regression that result in a maximum correlation between a dependent (response) random variable and multiple independent (predictor) random variables. Xue et. al.<sup>27</sup>, went further to develop a non-parametric approach that optimizes based on no predetermined functional form, derived solely based on the data set.

Discriminant analysis – This is a multi variate technique designed to separate samples into groups based on relationships found in a training set of data. The relationship must be such that they can be defined explicitly and must be linear combinations of functions of the predictor variables.

### ***Implicit probabilistic techniques***

Probabilistic or database methods are intrinsic (or implicit) relationships of data compiled in a multi dimensional database. A value of y is read from a database corresponding to a value of x. In this way the implicit relationship between the data are preserved.

N-Dimensional histogram – When the x corresponding to y concept is expanded to include additional variables, the approach becomes an ‘n-dimensional histogram’, and the discrimination of the dependent variable is generally improved. This method has the following advantages over regression techniques in that it has the ability to preserve the subtle relationships between variables, it fully utilizes the shape characteristics of the data and it has the ability to incorporate soft data such as facies type into the database to define the categories of qualitative histograms.

Cluster analysis – This is a multi-variate technique for classification of samples into groups based on little or no prior knowledge of that grouping. Simple cluster analysis does not use the information on facies known from the cored interval, but instead attempts to find natural groupings, called clusters based on the estimator variable.

### **Porosity estimation**

Porosity is determined from 3 basic log types that measure porosity directly (neutron) or indirectly (density and sonic). Where a neutron count based porosity value is known from the older neutron logs, a conversion algorithm<sup>28</sup>, may be used to convert counts per second or any CPS derived unit (environmental units, API cps, etc) which exhibits a logarithmic scale of porosity to porosity values on a linear scale.

Where the density, neutron porosity and photoelectric effect curves are available, porosity measurements based on shale corrected lithology model can be reliable and consistent over a wide range of rock types<sup>29</sup>. No matrix parameters are required for this model unless light hydrocarbons are present. Shale corrected density and neutron data are used as input in this model and results depend on shale volume calculations and density and neutron shale properties selected for the model. Therefore porosity should be compared to core data and corrected accordingly till a suitable match is obtained between both data sets.

Where limited suite of porosity logs are available, a model based on the shale corrected density, shale corrected neutron or shale corrected sonic is used<sup>29</sup>.

### ***Gamma ray***

The Gamma Ray log is a continuous recording of the intensity of the natural gamma radiations emanating from the formations penetrated by the borehole vs. depth.

In sedimentary formations, since the radioactivity can be attributed mainly to the clay minerals, the gamma ray log can be used to distinguish between shale and non-shale formations and to estimate the clay content of shaly formations.

### ***Clay content***

Clay or shale content can be quantified using a shale index from values given by the gamma ray log. Different models are available for quantifying this index:

General linear form

$$V_{shl} = \frac{X_{raw} - GR_{clean}}{GR_{shl} - GR_{clean}} \quad (1.1)$$

Other models used to modify the index to account for various degrees of non-linearity between the gamma ray response and the clay content are available:

Larionov's model for tertiary rocks

$$V_{shl\_modified} = 0.083(2^{3.7V_{shl}} - 1) \quad (1.2)$$

Larionov's model for older rocks

$$V_{shl\_modified} = 0.33(2^{2.0V_{shl}} - 1) \quad (1.3)$$

Stiebers' model

$$V_{shl\_modified} = \frac{V_{shl}}{3 - 2V_{shl}} \quad (1.4)$$

Claviers' model

$$V_{shl\_modified} = 1.7 - (3.38 - (V_{shl} + 0.7)^2)^{0.5} \quad (1.5)$$

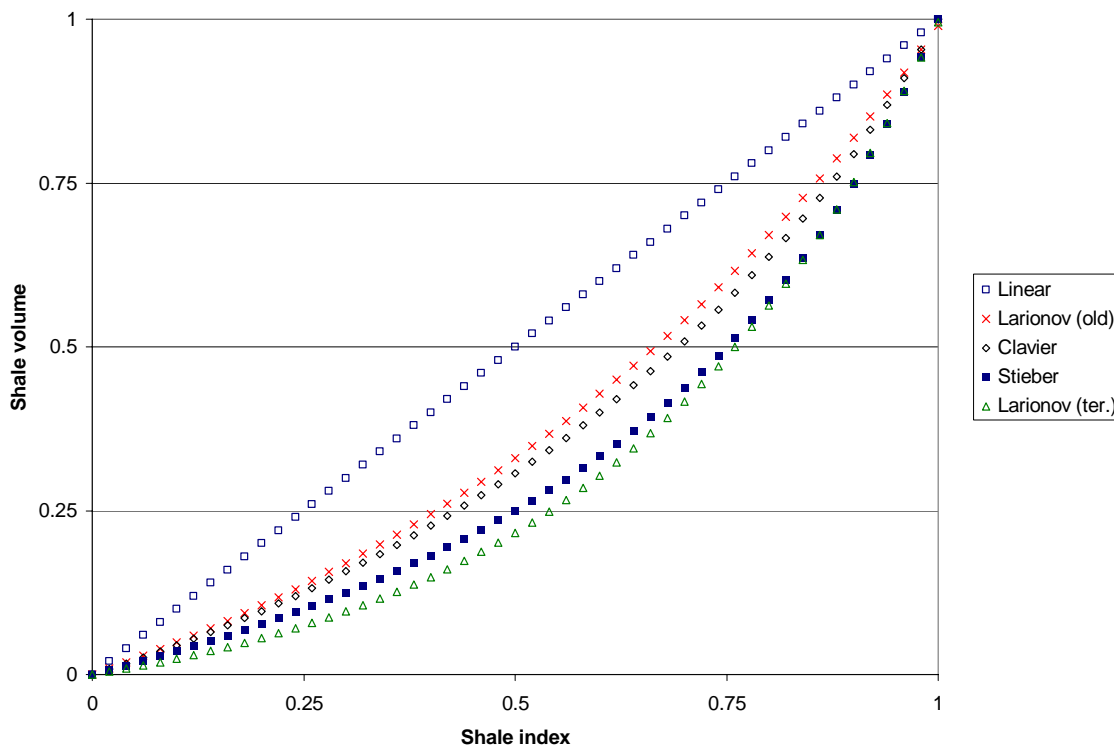


Fig. 1.5 - Non-linearity of the different models for estimating clay content using gamma ray.

### Log normalization

Well log normalization is a fundamental part of well log analysis, and is one of the necessary steps for arriving at accurate rock quality descriptors. The foundation of the integrated log analysis process is the core, well test and log database<sup>30</sup>. The shortcomings in the foundations of the analysis ultimately influence the quality of the final estimations of permeability, the interdependence of the descriptors are shown in Fig. 1.6.

Errors in the database will trickle up to affect shaliness, porosity and water saturation calculations. Also errors in shaliness calculation will cause additional errors in porosity and water saturation because these calculations also depend on shaliness. When everything is done correctly useful values of permeability and effective permeability can be obtained from integrated studies.



In excess of fifty percent of all well logs are erroneous, Neinast and Knox<sup>31</sup> base this percentage on an analysis of 1986 suites of well logs containing more than 34 million curve feet. The basic sources of error are tool malfunction, incorrect tool design, inconsistent shop and field calibration, and operator error. All but ten percent of the incorrect logs may be corrected and the data used quantitatively.

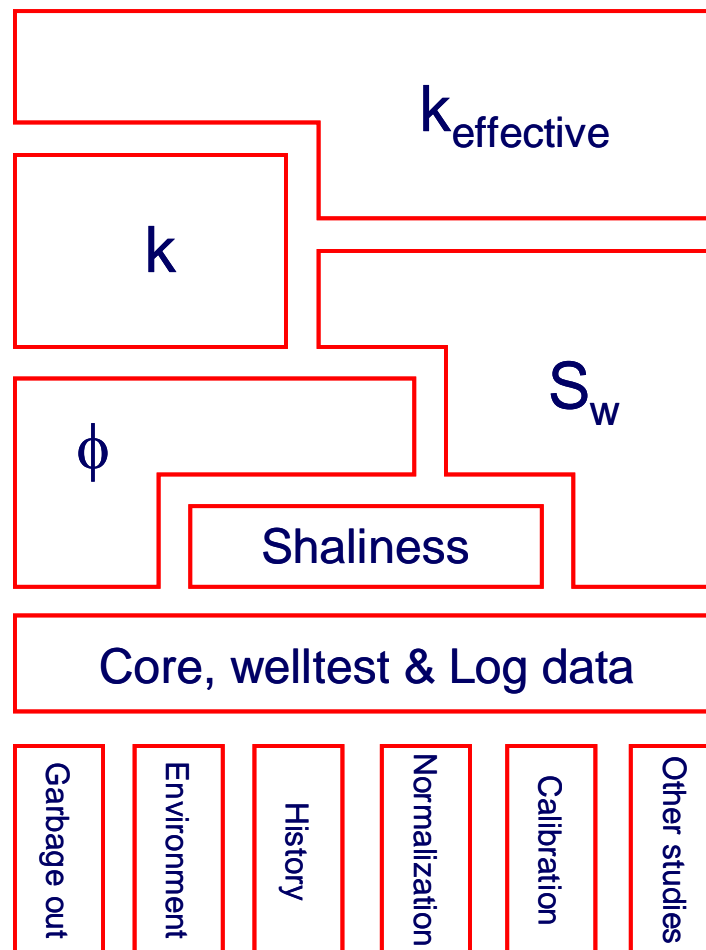


Fig. 1.6 – The log analysis process<sup>30</sup>.

Hunt<sup>30</sup> in his analysis, suggests that about 65 - 70% of gamma rays logs, 50% of density logs, 40% - 50% of neutron logs and 5% - 10% of sonic logs require some normalization to correct for variances in field calibrations of logging tools. After normalization well log data can be effectively integrated, correlated and calibrated with core data. The resulting correlations can be extended vertically to include layers that were not cored, and laterally

to wells across the study area. The difference in scale of measurement of the two data sets must be taken into account. Core data have a scale of cubic inches, while log data have a scale of cubic meters and well test data have a scale of acre-feet.

The normalization procedure to correct log data requires the following<sup>31</sup>:

- Digitize the well log data
- Select corresponding lithologic intervals
- Accumulate and present data in appropriate form (Histograms, etc)
- Compute porosity and water saturation
- Compare with core analysis
- Map to reveal anomalies

**Digitization** – The individual curves are depth matched either prior to data capture in ASCII format or if post processing software is available to correct depth anomalies. All heading data is combined with the log values to allow pertinent corrections to be made in subsequent calculations.

**Interval selection** – Correlation of stratigraphic intervals is of extreme importance. The earth changes radically in a vertical direction and gradually in a lateral direction. Appropriate corresponding lithological sections must be chosen so that comparison of similar intervals may be accomplished. Every effort should be made to eliminate pay zones or other zones of interest as data for correlation prior to normalization.

**Data presentation** – Data must be accumulated in a form that allows rapid and concise corrections. Variations in thickness of explicit sections is eliminated by presenting the information in statistical format. The basic concept is the formation of patterns that the analyst recognizes and compares to make the proper corrections. Three methods of data presentation are histograms, crossplots and overlay.

### ***Histogram***

The histogram is made by plotting the percent frequency of occurrence of data on the abscissa against the log unit value on the ordinate. The mean and standard deviation are calculated along with the mode, maximum and minimum values, and the net and gross number of samples used in the histogram. Histograms of discriminated or complete log values may be prepared for specific correlated intervals. The individual frequency histograms may be compared with similar histograms from other wells, with core derived histograms, or with mass histograms or entire regions or fields.

### ***Crossplots***

Crossplot techniques for lithology and porosity determination have been in use for several years. Additional advantage of dual porosity device data may be taken if the lithology is known or assumed. Errors in individual tools may be detected when the crossplotted data falls outside the range delineated by constant mineral lines. When three porosity logs are available, the data can be used to develop an M-N plot and allow corrections to properly compute porosity. The procedure is to first histogram and normalize individual logs, then verify and refine the normalization with crossplots.

### ***Overlays***

This is a simple process of correlating and overlaying similar type logs and noting the difference.

Computation and comparison – After the data has been normalized, the water saturation, porosity, lithology, permeability, etc. are computed on a foot by foot basis and compared to the weighted average core data to determine the degree of compatibility

Mapping – Contour maps are generated on selected intervals. Generally porosity and water saturation are the parameters used to confirm normalization. All drastic changes and abrupt highs and lows are rigorously verified as to validity.

**CHAPTER II**  
**DATA REVIEW (E.T. O’DANIEL)**

**Core sampling**

Cores samples were recently taken from six (6) wells within the ET O’Daniel unit, location of the wells are within the waterflood pilot area in the south east part of the lease (see Fig. 2.1). Though these samples are localized, they provide useful data towards verifying the established rock log model. Core data statistics are given in Table 2.1.

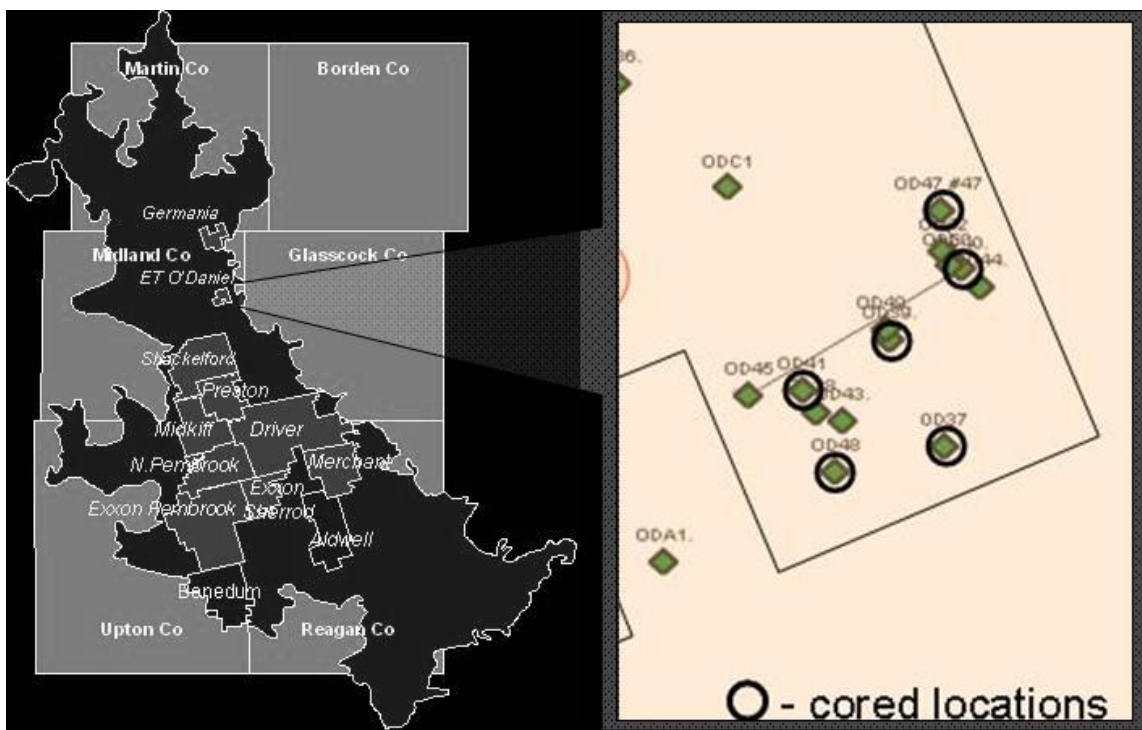


Fig 2.1 – Map of cored well locations in the ET O’Daniel pilot area.

The analysis was carried out by Reservoirs Incorporated. Procedure for estimating core parameters involved firstly correlating core to log depth by gamma ray scan of the cores, water and oil saturations were determined using the Dean-Stark extraction method and ultraviolet photographs taken. Sponge oil volumes adjacent to the core samples were reported as % pore volume and horizontal – vertical permeability to air was measured using a Hassler sleeve permeameter.

The core values obtained are integrated into the log database using the Geographix software, and depth matched using the log and core porosity response as a guide. This ensures that all data sampled from the logs with reference to the core data are for the same interval.

Table 2.1 – Summary of rock properties and saturations for ET O’Daniel wells.

Well	Flow Unit	Interval, ft	Sw, v/v	So, v/v	Por %	kmax, md	Gr. Den, g/cc	Bulk Den, g/cc	Fluorescence
ETO 37	1U	7040 - 7066	0.52	0.12	8.14	N/A	2.71	N/A	trace - 100
	5U	7216 - 7240	0.53	0.16	8.73	N/A	2.68	N/A	trace - 100
ETO 38	1U	7060 - 7087	0.41	0.06	10.07	0.57	2.65	N/A	25 - 100
	5U	7210 - 7237	0.34	0.08	10.39	1.36	2.65	N/A	no - 100
ETO 39	Core values previously integrated into LAS files								
ETO 40	1U	7088 - 7115	0.28	0.17	10.20	6.95	2.68	N/A	no - 100
	5U	7236 - 7264	0.34	0.15	9.06	N/A	2.67	N/A	no - 100
ETO 47	1U	7086 - 7108	0.47	0.08	8.38	0.14	2.70	2.48	N/A
	5U	7240 - 7267	0.48	0.11	8.59	0.19	2.69	2.46	N/A
ETO 48	Core values previously integrated into LAS files								

### Depth matched core-log playback

A depth matched playback for a cored well ET O’Daniel 37 displays the core derived parameters in tracks 2, 3 and 4 (core porosity / permeability, saturations and fluorescence).

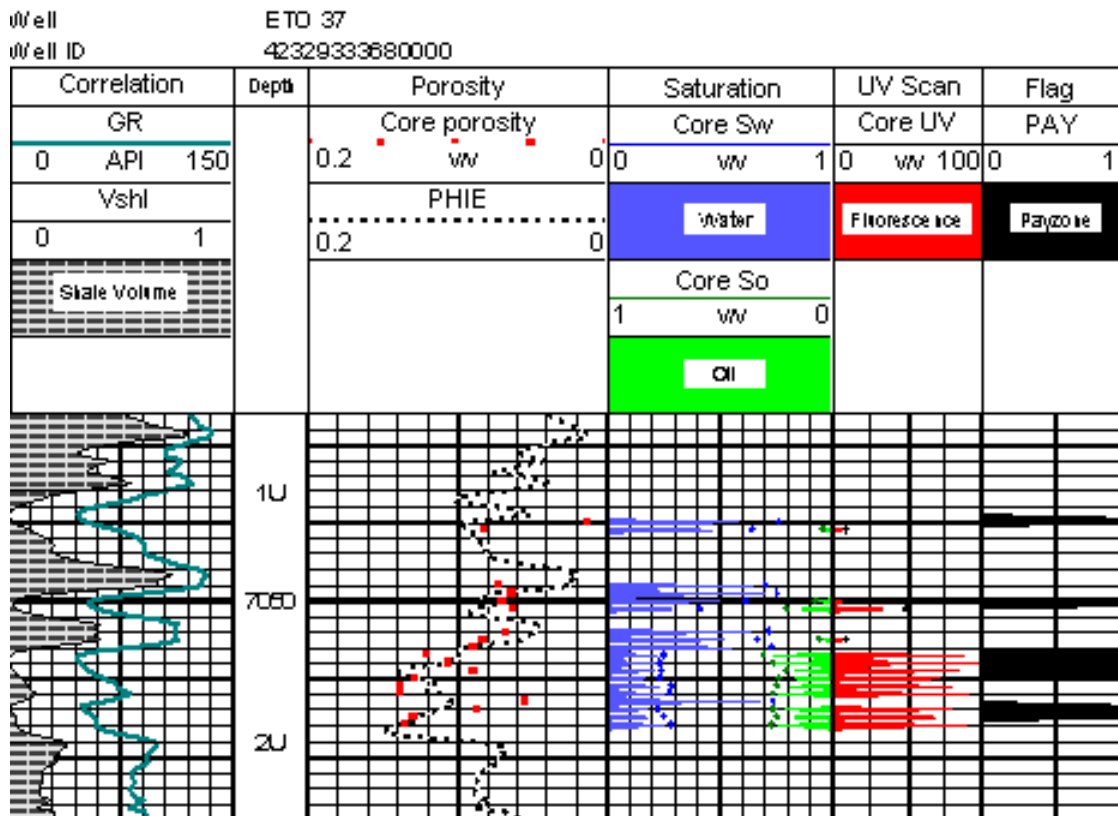


Fig. 2.2 – Typical core - log playback in the 1U interval.

Gamma ray and shale volume playback in track 1 are based on normalized data, track two displays porosity values from core and log data and permeability from core analysis. The agreement between core and log porosity is fairly good (track 2), but of more importance is the pay flag in track 5 based on the rock model. This pay flags strongly correlate with the fluorescing interval in track 4.

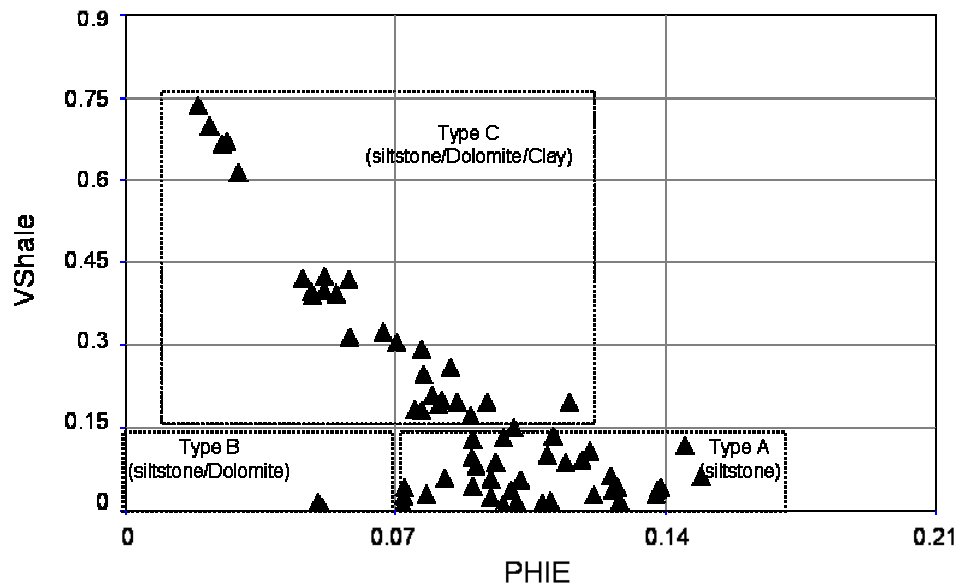


Fig. 2.3 – Crossplot of shale volume and porosity for ET 37, 1U sand.

The shale volume - porosity crossplot gives a quantitative indication of the rock types within the analyzed interval. In Fig. 2.3 the amount of rock type B is minimal, while type A and C are evenly distributed in the 1U interval for well ETO37.

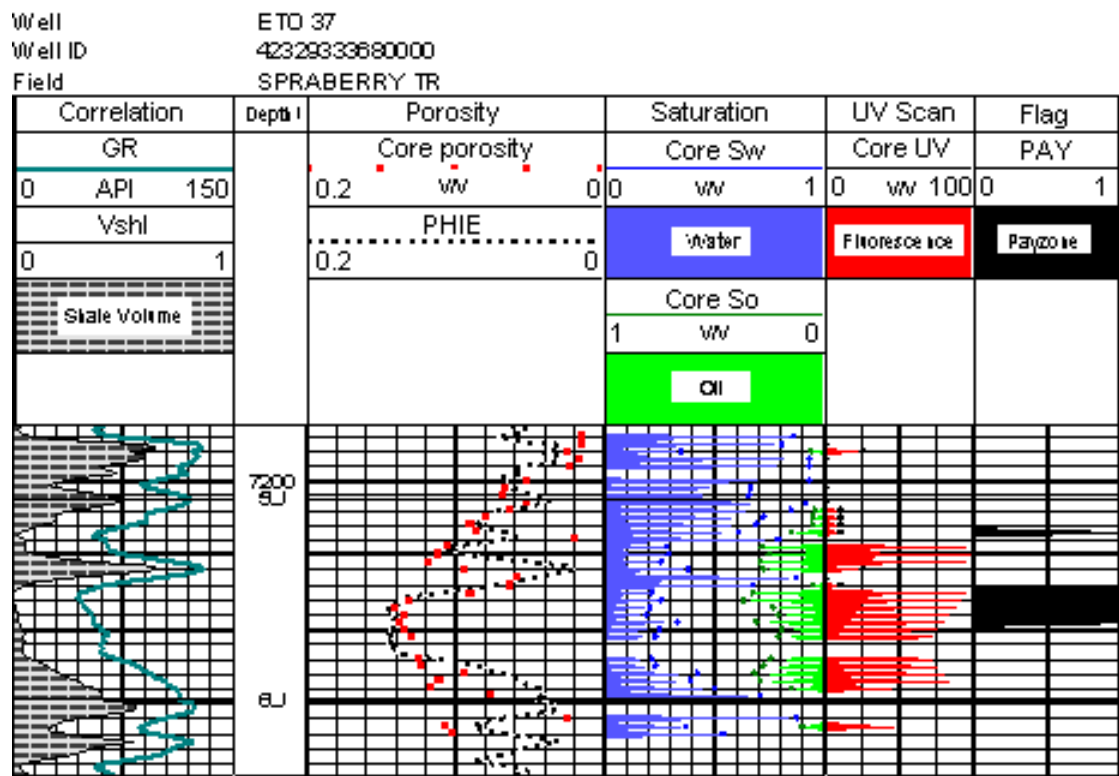


Fig. 2.4 – Typical core - log playback in the 5U interval.

The payflag and fluorescing interval for this unit (5U) correlate well after a depth shift based on core porosity and log porosity matching. The playback resulting from this optimal correlation is shown in Fig. 2.4.



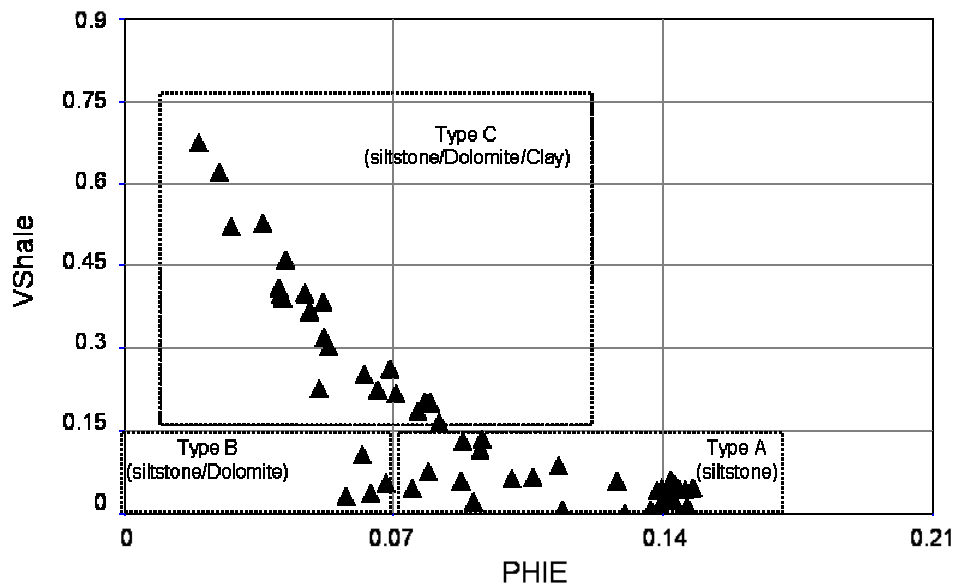


Fig. 2.5 – Crossplot of shale volume and porosity for well ET 37, 5U sand.

A number of observations are evident from figs. 2.2 to 2.5, these are that the low shale intervals of the 1U and 5U units are almost exclusively payzones or type A rocks, while the higher shale intervals are exclusively non-hydrocarbon bearing sands. Also a estimate of the productive intervals (net pay) account for about 50% of the gross sand in the 1U unit and about 40% of the gross sand in the 5U intervals. Other well analyzed also displayed similar trends as observed in wells ETO 37.

The 1U and 5U pay zones are easily identified by integrating whole core analysis and open hole logs into a calibrated shaly-sand model. The 2U, 3U and 4U zones are not consistent with this model<sup>5</sup>, this is due to the large concentration of dolomitic cements, thus rendering low gamma ray (low shale content) sands in this region as non-pay.

### Lithology

The density-neutron crossplots among other uses are invaluable as indicators for lithology and rock types. Figs. 2.6a – b, show the results of crossplots of neutron density in the wells in which they are available.

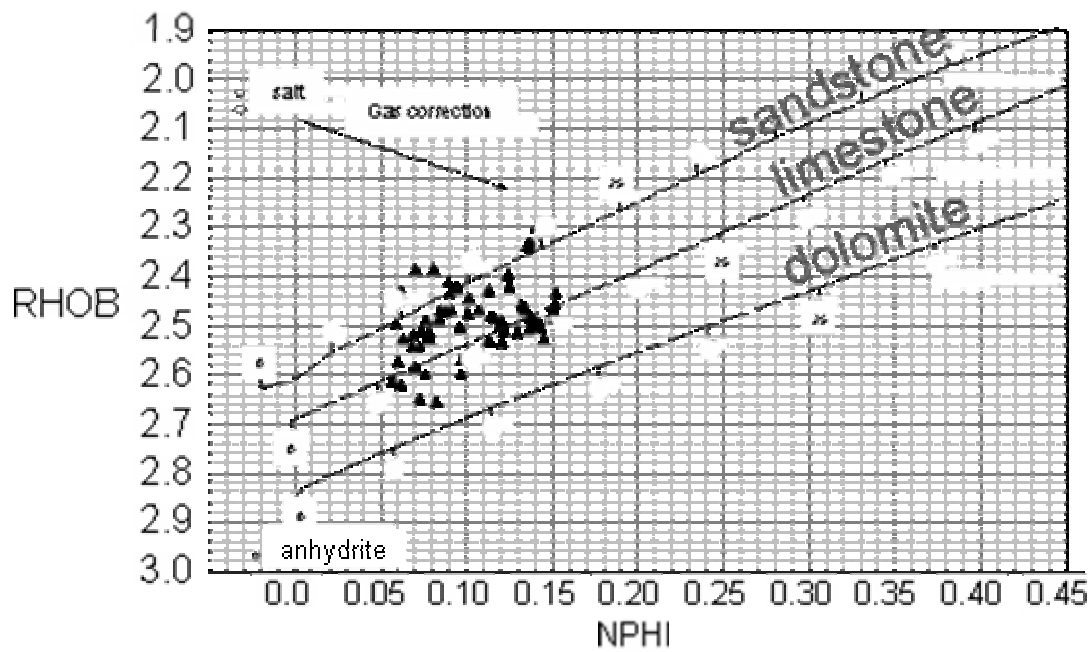


Fig. 2.6a – Crossplot for lithology identification in 1U sand for well ET 37.

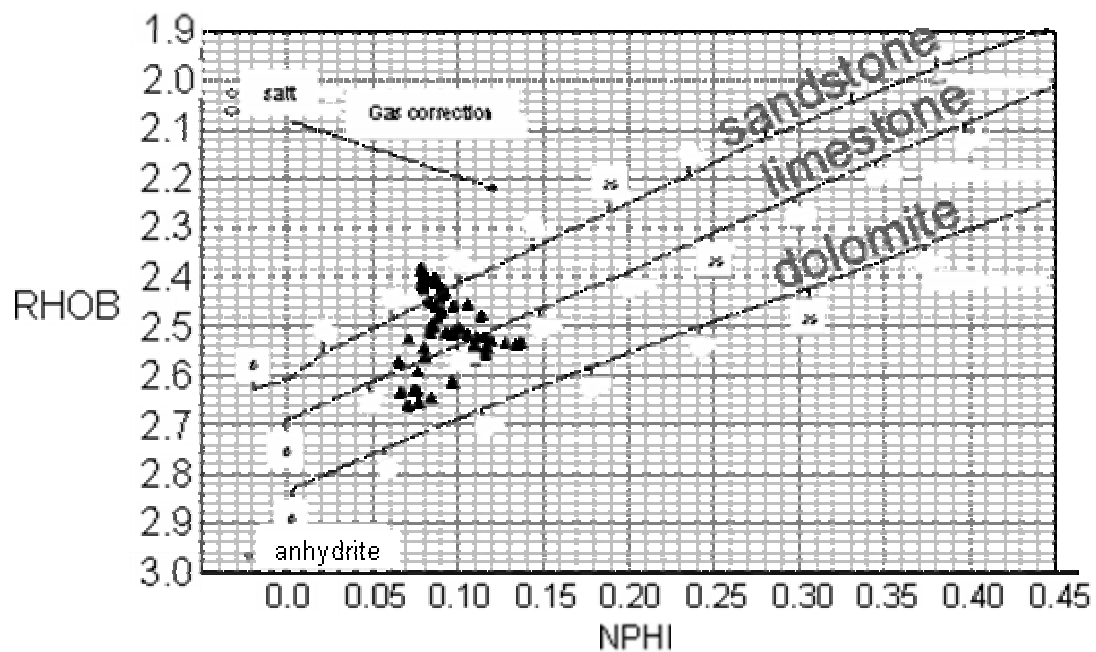


Fig. 2.6b – Crossplot for lithology identification in 5U sand for well ET 37.

The gas correction if applied will tend to shift the data down and right i.e. reduce density porosity and increase neutron porosity. Shale correction will depend on the type of shale (structural, laminated or dispersed).

## CHAPTER III DATA ANALYSIS

### **Log conversions and normalization**

26 logs are available within the ET O'Daniel unit, including log data for the cored wells. The wells are a variety of observation wells, injectors and producers.

59 well logs are available within the Germania Spraberry unit. Most of the logs are neutron logs taken as far back as 1950, with a few recent porosity and resistivity logs.

Log normalizations are performed on both log data sets prior to any transformations or inferences as to the significance of the log analysis. Illustrative procedures are shown for ET O'Daniel in the proceeding sections.

### ***Gamma ray***

This log forms the basis of pay identification within the Spraberry rock model. It is therefore important that the gamma ray is scaled appropriately to enable a consistent shale volume calculation from well to well.

Gamma ray curves for all the logs within the ET O'Daniel database were analyzed, and it was discovered that no two logs gave the same values at any chosen marker. Though this is expected, the wide variance in the response across these markers indicate the necessity for normalization of the gamma ray logs. More so, due to the fact that for a multi-well analysis, the Shale volume calculations will need to be revised for every well log if this process is not carried out.

### **Gamma ray maps**

Often mapping techniques are used to discern trends of gamma ray values. These gamma ray values may sometimes show systematic variation that may often be mistaken as tool

or calibration errors, we therefore need to map the lower and upper limits of the gamma ray values to verify whether or not trends exist rather than assume the need for normalization of gamma ray values.

Figs. 3.1 and 3.2 show maps of minimum and maximum raw gamma ray values obtained within 1U sand interval. Values are obtained by taking lowest and highest gamma ray observations within the interval of interest from digitized data.

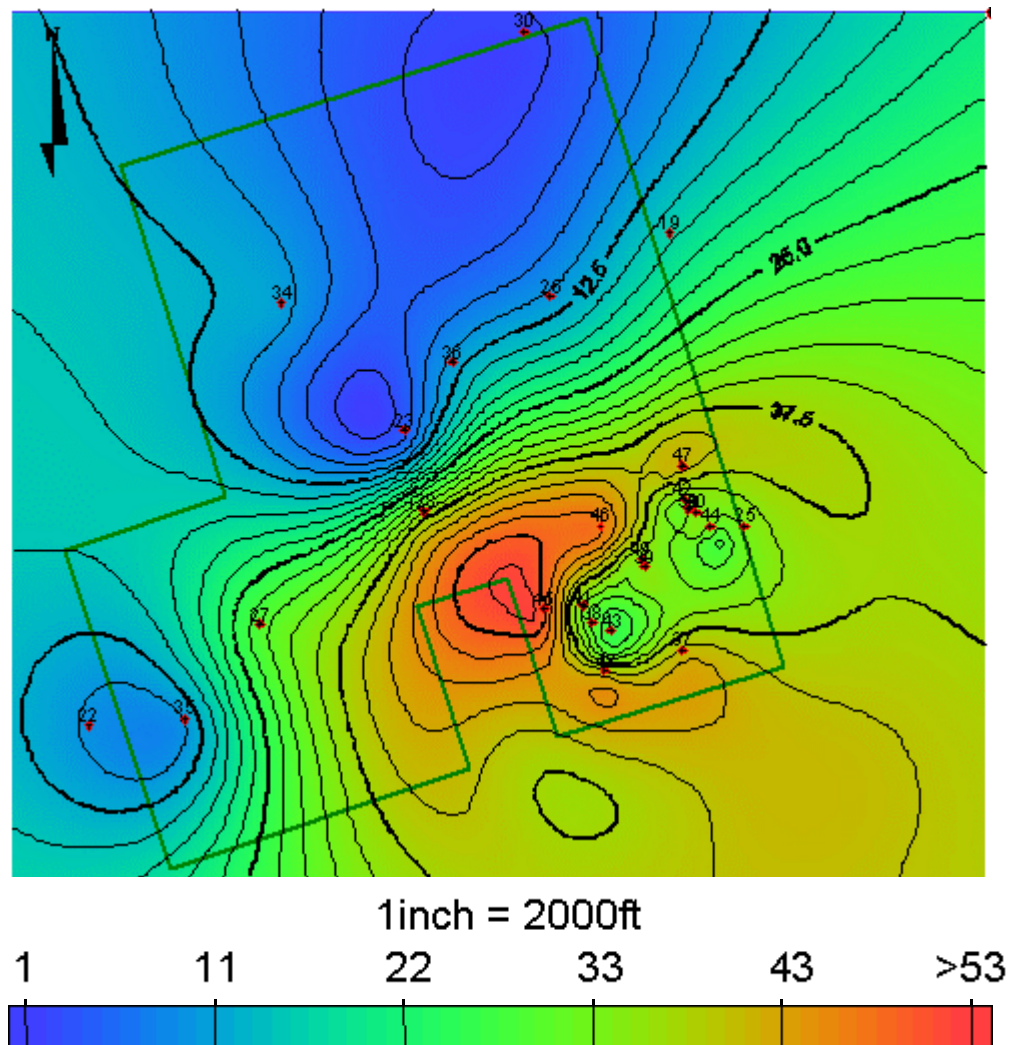


Fig. 3.1 – Minimum gamma ray values for ET O'Daniel unit in the 1U sand interval.

Often a bulls eye pattern on a contour map will give away the fact that the data points are random or lack any systematic variation in space. From the figure above we see that the NW section of the area is consistently low and the SW is consistently high, this might indicate a systematic trend. From the maximum gamma ray values in the 1U interval (Fig. 3.2) we do not see this trend, instead we see bullseye patterns, this will suggest that the trend in the 1U lacks consistency and hence indicate that normalization is required.

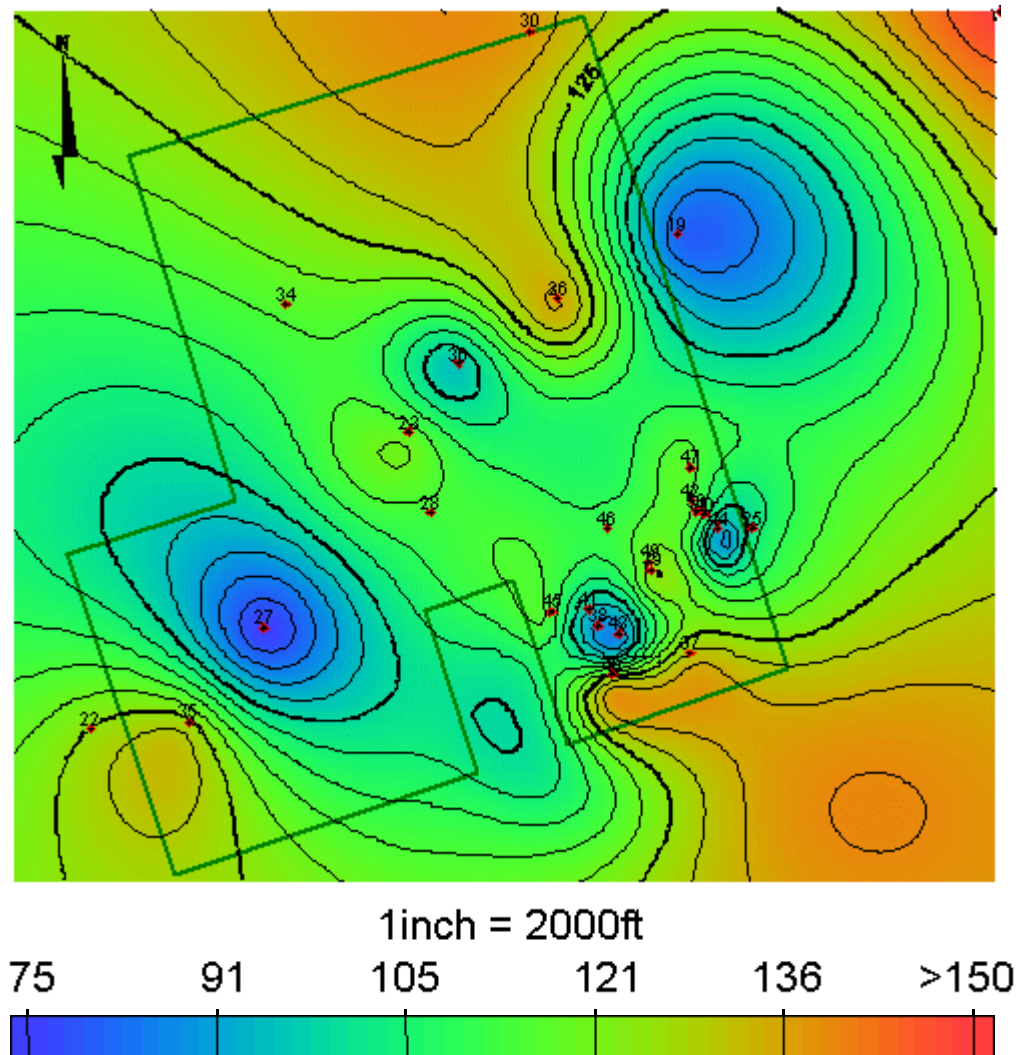


Fig. 3.2 – Maximum gamma ray values for ET O'Daniel unit in the 1U sand interval.

The same plots were generated for the 5U interval and the same conclusion was drawn based on the seemingly random distribution of the gamma ray values on both the minimum and maximum value distributions (see appendix B for figures).

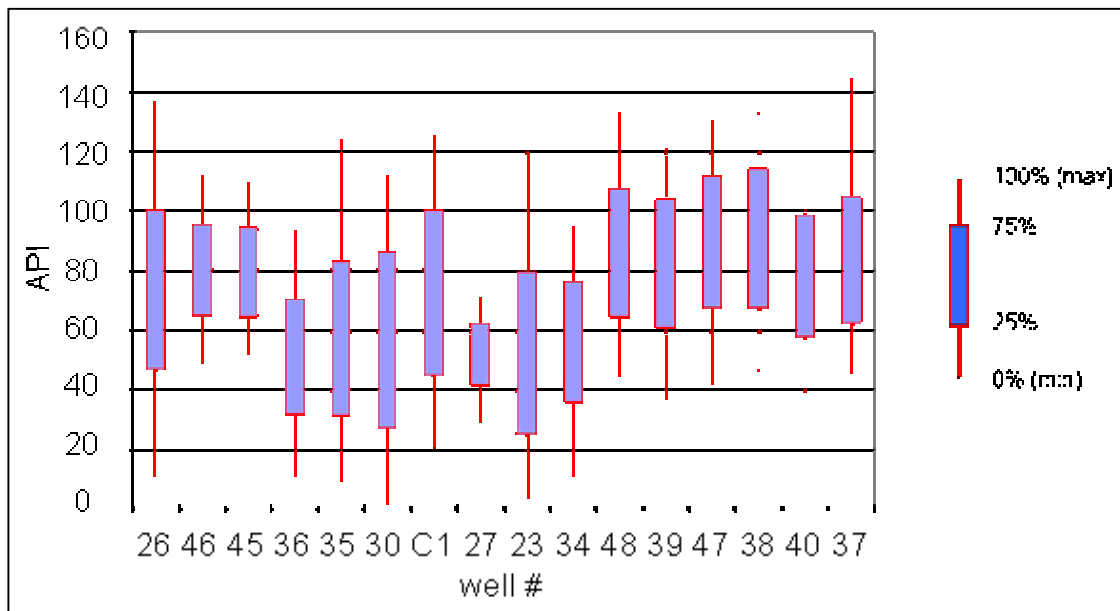


Fig. 3.3 - Variations in response from the gamma ray curves in ET O'Daniel.

### Gamma ray normalization

It can be inferred that the field standard based on the limited database is the range with the highest number of occurrence. Wells 37, 38, 39, 40, 47, 48, C1 and 26 are spread across the 20 – 140 API range and are the group exhibiting similar ranges.

A histogram for a type well representing the field standard is used to adjust all other wells deemed to require normalization. Fig. 3.4 shows the histogram and cumulative density functions for well 36 before and after normalization using well 26 as the standard.

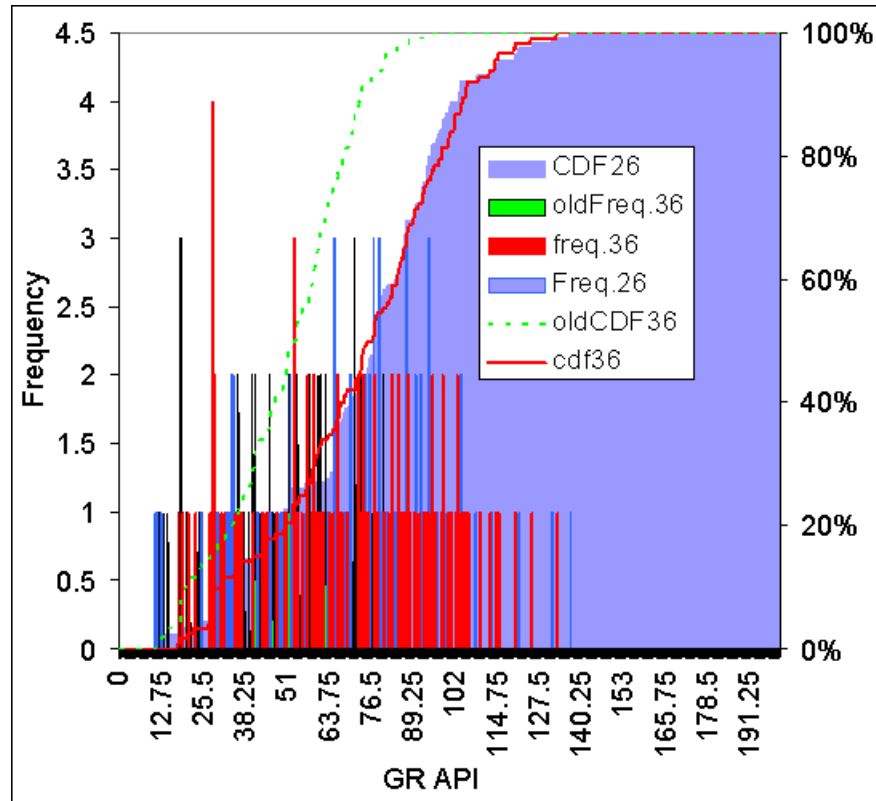


Fig. 3.4 - Histogram and CDF for wells 36, before and after normalizing against well 26.

A single equation for applying linear adjustments to log data is given by Shier<sup>28</sup>.

$$X_{norm} = R_{low} + \frac{(R_{high} - R_{low})(X_{raw} - W_{low})}{(W_{high} - W_{low})} \quad (3.1)$$

A different method used to adjust well log data involves the adjustment of each data point by a constant value such that the mean of the sample data equals the mean of the type log data. Thereafter, an 'Affine' correction is then applied to the sample data such that the variance of the sample equals the variance of the type log data. A computer program may be used to solve for the appropriate shift and correction factor required to match the mean and variance of the type log data.

Affine Correction<sup>32</sup>.

$$X_{norm} = \sqrt{s.f.}(X_{raw} - \mu) + \mu \quad (3.2)$$



$X_{norm}$	-	Normalized well value
$X_{raw}$	-	Actual well value
$R_{low}$	-	Regional low normalization value
$R_{high}$	-	Regional high normalization value
$W_{low}$	-	Wells lithological low value
$W_{high}$	-	Wells lithological high value
s.f	-	Correction factor
$\mu$	-	Population mean

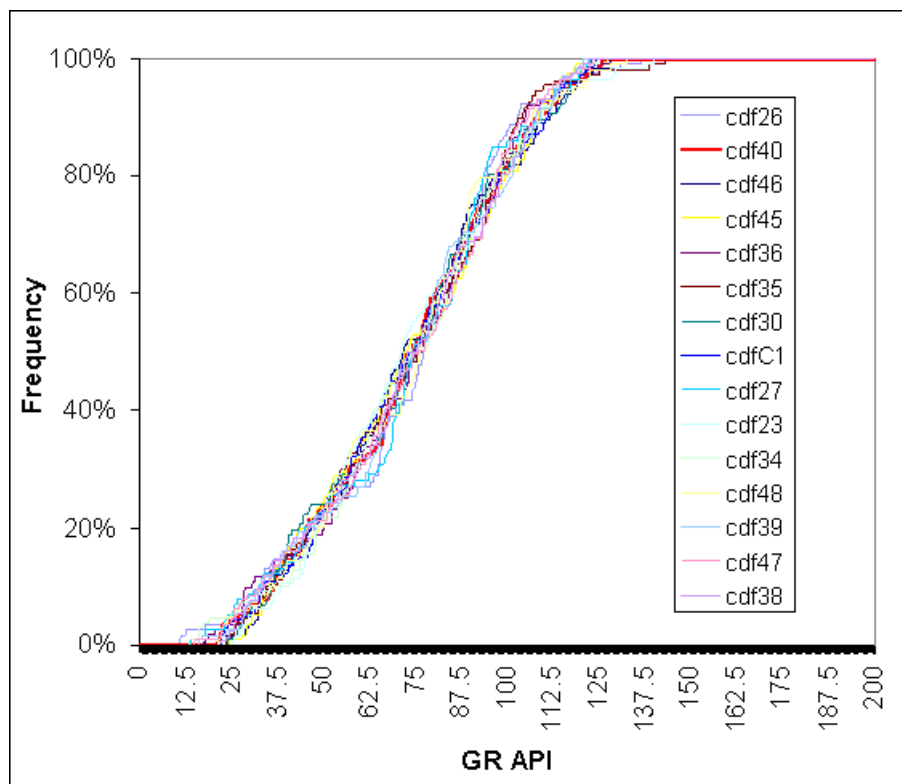


Fig. 3.5 – Corrected gamma ray distribution for ETO'Daniel wells.

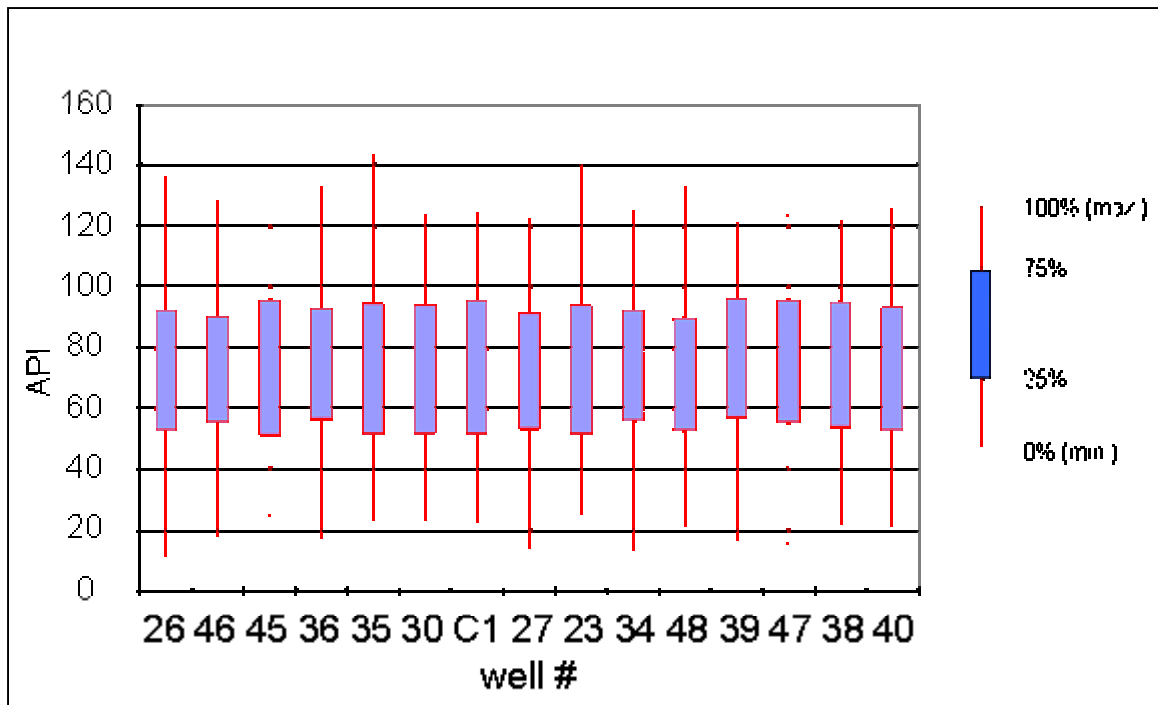


Fig. 3.6 – Normalized gamma ray values in 1U and 5U regions of upper Spraberry, ET O’Daniel unit.

## *Neutron logs*

### Standardization of neutron log units

The most common measure of porosity within the GSU log database is counts per second (cps) and is a measure of the amount of neutrons detected after bombarding the formation with energetic neutrons at the rate of several millions per second.

The neutron density decreases almost logarithmically with hydrogen richness, which is why porosity is a logarithmic function of neutron deflections.

The API RP33 recommends a system of neutron unit of calibration in the standardization-well-logging pit of the University of Houston.

One API neutron unit is defined as 1/1000 of the difference between instrument zero (tool response to zero radiation) and log deflection opposite a 6ft zone of Indiana limestone of 19% porosity.

### Conversion from neutron units to linear porosity units

A useful equation for converting a linear scale with respect to counts per second (logarithmic with respect to porosity), to a linear scale with respect to porosity is given by Shier<sup>28</sup>. This method is also known as the two – point method.

$$X_{norm} = 10^{\frac{y}{(W_{high\_cps} - W_{low\_cps})}} \quad (3.3)$$

where  $y = X_{raw} (\log R_{high\phi} - \log R_{low\phi}) + (W_{high\_cps})(\log R_{low\phi}) - (W_{low\_cps})(\log R_{high\phi})$

$X_{norm}$	-	Normalized well value (porosity, v/v)
$X_{raw}$	-	Actual well value (cps, API, EU)
$R_{high\phi}$	-	Value for high porosity location from core or reliable log data (known for a particular region, unit – v/v).
$R_{low\phi}$	-	Known value for low porosity location from core or reliable log data (known for a particular region, unit – v/v).
$W_{high\_cps}$	-	Well value at $R_{high\phi}$ location (cps, API, EU)
$W_{low\_cps}$	-	Well value at $R_{low\phi}$ location (cps, API, EU)

(Note: R in this case is not resistivity, but is used to denote regional value of parameter)

This equation is valid for all neutron curves measuring neutron counts irrespective of units.

The normalization equation requires the input of two lithologies from both a “type” well and the well being normalized. One lithology input is from a log interval that produces a

high log reading and the other is from an interval that produces a low log reading. These lithology intervals that bound the normalization process are known as normalization zones. Normalization zones should have a well log response that is consistent from well to well (as is the case of lithology intervals consisting purely of salt and anhydrite). If such zones are unavailable, the analyst chooses zones whose behavioral changes are understood from location to location. This implies that for any one field, many normalization zones may have to be selected in order to properly limit the high and low readings of the different curve types being adjusted.

After identifying lithology intervals that will be used for normalization, the characteristic values of  $R_{low}$  and  $R_{high}$  in these zones must be determined. This is accomplished by picking a “type” well (or wells) containing normalization zones considered by the analysts to have the correct well log response. This “type” well (or wells) is then defined as the standard to which all other curves will be adjusted.

### **Porosity**

Various logs are available that give a direct indication of porosity or matrix density. The database has mostly cased neutron logs that require conversion from API, cps or EU units to porosity units (Eq. 3.3). A few other wells have neutron porosity (NPHI, TNPH, TPHI) or density or acoustic (DT), the later two do not directly measure porosity.

When matrix lithology is known, shale free, and filled with water, all three porosity logs give the same values of porosity. These conditions are rarely encountered and therefore adjustments must be made for each of the different logs based on characteristic response in hydrocarbons and water.

The density log overestimates porosity in hydrocarbons, neutron logs underestimate porosity in hydrocarbons, and the acoustic log overestimates porosity in hydrocarbons<sup>30</sup>. To balance these anomalies out, an average porosity is often taken of the density and

neutron logs, in the absence of the density log either the neutron or sonic is used to estimate porosity.

$$PHIA = (DPHI + NPHI) / 2 \quad (3.4)$$

### *Corrections for porosity*

Porosity as earlier mentioned in chapter I, can be obtained from a combination of the different porosity logs. The preferred log suite will be the density porosity and the neutron porosity or sonic porosity, unfortunately few wells have the desired combination and porosity is often resolved from a one dimensional analysis of the available log (mostly neutron porosity). The playbacks used for analysis are chosen based on availability of porosity curves for the particular well.

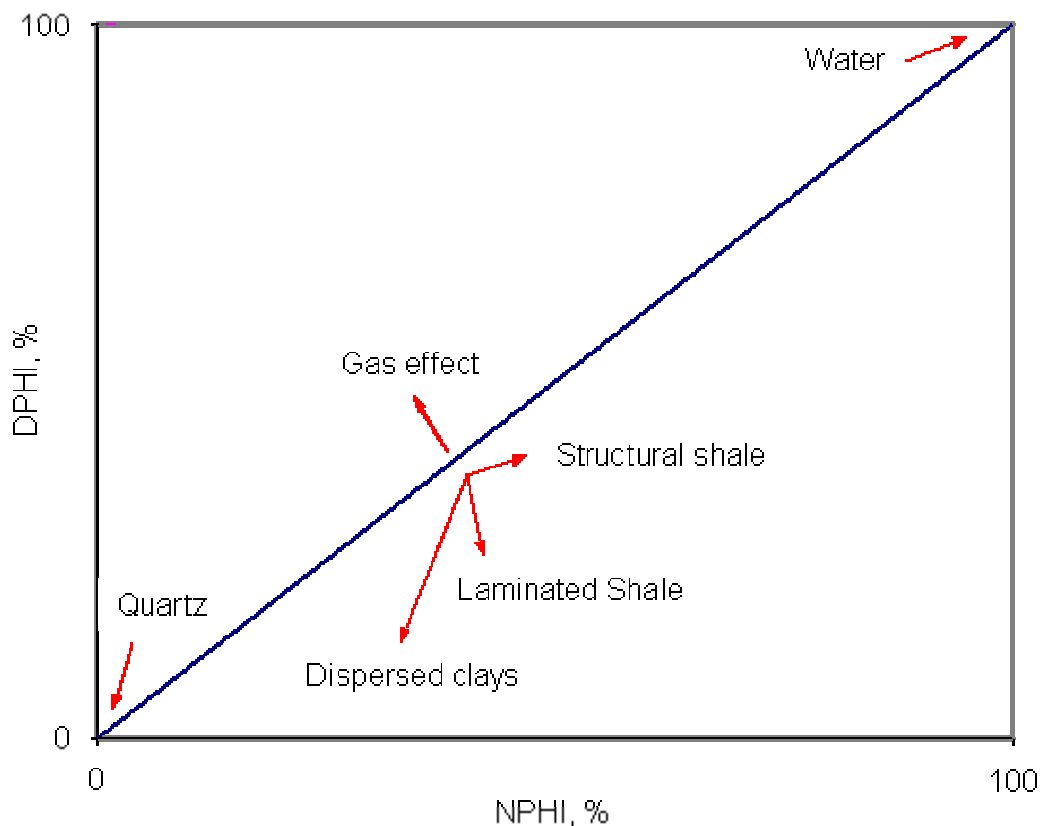


Fig. 3.7 – Effects on quality of porosity data from the density and neutron porosity tools.

Shale corrections are highly dependent on mode of shale features within the formation<sup>33</sup>. Shaliness affects the porosity log response in proportion to the amount, type and distribution of shale. This distribution may be structural laminated or dispersed shale. In the 1U and 5U sand units the shale distribution is in the form of laminae. Fig. 3.7 shows the effects of shaliness and gas on porosity values obtained from neutron and porosity logs.

Effective Porosity – The Effective porosity is less than the total or log measured porosity. This is due to the residual porosity within the unconnected pore spaces particularly within the clay minerals. Effective porosity (PHIE) can often be estimated by correcting for the presence of shale, given by:

$$PHIE = PHIA (1 - V_{shl}) \quad (3.5)$$

### **ET O'Daniel log-core model**

#### ***Log porosity – core porosity x-plots***

The core and log porosity crossplots indicate the level of agreement between core data and log data. If there is sufficient agreement between both porosities or a relationship between both data sets can be consistently established, further analysis can be confidently carried out on the basis of log porosity.

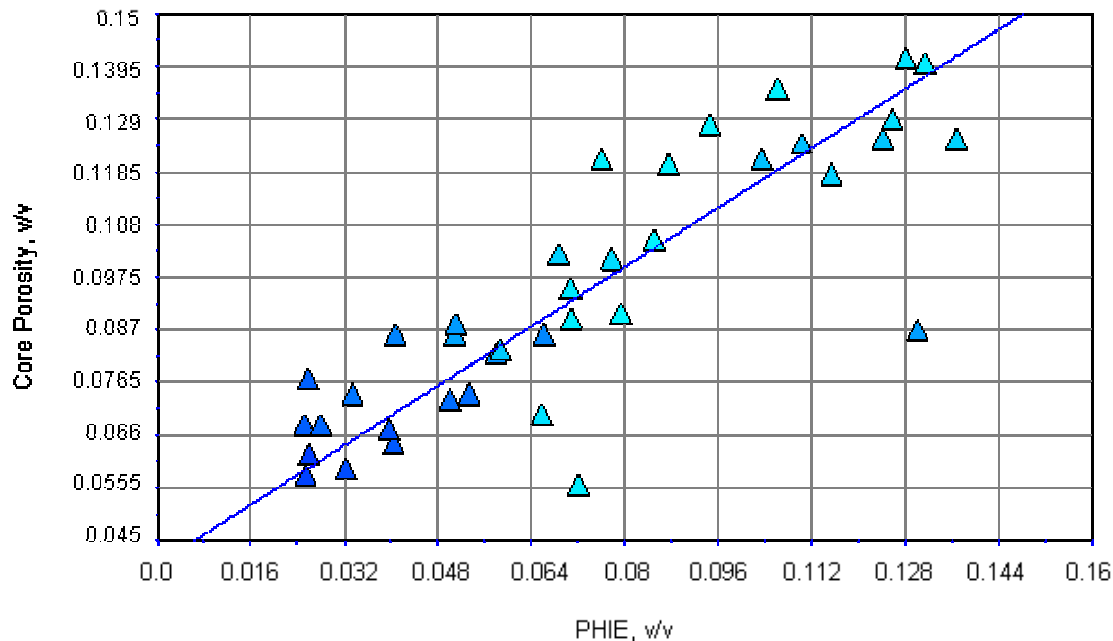


Fig. 3.8 - Crossplot core porosity vs. log porosity for ETO'Daniel 39, 1U sand. Light to dark markers represent a 3rd dimension of increasing shale content on a scale of 0 to 1.

A depth match is performed prior to a crossplot of both porosity values (core and log). The depth match may be improved by analyzing the degree of correlation obtained for crossplots based on depth shifting the core data. This is done if a 'clear' relationship cannot be established just by visual analysis.

From regression analysis a best fit equation for the x-plot in 1U was found to be:

$$Y = 0.050342 + 0.539983X \text{ and } R^2 = 0.677$$

And for 5U:

$$Y = 0.05810 + 0.560472X \text{ and } R^2 = 0.620651$$

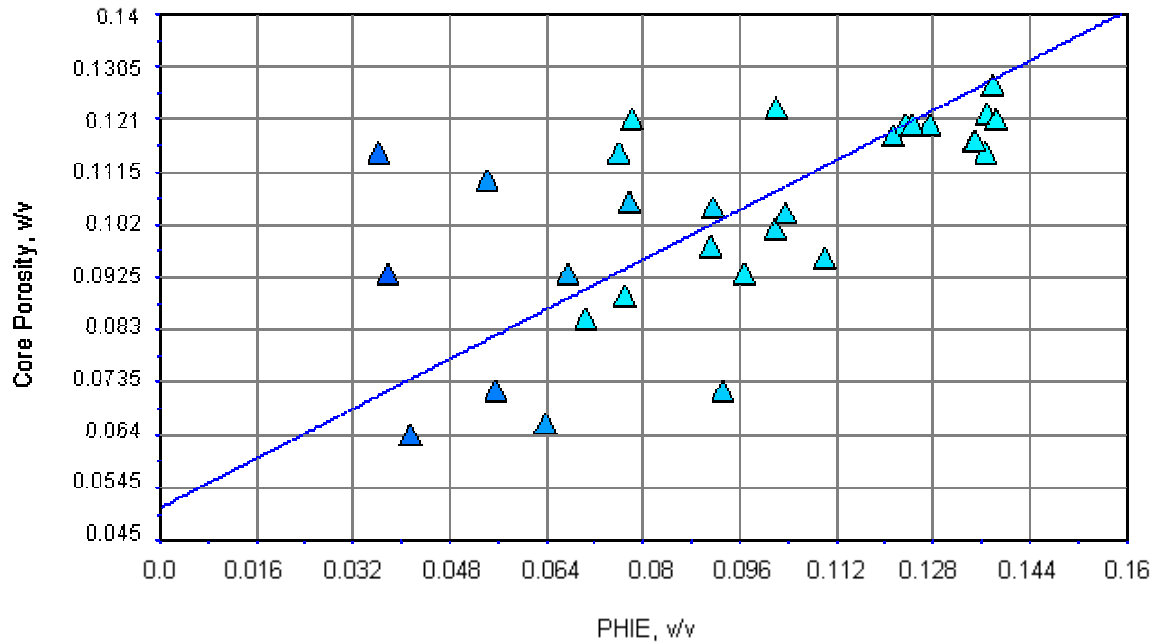


Fig. 3.9 - Crossplot core porosity and log porosity for ET 39, 5U sand.

The ET O'Daniel 39 well gave the most consistent core to log relationship of all the cored wells analyzed, more so within the 1U interval. Table 3.1 shows the summary of regression results obtained from the crossplots of cored wells in the ET O'Daniel field.



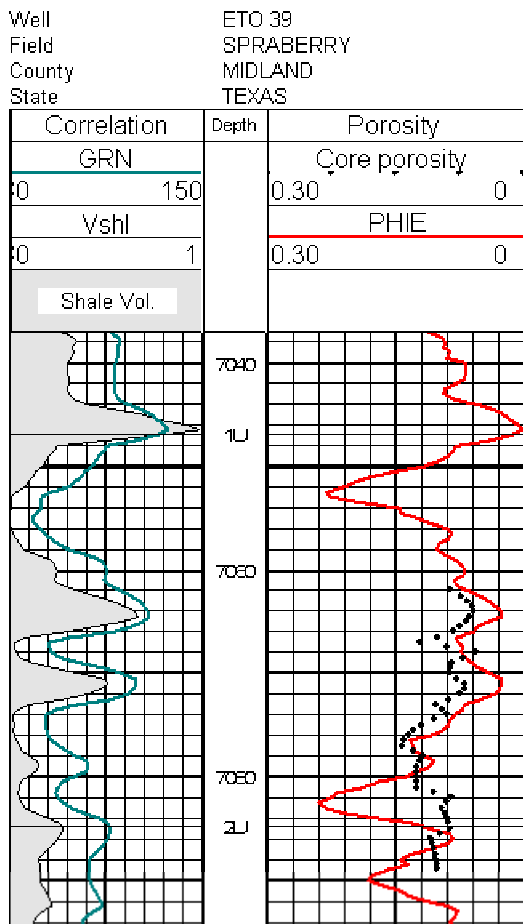


Fig. 3.10 – Log playback of log and core porosity in ET 39, 1U sand.

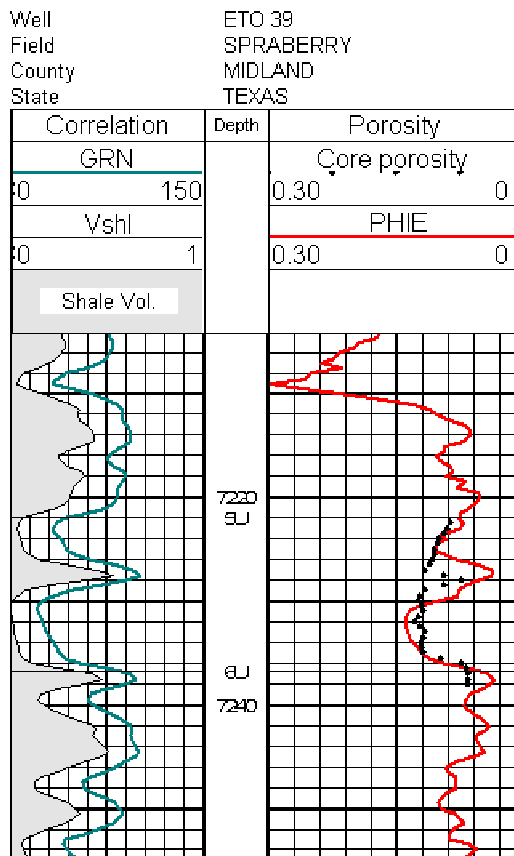


Fig. 3.11 – Log playback of log and core porosity in ET 39, 5U sand.

Table 3.1 – Regression from crossplots of core – log porosity for cored ET O’Daniel wells.  
(Best results are obtained in ETO#39 well).

Well	1U		5U	
	Least Sq. Regression	R2	Least Sq. Regression	R2
37	$y = -0.018494 + 1.12948x$	0.542	$y = -0.024442 + 0.949273x$	0.106
38	$y = -0.024815 + 1.049007x$	0.230		
39	$y = 0.050342 + 0.539983x$	0.677	$y = 0.050810 + 0.560472x$	0.621
40	$y = 0.050857 + 0.520833x$	0.509	$y = 0.028280 + 0.662358x$	0.396
47	$y = 0.017356 + 0.560368x$	0.073	$y = -0.021898 + 1.243577x$	0.073
48	$y = 0.014259 + 1.042477x$	0.519	$y = 0.034999 + 0.748994x$	0.776

$y =$  core porosity,  $x =$  log porosity

Core – log porosity discrepancies are observed from the log playbacks and regression correlations, this is often due to bound water contained in the clays. This is also referred

to as residual porosity earlier mentioned, this results in porosity estimates from logs exceeding that determined from cores.

### **Variables influencing permeability**

#### ***Regression analysis***

Various variables often influence the flow capacity of the rock, such as clay mineral content (shale), distribution, pore throat size / capillary pressure, connate water saturation, porosity etc. Crossplots of these variables and permeability will often reveal underlying relationships, furthermore, regression analysis may produce a functional mathematical model to represent this relationship.

Readily available are porosity and shale volume data obtained from the neutron, density or acoustic logs and gamma ray logs respectively. Porosity values (PHIE) are verified against core porosity data (Figs. 3.10 and 3.11).

Figure 3.12 a – b show the shale volume - permeability relationship for wells 39 and 47. The trend is consistent for all the wells investigated i.e. permeability decreasing with increasing shale content.

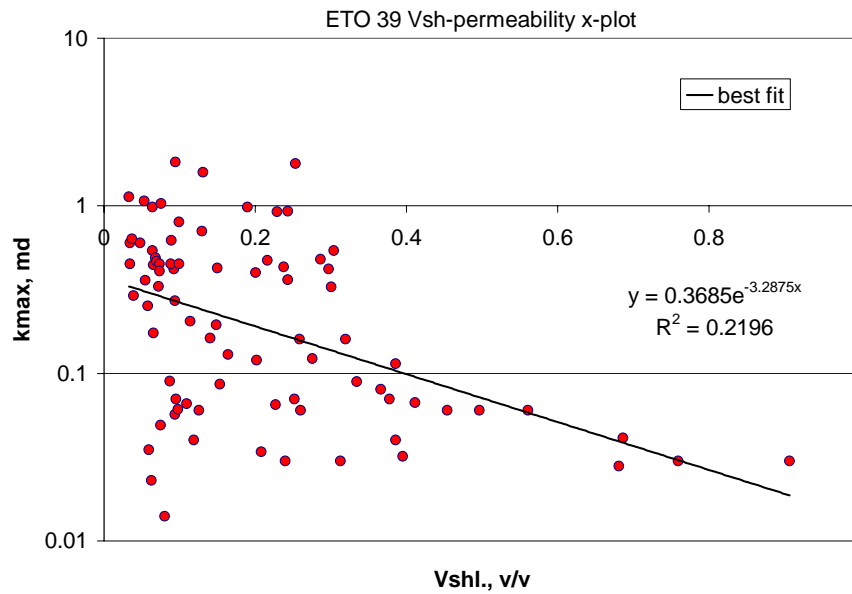


Fig. 3.12a - ET 39 crossplot for shale volume and permeability.

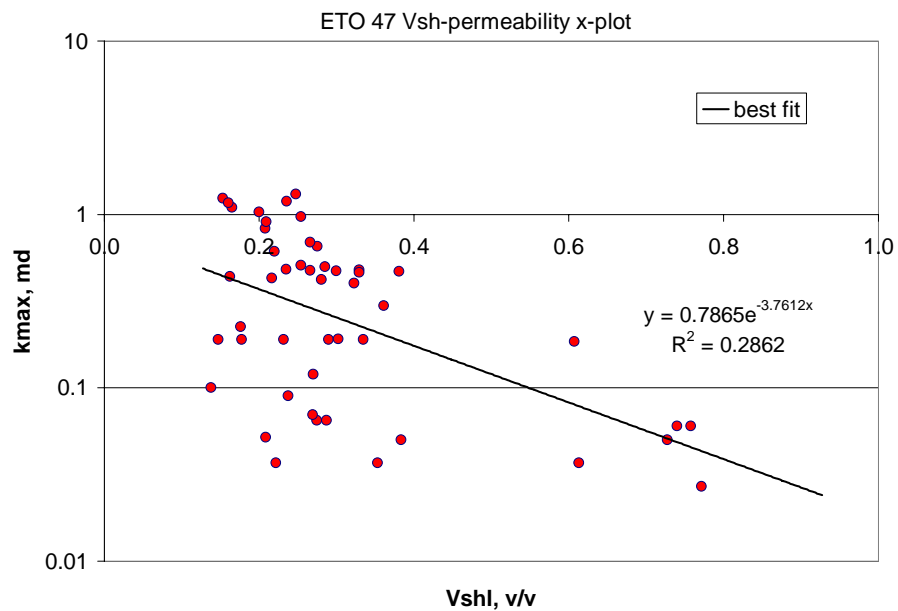


Fig. 3.12b - ET 47 crossplot for shale volume and permeability.

### *Shale effects on porosity and permeability*

Figs. 3.12a and b show the relationship between shale volume and core permeability values. Within the shaly Spraberry sands, shale is in the form of laminae and therefore we

expect a significant effect on the density and neutron porosity log values. Gas effects are negligible in the Spraberry payzones due to the absence of a gas cap, therefore any corrections to be made are for shaliness.

Shale corrections are applied to the neutron porosity data as given in Eq. 3.5.

Figs. 3.13a and b show the relationship between the uncorrected neutron porosity data and permeability. From established correlations for porosity and permeability<sup>28</sup>, we expect to observe an increase in permeability associated with an increase in porosity, but in the figures below, this trend is masked by the effects of the shale laminae in the logged intervals.

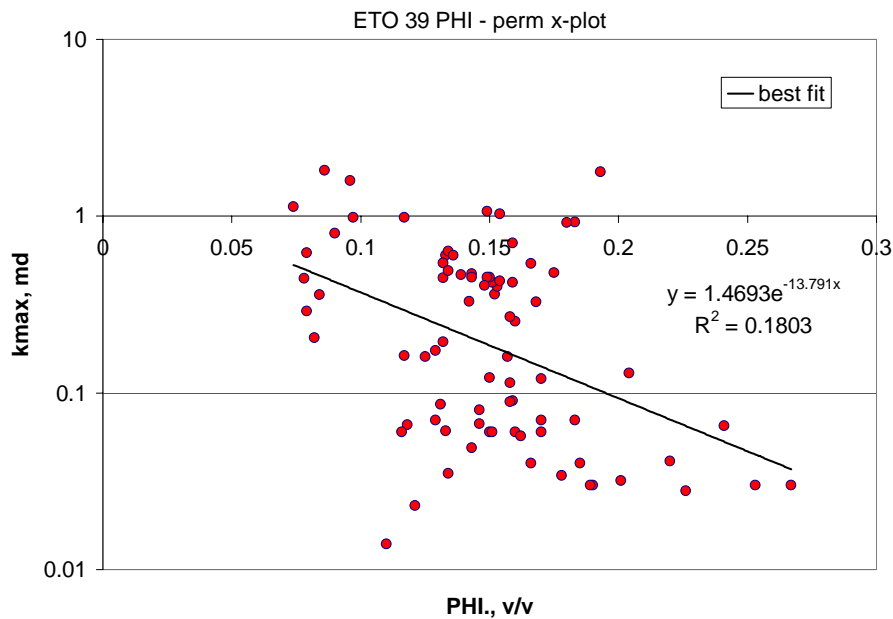


Fig. 3.13 a - ET 39 crossplot for log porosity and permeability.

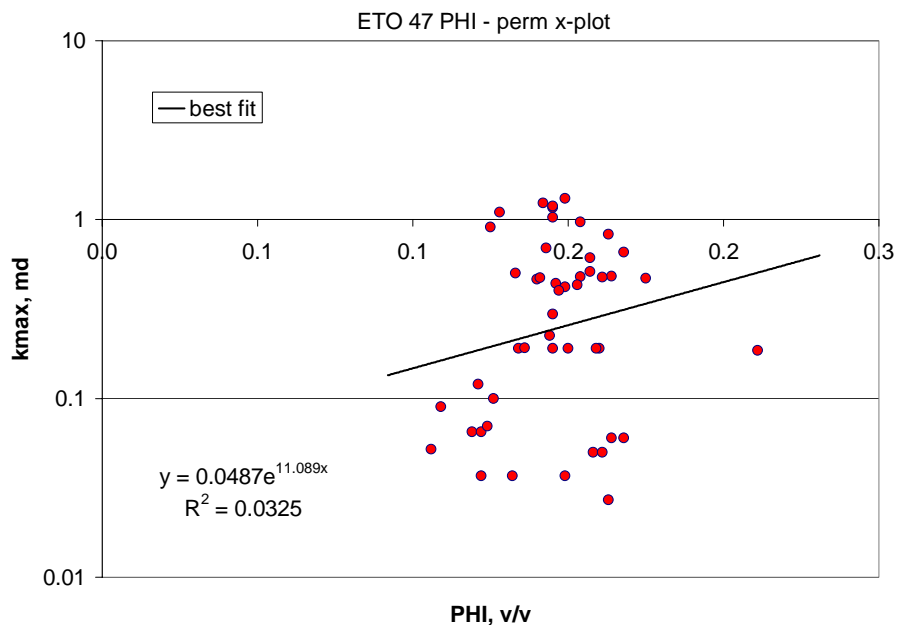


Fig. 3.13 b - ET 47 crossplot for log porosity and permeability.

From Figs. 3.12, we can see that the shale volume clearly influences the permeability, therefore we must apply corrections to the log porosity to obtain a useable model for predicting permeability.

After correcting for shaliness, plots generated for porosity-permeability (Figs. 3.14a and b) show the functional relationships for predicting permeability based on porosity.

The porosity values from the neutron log are used for this prediction exercise as this is the available porosity log type within the database, with the exception of only a few wells which may have both or the three porosity types.

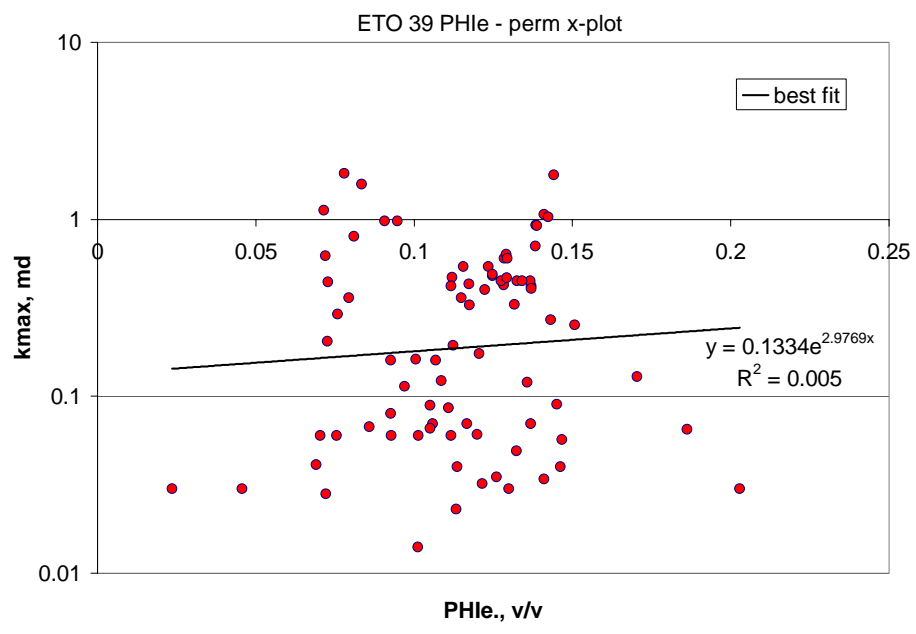


Fig. 3.14a – ET 39 crossplot for shale corrected porosity and permeability.

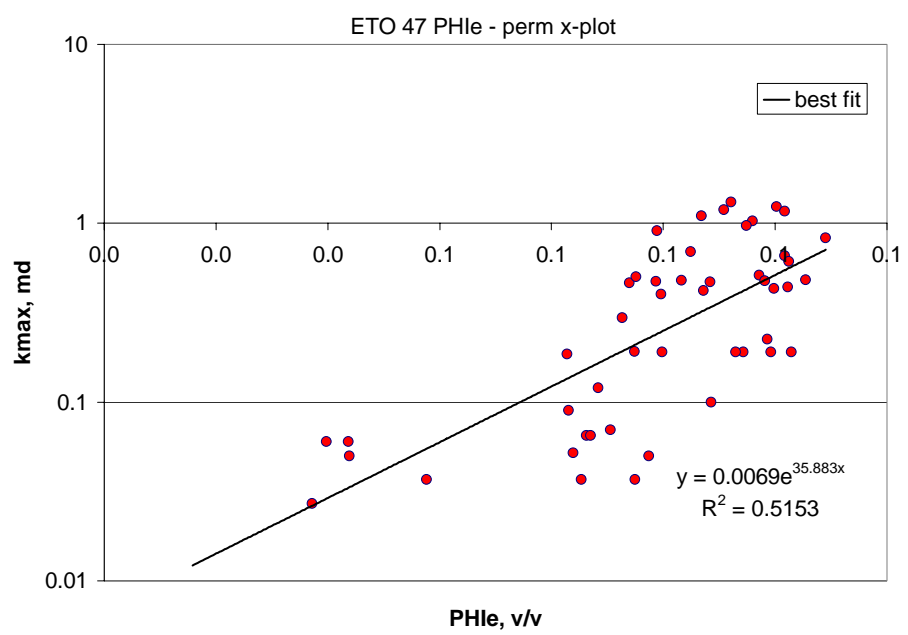


Fig. 3.14b - ET 47 crossplot for shale corrected porosity and permeability.

Figures above show the crossplots of 2 of the control wells used to establish a porosity - permeability relationship. The porosity is corrected for shale (PHIE), and this corrected porosity is regressed against corresponding core permeability values for each of the wells

analyzed. Well ETO 47 gives the best correlation, the resulting relationship between porosity and permeability is given as:

$$Y = 0.0069e^{35.883X} \text{ and } R^2 = 0.515$$

where y = permeability and x = effective porosity for a given well in the zones of investigation (1U and 5U in this case).

### ***Data conditioning ('ACE')***

Besides porosity, rock type, clay content and lithology, initial water saturation and pore throat size most probably have an influence on effective permeability. The limitation of any log derived permeability is in the fact that these variables are static volumetric terms, whereas permeability is a measure of the movement of fluid through rock (Hunt, Pursell, 1997). Any permeability correlation between porosity and or water saturation will not likely have a wide geographic or geologic application. The only way to obtain a robust permeability distribution is by acquiring field wide core and well test data.

Correlating permeability in the Germania unit is hampered due to an absence of core data, production data is available, and is beyond the scope of this project. Therefore we are limited to methods which use static properties to correlate the permeability, specifically the 'Alternating Conditional Expectation' (ACE) method.

From the established rock model (Table 1.1), the upper Spraberry has been classified into 3 rock types based on shale content and porosity. As the rock type is classified based on porosity and shale volume it will not be used as a variable in the estimation of the permeability transform. Therefore, 2 independent variables will be used: shale volume and porosity in calculating the dependent variable, permeability.

### *The 'ACE' transformations*

The optimized multi-variate regression was performed to determine the optimal transformation for porosity type data (density or neutron porosity).

The resulting playback for the 1U and 5U intervals (Fig. 3.15) shows the match from conventional regression from cored wells and from the ACE algorithm.

The following transformations were used to obtain the ACE model:

$$\text{NPHI}_{\text{transform}} = -303.86\phi^2 + 125.24\phi - 11.738$$

$$\text{Vshl}_{\text{transform}} = -3.8536V^2 - 0.63206V + 0.66875$$

$$k_{\text{ACE}} = 0.40339A\Sigma_{\text{transform}}^2 + 0.64404\Sigma_{\text{transform}} + 0.018403$$

$$\text{where } \Sigma_{\text{transform}} = \text{NPHI}_{\text{transform}} + \text{Vshl}_{\text{transform}} \text{ and } R^2 = 0.77$$

The correlation coefficient obtained using the ACE algorithm is higher than that from conventional regression, but it is obvious from the playback in fig. 3.15 that both methods do not adequately model the permeability using porosity and clay content. In a separate study<sup>34</sup>, NMR core analysis was performed on two samples from wells within the ET O'Daniel unit to develop an empirical NMR permeability model for the upper Spraberry sandstones. NMR permeability was derived for reference using  $K = 4.6T_{2\text{ml}}^2\phi^4$ , where  $T_{2\text{ml}}$  is the logarithmic  $T_2$  of the  $T_2$  distribution curve. Such a study emphasizes the complexity of modeling permeability based on primary reservoir properties, albeit, no NMR data is available in the database to enable a comparison of the ACE model and the NMR model.



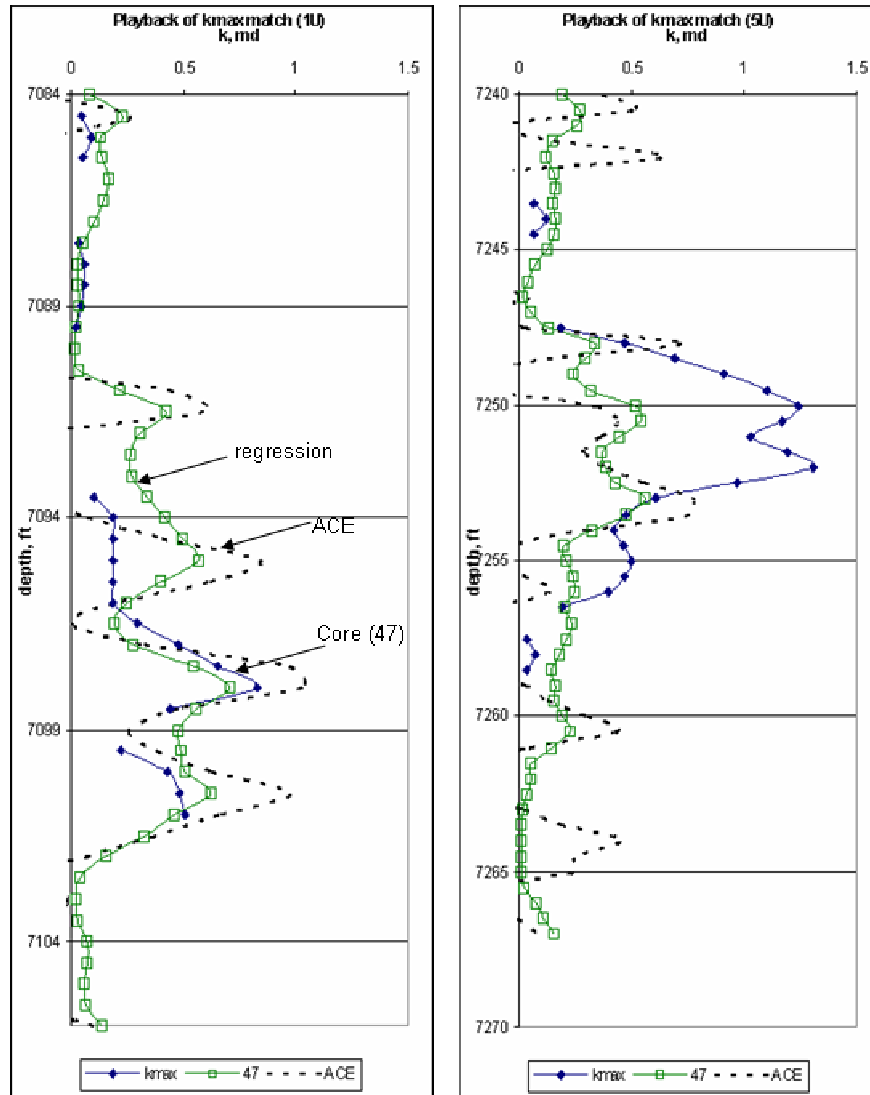


Fig. 3.15 – Playback of results from conventional regression and ACE regression.

### Water saturation

Table of values for Archie parameter values for use in the quantitative analysis of Spraberry sands have been published<sup>11</sup> based on log data analysis in the Spraberry sands by Schlumberger. Table 3.2 gives expected range of values for the Spraberry.

The Archie equation has been used extensively in the Spraberry<sup>5,11</sup> to successfully estimate saturations within the upper Spraberry interval. A match of the saturation profile

of the Shackelford I-38 was made with 1, 1.66 and 1.46 for a, m and n respectively. These values agree with the averages proposed in Table 3.2.

The tortuosity exponent (a), usually varies from 0.62 to 1.2 but 1 is often used as it has a narrow range of variation and is not related exponentially to the formation factor, F.

$$R_o = F \cdot R_w, \text{ where } F = a/\phi^m = R_o/R_w$$

Cementation factor (m) may vary from 1 to as much 4, rocks with fractures or fissures may have low cementation values often close to 1. The saturation exponent (n) is usually 2, for shaly sands this value is less than 2.

Table 3.2 – Archie parameters used in determining saturation in the upper Spraberry.

	Min	Max	Average	Comment
R <sub>w</sub>	0.03 ohm-m	0.04 ohm-m	0.35	Measured at 130F
R <sub>o</sub>	0.7 ohm-m	3 ohm-m	1.3	Min and max values are for porosity ranging from 8 to 20%
				Average value for porosity of 12%
m		1.8		Possibly lower for clean sands
F	20	100		
φ	8%	20%	12%	Average for upper spraberry
n	1.5	1.9		Usually less than 2.0 for shaly sands

The generalized form of the Archie equation is  $S_w^n = aR_w/\phi^m R_t$

This equation is applied in the wells that have resistivity log values over the 1U and 5U sand intervals to estimate average saturations. In applying Archies equation, certain parameters will be varied so as to match the measured core saturations. Going by table 3.2, the R<sub>w</sub>, a, and n values are fixed at 0.035 ohm-m, 1 and 1.7 respectively, while R<sub>t</sub> - true resistivity is obtained from the laterolog or induction log. The parameter whose sensitivity will determine the match based on measured core saturation will be m, the cementation exponent.

Figure 3.16 (saturation track) shows the match between the Archie calculated water saturation and the core derived saturation. A cementation exponent of 1.7 gave a good match on most of the cored wells (see Figs. 3.16 and 3.17). A crossplot of Core and

Archie derived saturation values was used to evaluate the optimal match by choosing a cementation exponent value (m) that results in the best correlation coefficient for the compared wells. In some wells the match was not optimal i.e well #47 and # 40 (1U), but all wells considered, m of 1.7 gave a good fit.

From depth averaged Archie calculated saturation values, Table 3.3 was developed for wells with core and / or resistivity data.

Table 3.3 – Interval averaged water saturations for well with resistivity curves.

Well	Int.	Avg. SwA	Avg. Core Sw	Date Logged
37	1U	N/A	48.04%	10/19/1995
	5U	N/A	63.60%	10/19/1995
38	1U	28.16%	29.07%	8/14/1998
	5U	N/A	22.91%	8/14/1998
39	1U	42.05%	N/A	7/5/1998
	5U	42.00%	N/A	7/5/1998
40	1U	30.18%	22.76%	9/4/1998
	5U	31.05%	31.15%	9/4/1998
47	1U	33.16%	52.66%	7/22/1998
	5U	N/A	48.65%	7/22/1998
48	1U	29.04%	N/A	9/24/1998
	5U	36.00%	N/A	9/24/1998
49	1U	36.82%	N/A	2/15/2001
	5U	35.37%	N/A	2/15/2001
50	1U	50.86%	N/A	2/15/2001
	5U	36.37%	N/A	2/15/2001

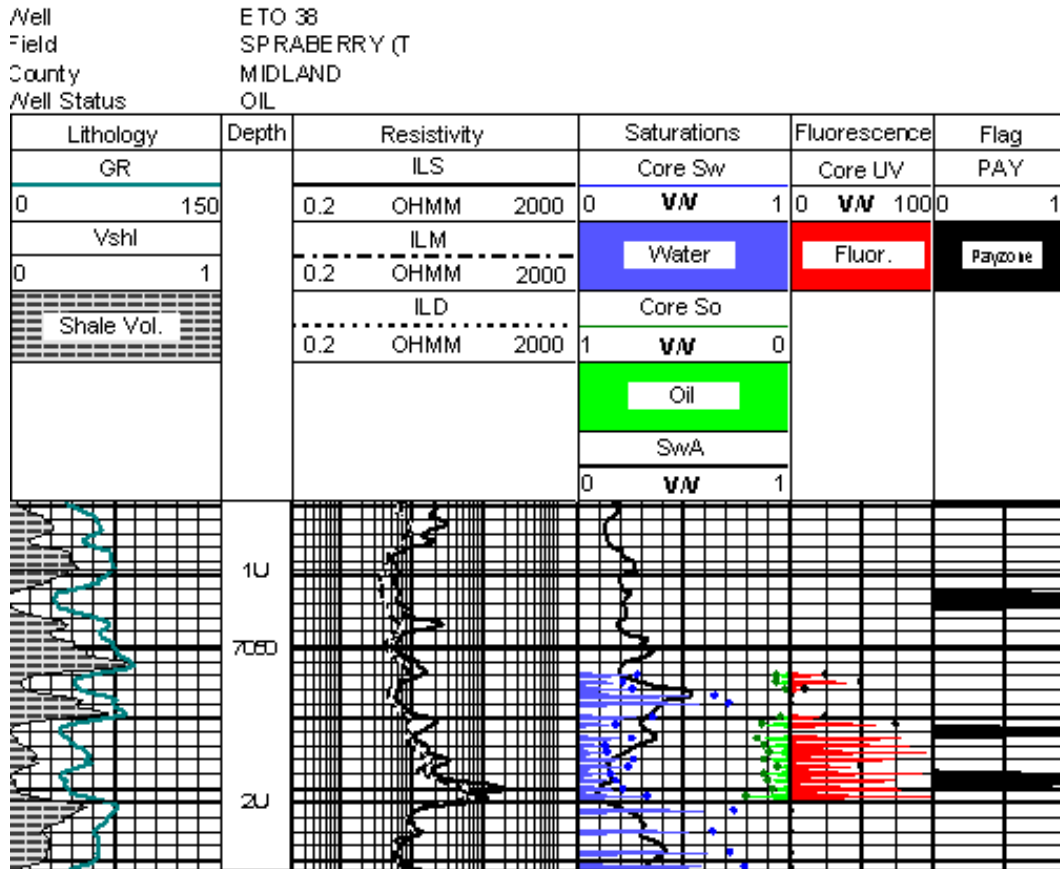


Fig. 3.16 – Saturation profile matched for ET 38, 1U using  $R_w$  0.035 ohm-m and  $m$  1.7.

Determining  $S_w$  in a fractured reservoir using the Archie equations is complicated because the cementation exponent,  $m$ , may be as low as 1. Rasmus<sup>35</sup>, proposes an equation for calculating  $m$  in fractured reservoirs.

$$m = \frac{\text{Log}[\phi_s^3 + \phi_s^2(1 - \phi_t) + (\phi_t - \phi_s)]}{\text{Log} \phi_t} \quad (3.6)$$

where

$m$  = Archie cementation exponent

$\phi_s$  = matrix porosity calculated from Sonic log

$\phi_t$  = total porosity from neutron or density logs

From well #47, a single well average of log values for  $\phi_s$  and  $\phi_t$  are 0.1236 and 0.1512, after evaluating for m using Eq. 3.6, the resulting value of m equal to 1.667 which is in the range of the optimal value previously determined from core Sw and SwA comparison.

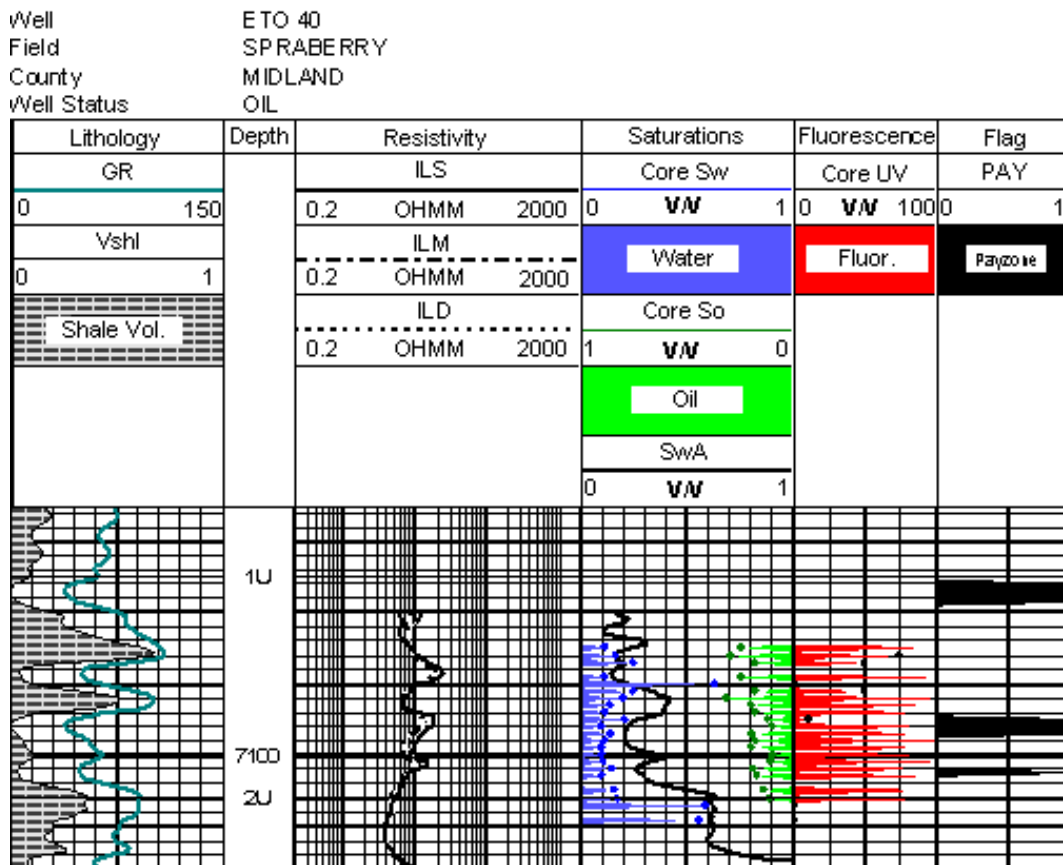


Fig. 3.17 – Saturation profile matched for ET 40, 1U using  $R_w$  0.035 ohm-m and m 1.7.

## CHAPTER IV

### ET O'DANIEL AND GERMANIA ANALOGY

On the basis of available log data, shale volume determined from gamma ray logs and porosity response will form the basis of comparison of the two units. Permeability of the matrix in the Spraberry unit is low in general and flow capacity is enhanced as a result of the interconnected natural fractures, for this reason, it can be established at this early stage that one of the three major indices (matrix permeability) for comparing the two fields show sufficiently similar response, although there is no core permeability data in the Germania unit to correlate.

#### Shale volume

Figs. 4.1 and 4.2 show the distribution of average shale volume fraction within the 1U and 5U intervals in the ET O'Daniel unit. The values are averaged every 0.5 feet of depth and these values used are based on the normalized values determined in chapter III.

The shale volume indices clearly follow a normal distribution and summary statistics for each interval are as shown alongside the distribution.

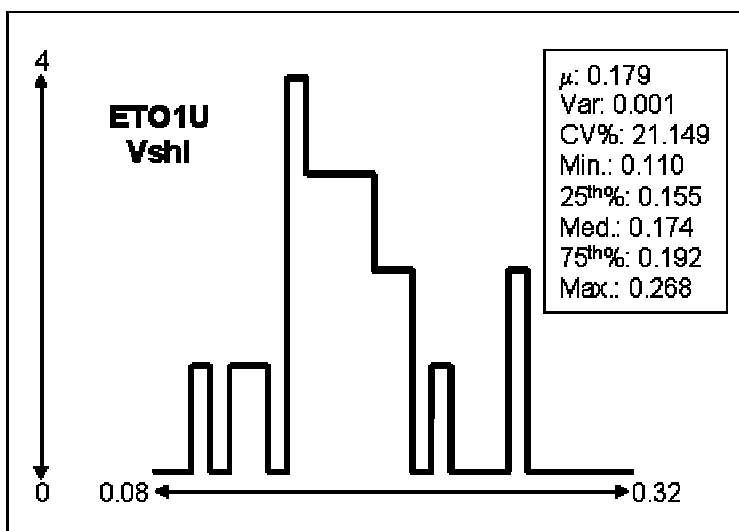


Fig. 4.1 – Statistics of Vsh values for ET O'Daniel, 1U sand.

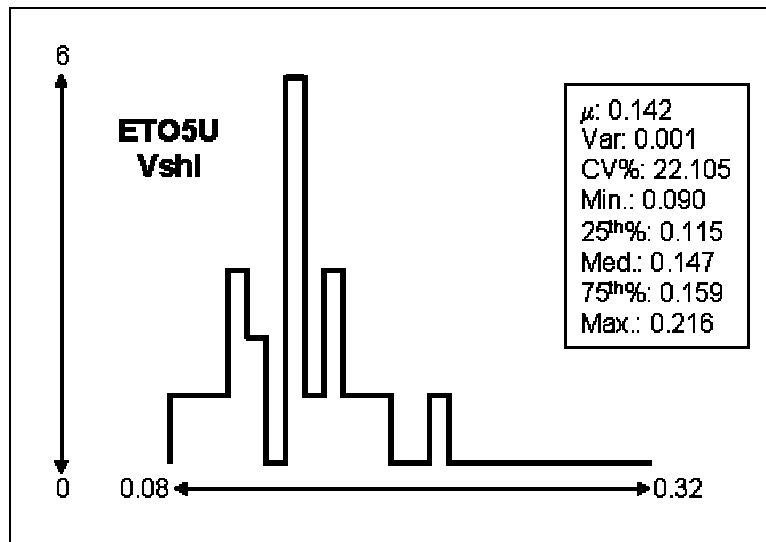


Fig. 4.2 – Statistics of Vsh values for ET O’Daniel, 5U sand.

Figs. 4.3 and 4.4 similarly show shale volumes in the Germania unit, and like the distribution follows a normal distribution.

When comparison of the two fields are made based on the shale volumes, we observe similarities in the mean and Inter-Quartile range (IQR) for both the 1U and 5U units.

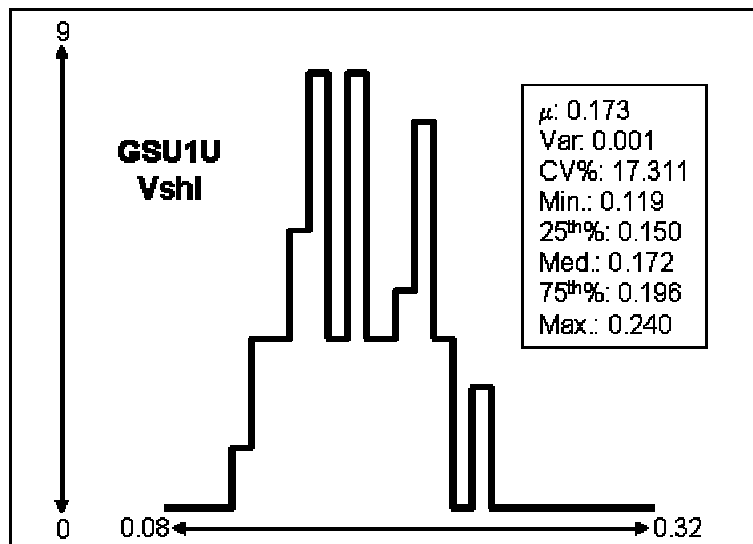


Fig. 4.3 – Statistics of Vsh values for Germania, 1U sand.

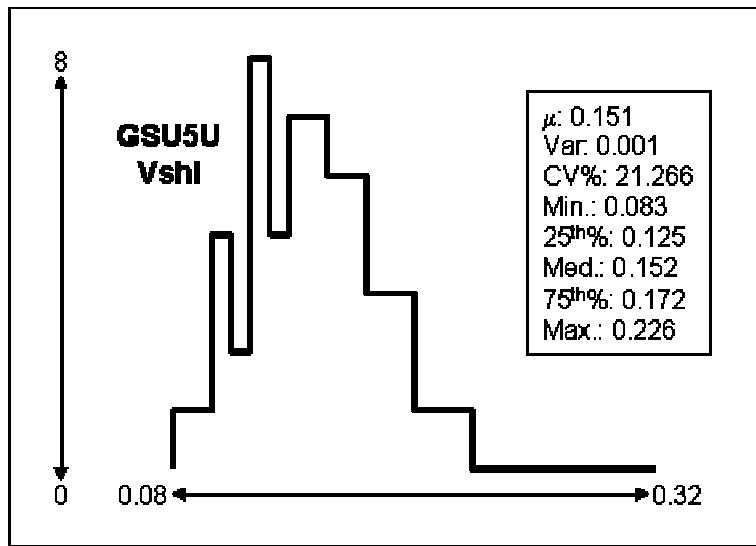


Fig. 4.4 – Statistics of Vsh values for Germania, 5U sand.

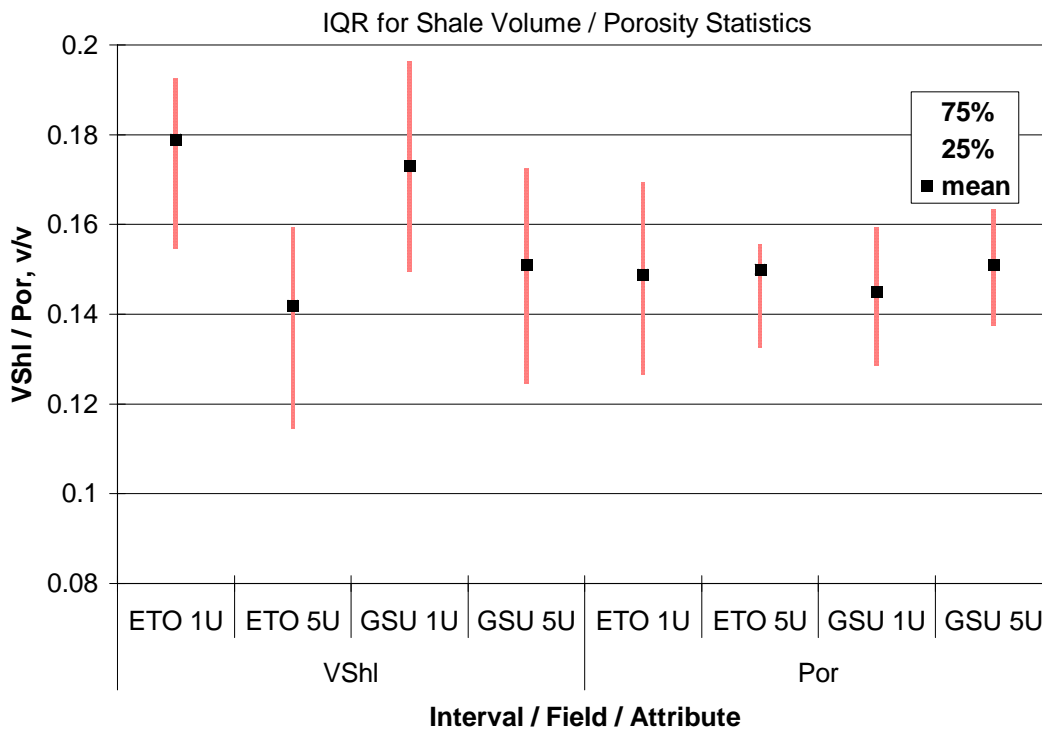


Fig. 4.5 – IQR and mean values of shale volume and porosity for ET O’Daniel and Germania units.



Fig. 4.5 compares the mean and IQR for the shale volume and porosity between sand members in each unit. The 1U in the ET O'Daniel and Spraberry are almost identical in mean, quartile distribution and most other statistical measures for the shale volumes distribution.

The 5U also shows similarities in most measures, but generally exhibits a lower range of porosities, and a slightly lower mean with respect to the 1U interval.

### Porosity

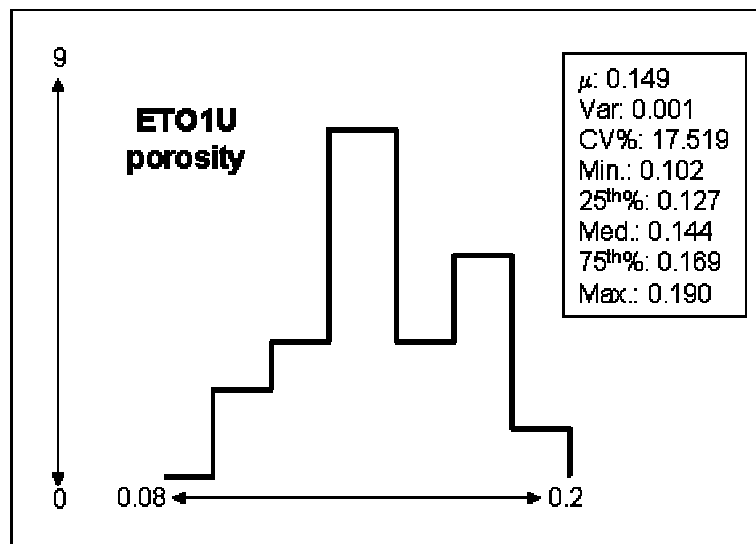


Fig. 4.6 - Statistics of porosity values for ET O'Daniel, 1U sand.

Porosity values are similar within the 1U interval in both units as seen in figs. 4.6 to 4.9, with a slight skew observed in the Germania 1U and 5U interval. Besides the skew, the mean and IQR indicate that the sands (1U and 5U) have similar range of values. The sands are generally of low porosity and permeability, and shale is laminated, however, on the average shale tends to be relatively low as observed in the Shale volumes obtained from well averages in the sand intervals.

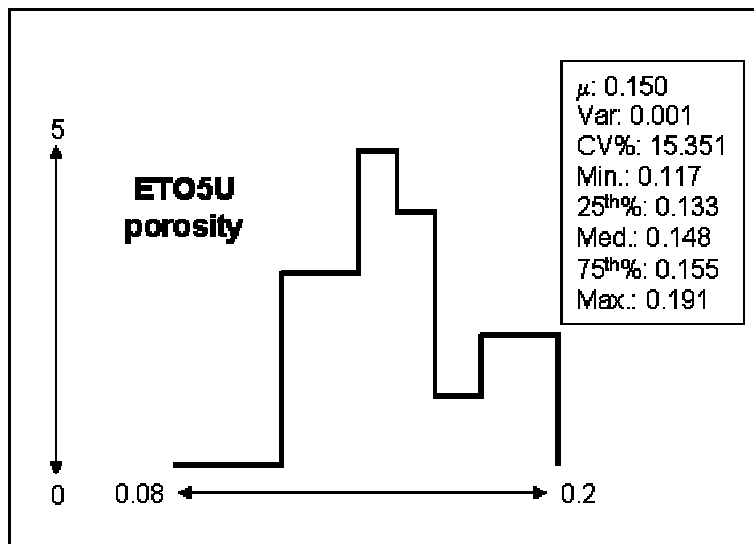


Fig. 4.7 - Statistics of porosity values for ET O'Daniel, 5U sand.

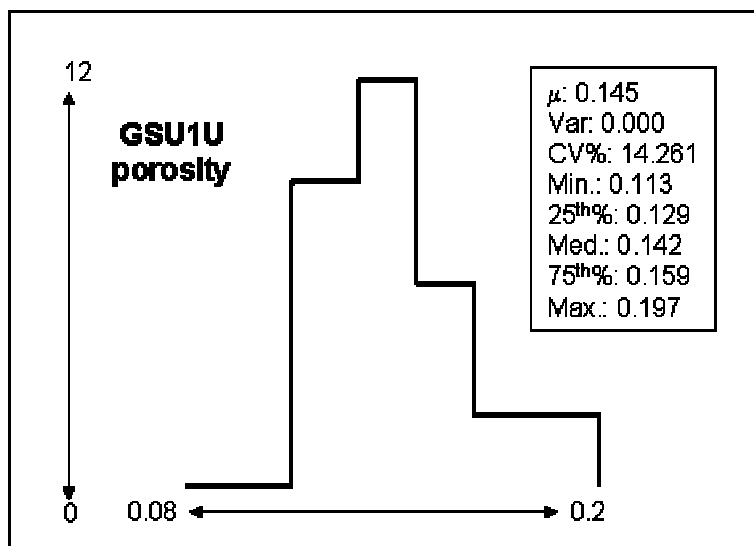


Fig. 4.8 - Statistics of porosity values for Germania, 1U sand.

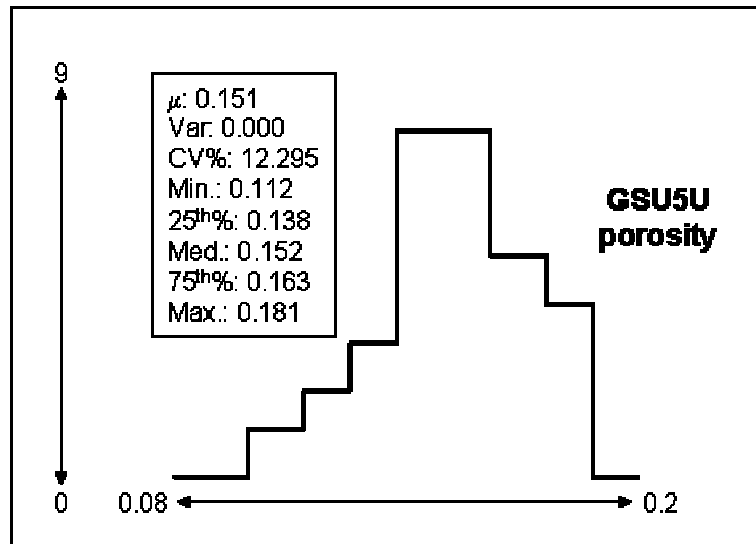


Fig. 4.9 - Statistics of porosity values for Germania, 5U sand.

### Kolmogorov – Smirnov test for porosity and shale volume

This test is based on measuring the maximum vertical separation between two empirical CDF's<sup>36</sup> given as  $d_{\max}$ . This method makes it possible to compare entire distributions rather than any single statistical measure.

For a one sided test at the 5% confidence level, the value of  $1.36(I_1 I_2)^{0.5} (I_1 + I_2)^{0.5}$  must exceed  $I_1 I_2 d_{\max}$  for the two empirical distribution forms to be considered the same.

Sample size for data set 1,  $I_1 = 31$

Sample size for data set 2,  $I_2 = 22$

Critical value not to be exceeded is given by  $I_1 I_2 d_{\max}$ , and the test value is given by  $1.36(I_1 I_2)^{0.5} (I_1 + I_2)^{0.5}$ . From Fig. 4.10, the value of  $d_{\max}$  is given by the maximum vertical distance between the two functions.

Resulting values are 47.06 and 258 respectively, this indicates that the distributions are somewhat different. A limitation<sup>37</sup> of this test is that it is more sensitive close to the

center of the distribution, than at the tail, evidenced by the Fig. 4.10 where  $d_{max}$  occurs about the center.

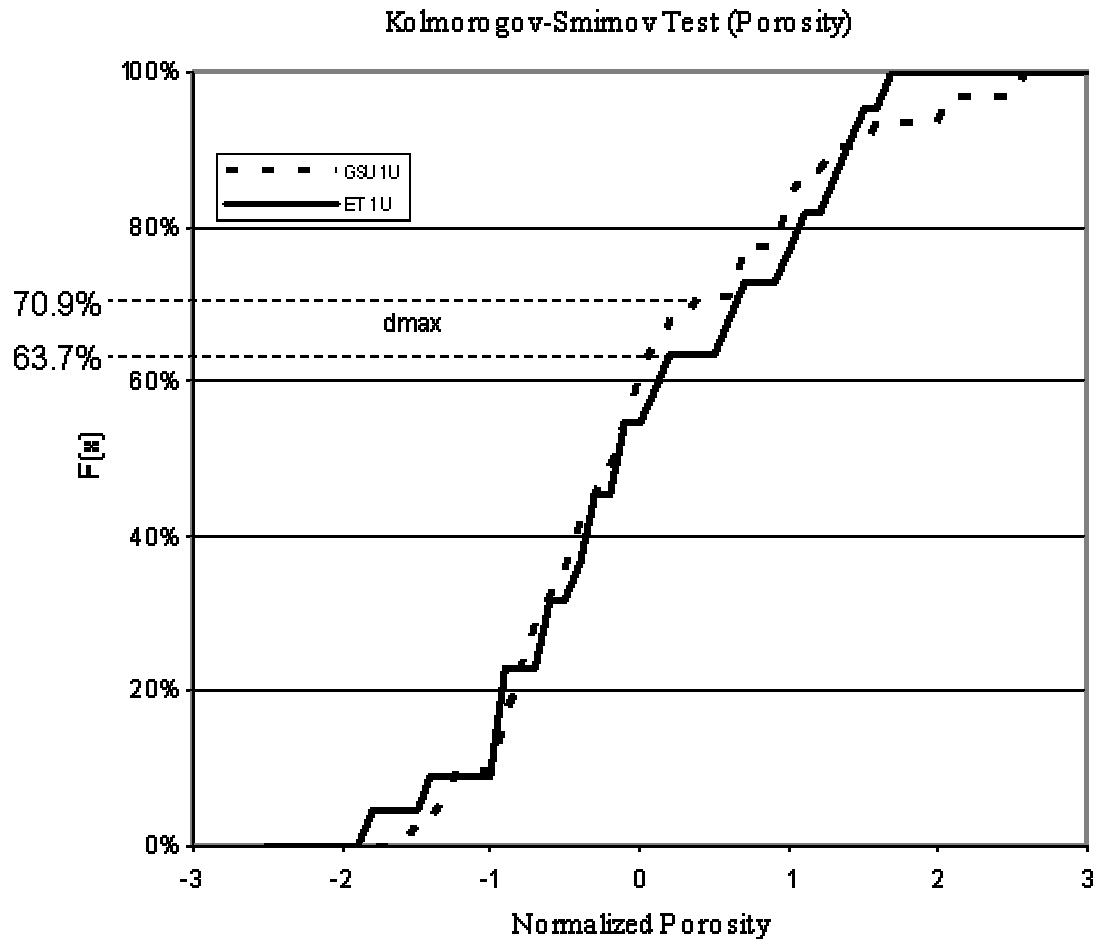


Fig. 4.10 – Kolmogorov - Smirnov test on porosity function, 1U sand.

Results of other comparisons between the units of ET O’Daniel and Germania for porosity and shale volume are summarized in table 4.1 below.

A further limitation in the value of any inference as a result of a comparative analysis of Germania and ET O’Daniel lies in the sample size. The ET O’Daniel dataset is about half the size of the Germania dataset for shale volume, it is therefore a possibility that improvement in correlations will be made as the database is expanded. See appendix B11

for illustration of effect of varying sample sizes on the Kolmogorov – Smirnov test for a normal distribution.

Table 4.1 – Kolmogorov-Smirnov test for porosity and shale volume.

	$I_1$	$I_2$	$d_{max}$	Critical	Test
<b>Porosity 1U</b>	31	22	6.90%	47.06	258.56
<b>Porosity 5U</b>	31	20	10.60%	65.72	241.84
<b>Vshl 1U</b>	50	23	7.10%	81.65	394.05
<b>Vshl 5U</b>	50	21	6.00%	63.00	371.33

### **Litho- stratigraphic section**

Another factor that lends itself to the verification of the ET O’Daniel and Germania units being analogous to one another is the depositional continuity over the two fields.

The 1U and 5U sands as well as the over and underlying intervals are well defined in both fields, and are at approximately the same depth horizons, and most of all, are picked by all the wells analyzed. Similar depositional characteristics are also observed i.e. prominent shale markers and fining/coarsening sand trends.

Figs. 4.11 and 4.12 show gross thickness map of both fields with line of section (A-A’) indicated and the litho-stratigraphic section displaying the 5 sand units in the upper Spraberry.

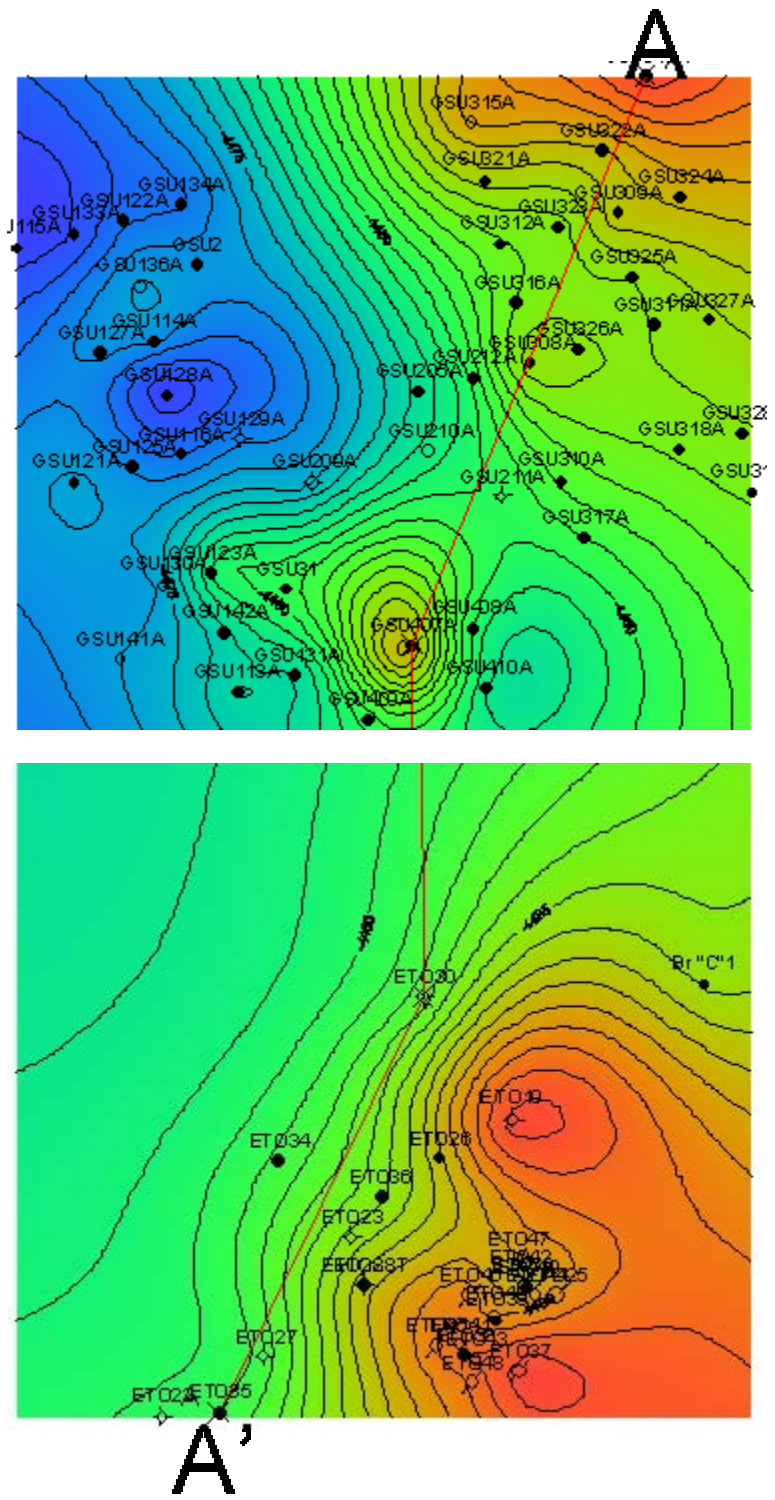


Fig. 4.11 – Gross thickness map of the 1U sand.  
(Section A-A' along the north–south dip wise axis of the Spraberry trend area).

Line of section A-A' shows a section taken in the paleodip direction of the Spraberry. In the previous literature<sup>2,16</sup>, it is suggested that deposition of terrigenous clastic sediments were southward thinning forming elongate fan shaped sand wedges.

Wells GSU#314, GSU#407, ETO#30 and ETO#35 are used for this section and are in sequence from North-East to South-West. Interwell distances are large, but intermediate wells exhibit same sand sequence and as such, wells spanning across both units were chosen to emphasize the lateral continuity of the 1U, 5U and intermediate sand intervals.

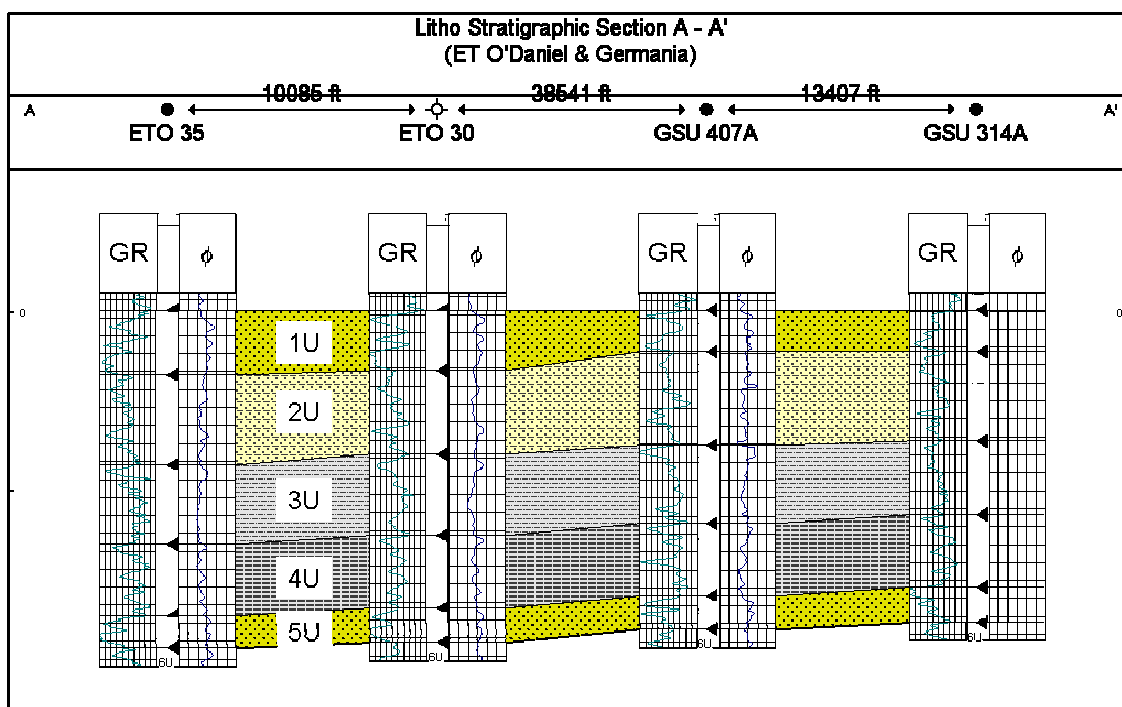


Fig. 4.12 – Lithostratigraphic section A-A' with datum at top of 1U interval.

## CHAPTER V MODEL APPLICATION IN GERMANIA UNIT

### Germania

#### *Picks and interval properties*

The Germania unit shows through the gamma ray logs, the characteristic response observed in the ET O’Daniel unit within the five reservoir units (1U thru 5U). The formation markers were generally distinguishable and continuous over the lateral space between both units. Application of the log based rock model to distinguish reservoir and non-reservoir quality rock through porosity and shale indicators will form the basis of the reservoir description process and the generation of structure and isopach maps that describe this unit.

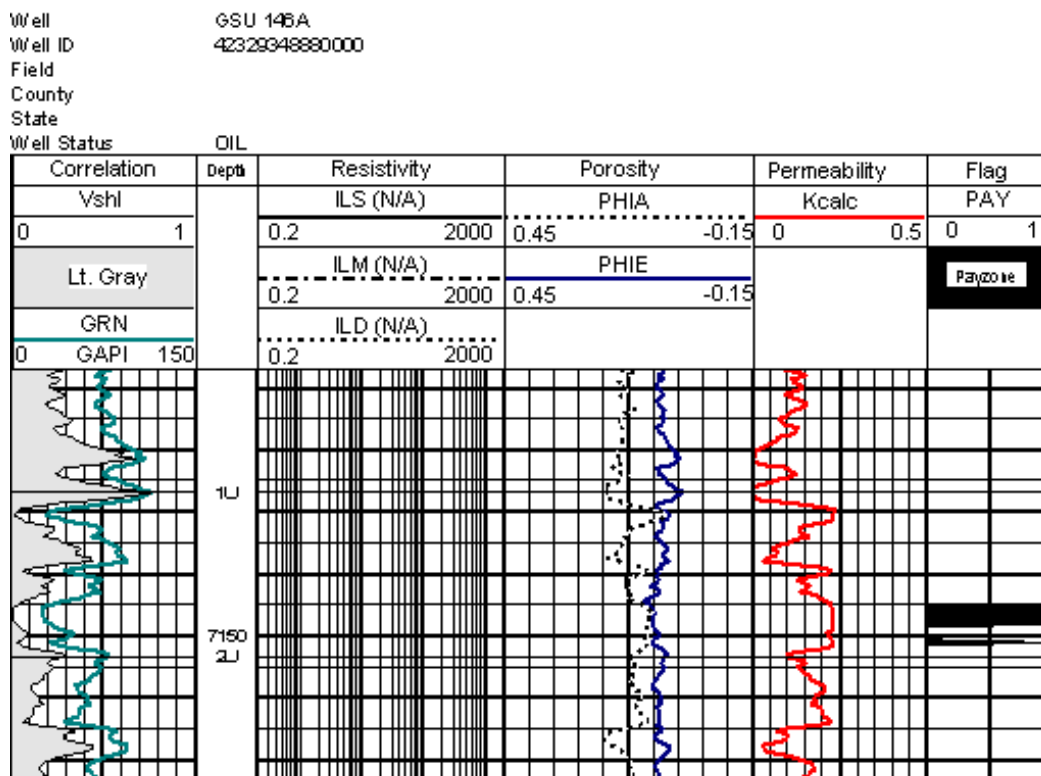


Fig. 5.1 – Payzone prediction based on rock model for GSU146A, 1U sand.



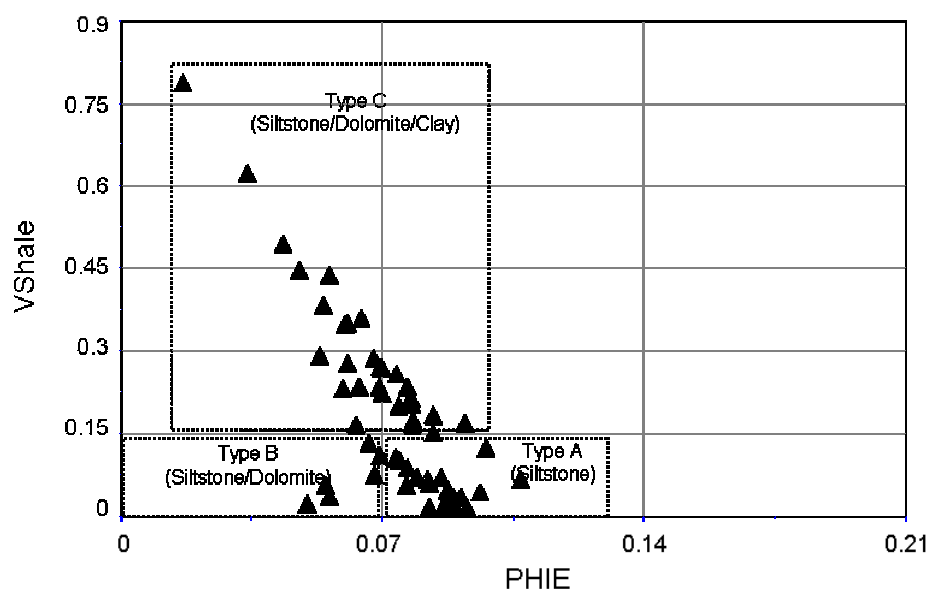


Fig. 5.2 – Estimate of rock types in GSU146A, 1U sand from shale volume - porosity crossplot.

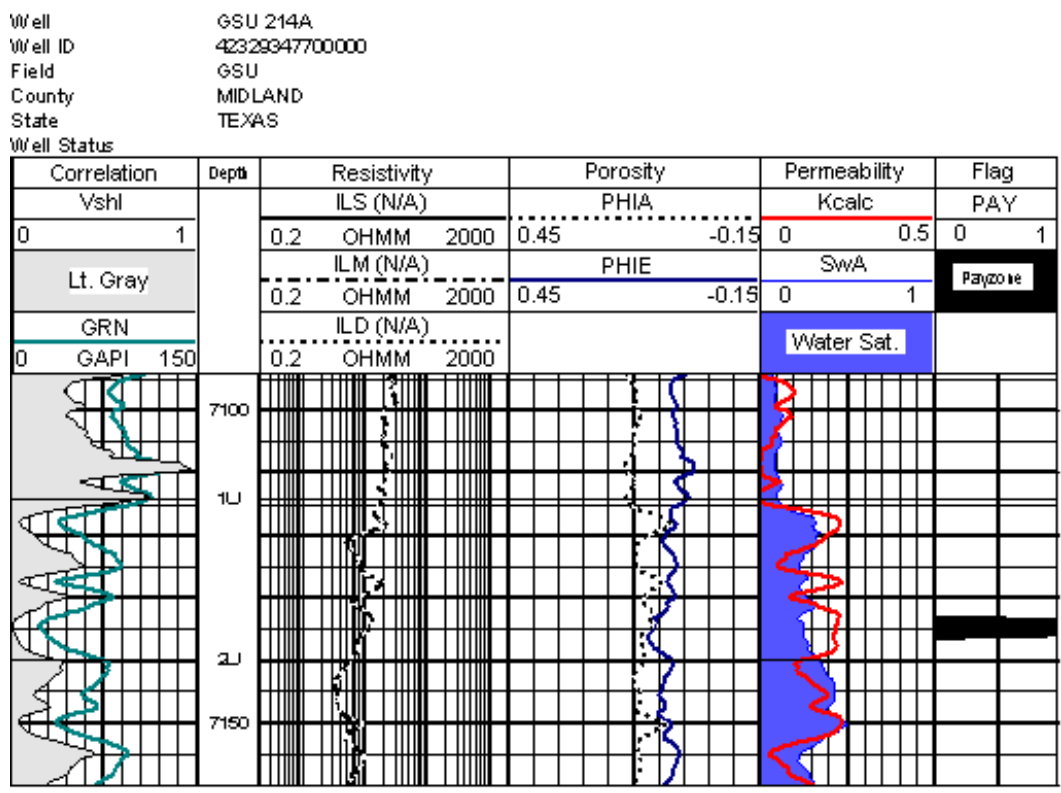


Fig. 5.3 – Payzone prediction based on rock model for GSU 214A, 1U sand.

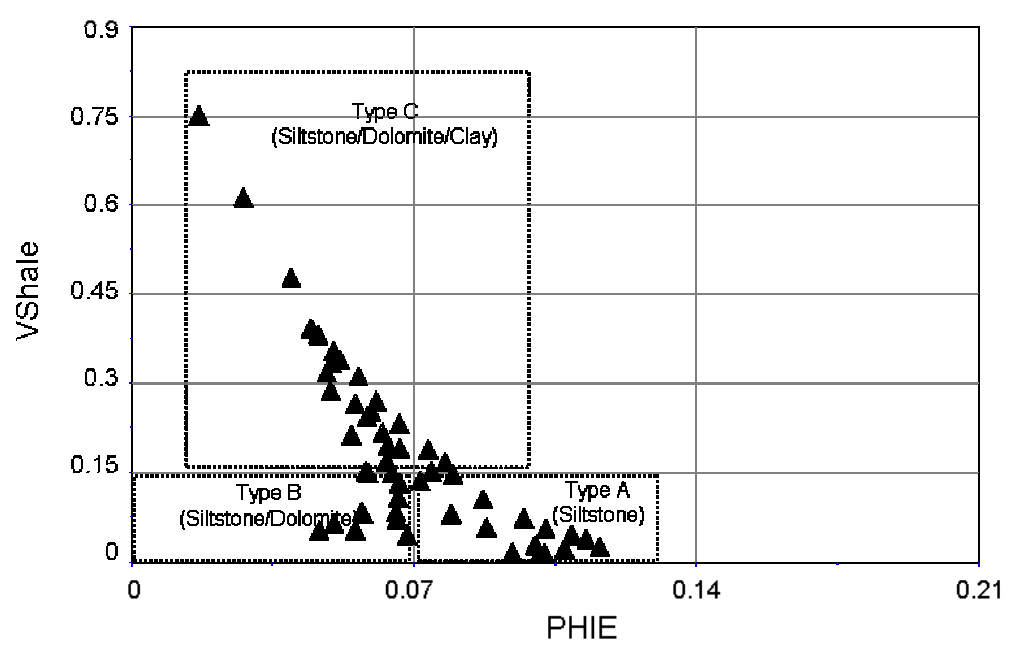


Fig. 5.4 – Vshale crossplot for GSU 214A, 1U sand.

Well GSU 214A  
 Well ID 42329347700000  
 Field GSU  
 County MIDLAND  
 State TEXAS  
 Well Status

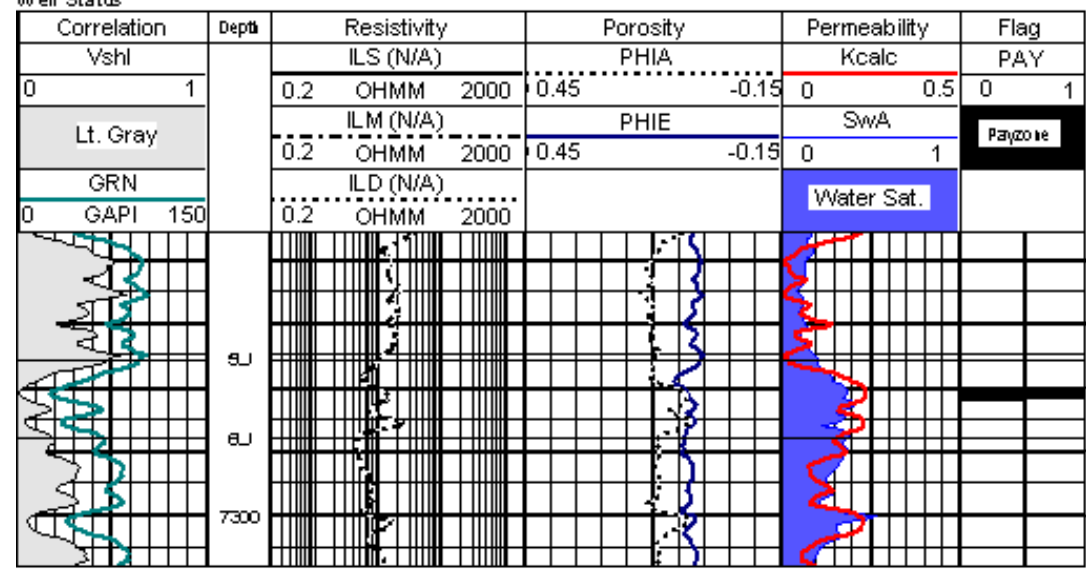


Fig 5.5 – Payzone prediction for GSU214A, 5U sand.

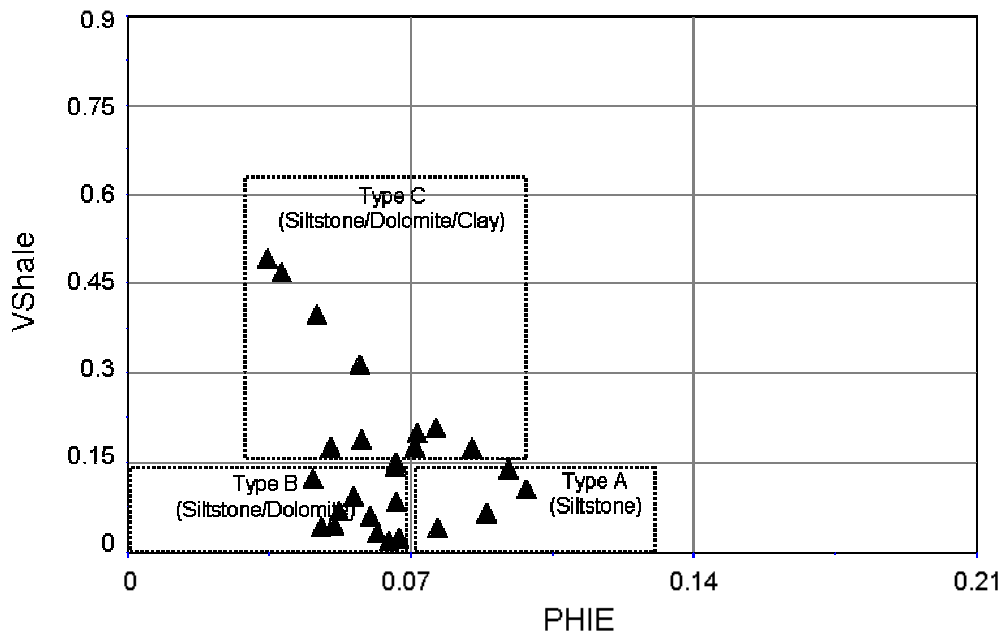


Fig. 5.6 – Vshale crossplot for GSU 214A, 5U sand.

The log based rock model developed from log analysis and petrographic studies in the ET O’Daniel unit, was applied with partial success in the Germania Spraberry unit. From observation within the GSU log playback, the rock model consistently underestimated the pay interval compared with the average ET O’Daniel interval.

Figs. 5.1 to 5.6 provide a visual means of quantifying the net sand with respect to the gross sand thickness. It is evident that the net to gross sand ratio drastically reduces based on the rock – log model estimates in the Germania unit with respect to the ET O’Daniel prediction estimates.

The 1U sand shows a net to gross ratio of about 30% as compared to 50% in the ET O’Daniel unit. A dissimilar trend is also observed, in that the low clay sands are not exclusively rock type A, but are mostly type B – dolomitic siltstone. In the 5U unit, the net to gross ratio observed here is about 20% compared to the 40% observed in the equivalent ET O’Daniel unit.

On the other hand, the more recent neutron porosity logs did yield consistent results with the application of the rock – log model in the Germania Spraberry unit. The logged well pay estimates ranged within the 50% and 40% values for the 1U and 5U units as in ET O’Daniel.

## **Uncertainties**

### ***Porosity***

Porosity derived from neutron logs are susceptible to errors when gas is present near enough to the wellbore. The normalization and conversion process does not eliminate these errors completely, especially due to the lack of unit standardization and well-bore environmental corrections. Hence due to the large number of neutron logs converted to porosity values in comparison to the ‘more reliable’ neutron porosity logs in the database used to perform the study, inferences based on the resulting porosity values are prone to errors. Quantification of the errors is not estimated in this study.

### ***Permeability***

The flow capacity of the rock may be dependent on many factors such as depositional porosity, pore throat size, irreducible water saturation, clay content, and in the case of diagenetically modified rock, alteration by mineralization or dissolution. Investigating each of these factors on permeability is often hampered by the difficulty in acquiring quality data, hence permeability is often reduced to log data, pressure transient tests, and conventional core data analysis. There are no direct measurements of producibility from logs.

Shale volume and porosity were the only variables used to investigate permeability and, therefore, limited the reliability of the permeability predictions.

### *Water saturation*

An inverse approach was used in determining saturations, and as is often the case, there is non-uniqueness in the defining parameters. In this case, the Archie parameters have pre-established tolerances as shown in chapter II, but nevertheless different combination of Archie parameters within this tolerance may still yield consistent matches from well to well.

### *Net pay*

Due to the limitations in the porosity predictions earlier mentioned, the rock log model which is based on porosity and shale volume will equally be subject to errors. Therefore, even though tried and tested, the rock log model may fail to adequately predict the location and thickness of productive sub units.

## **CHAPTER VI CONCLUSIONS**

Electrofacies patterns within the ET O'Daniel are easily recognizable in the Germania Spraberry unit and this correlation is evident across the units of the upper Spraberry. The general reservoir structure is consistent across both unit and thus becomes the essence of the Germania unit characterization.

Studies in the analog unit - ET O'Daniel, provided valuable input towards the characterization effort of the Germania for a variety of reasons, the most fundamental being the log based rock model used for rock type discrimination.

The simplicity of the model makes it easy to use as a criteria for determining pay quality within the upper Spraberry, once the correlatable units are identified. Secondly, the core analysis performed by Reservoirs Incorporated enabled the development of porosity and permeability relationships that may be applied in the GSU, the result of which are porosity and permeability maps to guide further development and simulation studies.

### **Conclusions**

1. The Isopach maps indicate channel deposits and interdistributary flat features that are consistent with the depositional evaluation proposed by Handford et al. The facies indicate detrital clasts of both depositional episodes as evident in the lithology charts in chapter II which indicate that the 1U and 5U intervals are made up of terrigenous sandstones as well as dolomitic carbonate facies.
2. Particularly evident in the ET O'Daniel Isopach maps are the north - south thinning of the sandstone intervals, this is indicative of an energy source north of the Spraberry.

3. The Germania unit isopach (net thickness) is conservative in its estimation of net pay thickness, this is can be attributed to the limitations of the log based rock model in predicting payzones based on normalized cased hole neutron logs. Neutron logs alone do not lend themselves to corrections (environmental etc). Porosity correction techniques require a multi-dimensional array of porosity data i.e. density and neutron or sonic. Ideally, the density and neutron porosity logging devices should be run together so as to allow for necessary compensatory corrections in log data.
4. Optimal non-parametric regression techniques did not clearly improve the estimations of permeability based on shale volume and porosity. The method in itself is efficient, but alternative or more appropriate relationships specific to the Spraberry units need to be investigated. Additional studies on pore throat distribution based on core analysis may offer opportunities to improve the predictions.
5. Techniques for determining water saturation in the spraberry or shaly sands do not recommend using the Archie's equation. The Archie model is simplistic in its approach and is only considered a means of 'estimating' water saturation for this study.
6. Acquisition of core data within the Germania unit is not an option. To enable further evaluation of the GSU, core derived parameters must be available to guide simulation studies and inform fracture characterization to yield an integrated reservoir model.

## REFERENCES

1. Schechter, D.S., McDonald, P., Sheffield, T., and Baker, R.: "Reservoir Characterization and CO<sub>2</sub> pilot Design in the Naturally Fractured Spraberry Trend" paper SPE 35469 presented at the 1996 Permian Basin Oil and Gas Conference, Midland, 27-29 March.
2. Handford, C.R.: "Sedimentology and Genetic Stratigraphy of Dean and Spraberry Formations (Permian), Midland Basin, Texas" *AAPG Bulletin* (1981), **65**, no. 9, 1602.
3. Barfield, E.C., Jordan, J.K., and Moore, W.D.: "An Analysis of Large-Scale Flooding in the Fractured Spraberry Trend Area Reservoir" *JPT* (1959), **11**, 15.
4. Schechter, D.S.: "Advanced Reservoir Characterization and Evaluation of CO<sub>2</sub> Gravity Drainage in the Naturally Fractured Spraberry Trend Area" 2nd Annual Technical Progress Report, US DOE Contract No. DE-FC22-95BC14942, Socorro, New Mexico (August 1997).
5. Schechter, D.S.: "Advanced Reservoir Characterization and Evaluation of CO<sub>2</sub> Gravity Drainage in the Naturally Fractured Spraberry Trend Area" 1st Annual Technical Progress Report, US DOE Contract No. DE-FC22-95BC14942, Socorro, New Mexico (August 1996).
6. McDonald, P., Lorenz, J.C., Sizemore C., Schechter, D.S., and Sheffield, T.: "Fracture Characterization Based on Oriented Core from the Spraberry Trend Reservoir: A Case Study" paper SPE 38664 presented at the 1997 SPE Annual Technical Conference and Exhibition, San Antonio, 5-8 October.



7. Reservoirs Inc.: “Geological and Petrophysical Analysis of the Upper Spraberry Formation, Midland County, Texas” Report prepared for Parker & Parsley Development Co., Midland, Texas (1997), **1 & 2**.
8. Schechter, D.S., and Banik; A.S.: “Characterization of the Naturally Fractured Spraberry Trend Shaly Sands Based on Core and Log Data” paper SPE 35224 presented at the 1996 Permian Basin Oil and Gas Conference, Midland, 27-29 March.
9. Schechter, D.S., and Banik; A.S.: “Integration of Petrophysical and Geologic Data with Open-Hole Logs for Identification of the Naturally Fractured Spraberry Payzones” paper SPE 38913 presented at the 1997 SPE Annual Technical Conference and Exhibition, San Antonio, 5-8 October.
10. Mardock, E.S., and Myers, J.P.: “Radioactivity Logs Define Lithology in the Spraberry Formation” *Oil and Gas Journal* (Nov. 1951), 90.
11. Lyttle, W.J., and Rieke, R.R.: “Well Logging in the Spraberry” *Oil and Gas Journal* (Dec. 51), 92
12. Schechter, D.S., and Putra, E.: “CO<sub>2</sub> Pilot Design and Water Injection Performance in the Naturally Fractured Spraberry Trend Area, West Texas” paper SPE 71605 presented at the 2001 SPE Annual Technical Conference and Exhibition, New Orleans, Sept. 30-Oct. 3.
13. Putra, E.: “Reservoir Simulation of Waterflood Pilot in Naturally Fractured Spraberry Trend” paper SPE 54336 presented at the 1999 Asia Pacific Oil and Gas Conference and Exhibition, Jakarta, 20-22 April.
14. Schechter, D.S., and Buoyun, Guo .: “An Integrated Investigation for Design of a CO<sub>2</sub> Pilot in the Naturally Fractured Spraberry Trend Area, West Texas” paper

- SPE 39881 presented at the 1998 International Petroleum Conference and Exhibition, Villahermosa, 3-5 March.
15. Wilkinson, W.M.: "Fracturing in Spraberry Reservoir, West Texas" *AAPG Bulletin*, (Feb 1953), **37**, no. 2, 253.
  16. Schmitt, G.T.: "Genesis and Depositional History of Spraberry Formation, Midland Texas" *AAPG Bulletin* (Sept. 1954), **38**, no. 9, 1957
  17. Tyler, N., and Gholston, J.C.: "Heterogeneous Deep Sea Fan Reservoirs, Shackelford and Preston Waterflood Units, Spraberry Trend West Texas" University of Texas at Austin Bureau of Economic Geology, *Report of Investigations* (1998), **171**, 38
  18. Montgomery, S.L., Schechter, D.S., and Lorenz, J.: "Advanced Reservoir Characterization to Evaluate CO<sub>2</sub> flooding, Spraberry Trend, Midland Basin, Texas" *AAPG Bulletin* (2000), **84**, no. 9, 1247.
  19. Asquith, G.B.: *Log Analysis of Shaly Sandstone Reservoirs: A Practical Guide*, AAPG (1992), Tulsa Oklahoma
  20. Greder, H.N., Mus, E.A., Veillerette, A.M., Pellerin, and F.M.: "Derivation of a Core Permeability Log and Extrapolation to Uncored Intervals" Proc. 36th Society of Professional Well Log Analyst Symposium (1995), 12p.
  21. Balan, B., Mohaghegh, S., Ameri, S.: "State-of-the-Art in Permeability Determination from Well Log Data: Part I- A Comparative Study Model Development" paper SPE 30978 presented at the 1995 Eastern Regional Conference and Exhibition, Morgantown, 17-21 September.

22. Allen, J.R.: "Prediction of Permeability from Logs by Multiple Regression" Trans. 36th SPWLA Symposium (1995)
23. Van Den Bosch, R., Fulop, A., and, Pistre, V.: "Permeability Prediction from Well Logs – A Case Study in German Rotliegend Sandstones" Trans. 36th SPWLA Symposium (1995), 12p.
24. Hook, J.R., Nieto, J.A., Kalkomey, C.T., and Ellis, D.: "Facies and Permeability Prediction from Wireline Logs and Core – A North Sea Case Study" Trans. 35th SPWLA Symposium (1994), AAA1.
25. Saxena, V.: "Hydrocarbon Evaluation through Modulus Decomposition of Sonic Velocities in Shaly Sands" Trans. 37th SPWLA Symposium (1996), 14p.
26. Breiman, L., and Friedman, J.H.: "Estimating Optimal Transformations for Multiple Regression and Correlations" *Journal of the American Statistical Association* (1985), **80**, 580.
27. Guoping Xue, Datta-Gupta, A., Valko, P., and Blasingame, T.: "Optimal Transformations for Multiple Regression: Application to Permeability Estimation from Well Logs" paper SPE 35412 presented at the 1996 Improved Oil Recovery Symposium, Tulsa, 21 April.
28. Shier, D.E., Course Notes for Well Log Normalization Work Shop, Published privately by Energy Data Services, Golden, Colorado (1991).
29. Crain, E.R., Garrido, M.: "Qualitative Analysis of Older Rocks for Porosity and Permeability – Lake Maracaibo, Western Flank Reservoirs, Venezuela" Petroleos de Venezuela (PDVSA)

30. Hunt, E., Aly, A., and Pursell, D.: "Fundamentals of Log Analysis, Part 6, Determining Basic Log Analysis Parameters - a, m, n, and  $R_w$ " *World Oil*, (Oct. 1996), **217**, no.12, 59
31. Neinast, G. S., and Knox, C. C.: "Normalization of Well Log Data" Trans. 14th SPWLA Symposium (1973), 11.
32. Isaaks, E.H., and Srivastava, R.M.: *An Introduction to Applied Geostatistics*, Oxford University Press (1989).
33. Hunt, E., and Pursell, D.: "Fundamentals of Log Analysis, Part 7, Determining Shaliness from Logs" *World Oil*, (1996), **218**, no.3, 55
34. Reservoirs Inc.: "NMR Core Analysis: Upper Spraberry Formation, ET O'Daniel Lease Area, Midland County, Texas" Report prepared for Parker and Parsley Development Co., Midland, Texas (1997)
35. Rasmus J.C.: "Variable Cementation Exponent, m, for Fractured Carbonates" *The Log Analyst* (1983), 41.
36. Jensen J.L., Lake L.W., Corbett P.W., and Goggin D.J.: *Statistics for Petroleum Engineers and Geoscientists*, Prentice Hall (1997)
37. NIST/SEMATECH *e-Handbook of Statistical Methods*, <http://www.itl.nist.gov/div898/handbook/>
38. Gibson, G.: "The Relation of Fractures to the Accumulation of Oil in the Spraberry Formation" *Proc. 3rd Oil Recovery Conference, West Texas Petroleum Research Committee, Bulletin 15* (1951), 16.
39. Ogden, V., and Locke, J.: "Core Data Discussions" *ibid.*, *Bulletin 15*, 57.

40. Marshall, J.W.: "Spraberry Reservoirs of West Texas" *Geological Notes* (1952), 2189.
41. Lang, W.H., Jr.: "Porosity Log Calibrations" *The Log Analyst* (1980), **21**, no. 2, 14.
42. Shier, D.E.: "A Comparison of Log Response between Logging Companies and Different Vintages of Tools" *The Log Analyst* (1997), **38**, no. 3, 47.
43. Shier, D.E., and Sponable, D.M.: "Correcting Drift in GNT Neutron Log Data from West Texas" *The Log Analyst* (1997), **38**, no. 3, 16.
44. Hardle, W.: *Applied Non-parametric Regression*, Cambridge University Press, Cambridge (1990)
45. Reservoir Inc.: "Geological and Petrophysical Analysis of the Upper Spraberry Formation in Midland County, Texas" Report prepared for Parker and Parsley Development Co., Midland, Texas (1996)
46. Jensen, J.L., and Lake, L.W.: "Optimization of Regression Based Porosity Permeability Predictions" presented at the 1985 10th Canadian Well Logging Society, Calgary
47. Boardman, D.W. et al.: "Use of Effective Properties for Characterization of a Naturally Fractured Reservoir in East Venezuela" paper SPE 53881 presented at the 1999 Latin American and Caribbean Petroleum Engineering Conference, Caracas, 21-23 April.
48. Guevara, E.H.: "Geologic Characterization of Permian Submarine Fan Reservoirs of the Driver Waterflood Unit, Spraberry Trend, Midland Basin, Texas"

- University of Texas at Austin Bureau of Economic Geology, *Report of Investigations* (1988), no. 172, 44p.
49. Asquith, G.B.: "The Importance of Determining Pore Type from Petrophysical Logs in the Evaluation of a Permian Wolfcamp Reentry, Northern Midland Basin" *The Log Analyst* (1997), **38**, no. 3, 37.
  50. Ingerman V.G.: "Statistical Integration of Log Data for Lithology Determination and Formation Evaluation" *The Log Analyst* (1995), **36**, 38.
  51. Katahara, K.W.: "Gamma Ray Log Response in Shaly Sands" *The Log Analyst* (1995), **36**, 50.
  52. Gamboa, P., Reis, J., and Morris, S.: "Development of a Log Based Petrophysical Model for a Complex Dolomite Reservoir" *The Log Analyst* (1994), **35**, 47.
  53. Whatler, P.: "Core Data Quality Issues" *The Log Analyst* (1994), **35**, 43.
  54. Nelson, P.H.: "Porosity - Permeability Relationships in Sedimentary Rocks" *The Log Analyst* (1994), **35**, 38.

## **APPENDIX A**

### **BACKGROUND GEOLOGY AND STRATIGRAPHY**

#### **Geology/Geophysical Background**

The Spraberry trend area spans an area about 150 miles in length and 50 miles at the broadest width, and has been found to be productive in an area approximately 500,000 acres<sup>16</sup>. The trend is estimated to originally contain over 8.5 billion barrels of oil of which only 8 – 12% have been recovered thus far. Structural contours show that the Spraberry trend lies updip and to the east of current day Basinal axis, which exists adjacent to the central Basin platform (Figure A1).

#### **Regional Stratigraphy and Lithofacies**

The Midland Basin is known to be composed of largely of shallow – marine shelf to shelf margin carbonates, as well as deep Basin deposits<sup>2</sup>. Early opinions were that the Dean and Spraberry formations were wolfcampian in age, Silver and Todd<sup>2</sup> reported based on biostratigraphic and physical stratigraphic evidence that the formations are Leonardian in age.

Stratigraphic sections analyzed by Jeary<sup>2</sup> suggest that the Spraberry formation Leonardian in age and is coeval with the upper and middle Clearfork and Glorieta formations (Figures A2 and A3), these correlations become less obvious in other areas of the Basin due to discontinuity of clastic strata across shelf margins and well control reasons.

The Spraberry formation is approximately 1000ft thick and is generally composed of 852ft of black shale and silty shale, 131ft of siltstones and 5ft of thin bedded limestones or dolomites. This formation belongs to the lower Leonard and rests conformably on the Wolfcamp. The black fissile shales and thin dolomite beds of the Clearfork group which directly overlies the Spraberry are fractured similar to the Spraberry rocks and with the same lithologic appearance.

The mass of the Spraberry can be separated into 3 distinct and correlative units, which are classified as the upper, middle and lower Spraberry with each unit of approximately the same thickness. The texture and mineralogical character of the major constituents can be described based on rock types as follows:

Siltstones ~ Major percentage of grains fall within the silt size range ( $< 1/16$  mm), with about 60% between the grade limits of 0.03mm – 0.06mm. Grains range from angular

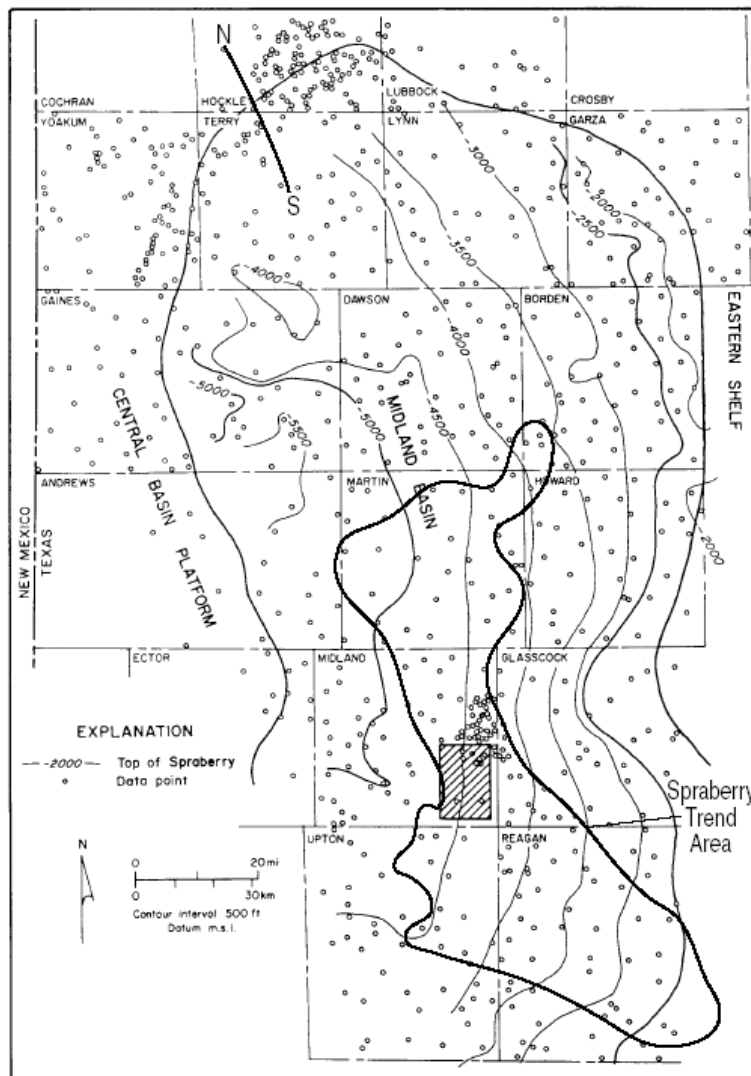


Fig. A1 - Structure contour data, top of Spraberry sandstone, Midland Basin, west Texas<sup>18</sup>.



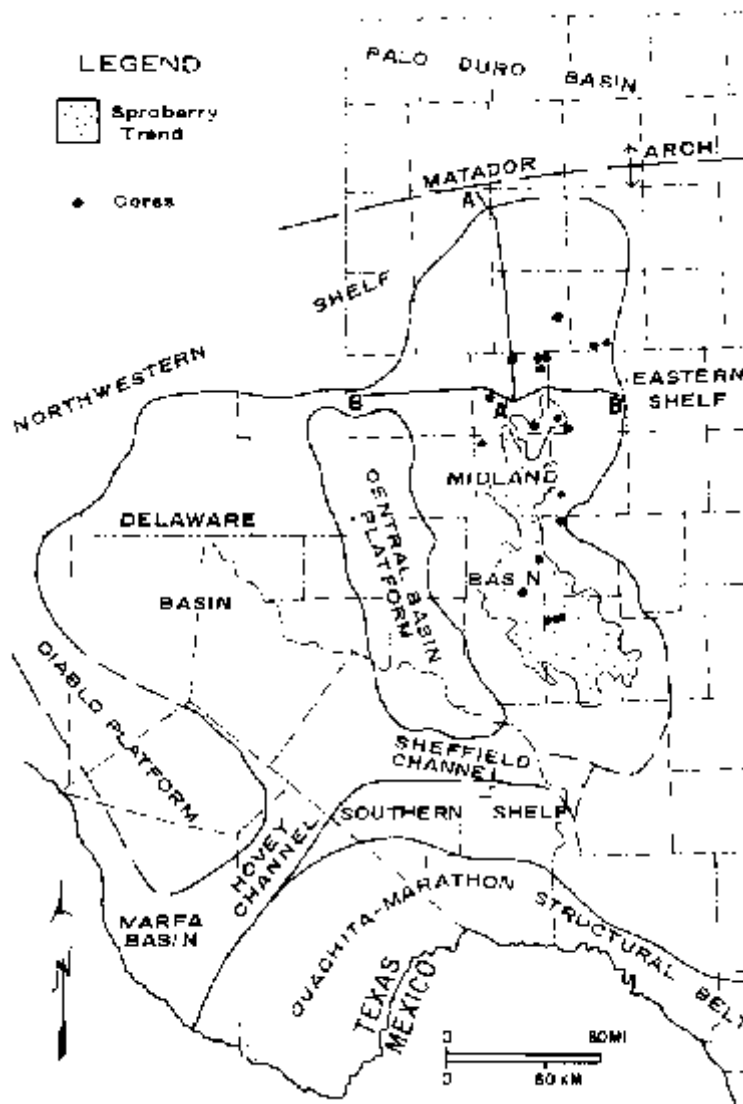


Fig. A2 - Regional geologic setting of Permian Basin, west Texas<sup>2</sup>.

to very angular and the sorting is from fair to poor. Primarily, the cementing agent is dolomite with some silica.

Dolomites ~ Vary in texture from fine to crystalline, the fine crystals being primary.

Shales ~ Several types of shales have been encountered, massive blocky as well as the commonly found fissile brittle type. Most of the shales have been classified as

carbonaceous, but in all petrographic slides examined, the shales were found to be silty and ferruginous.

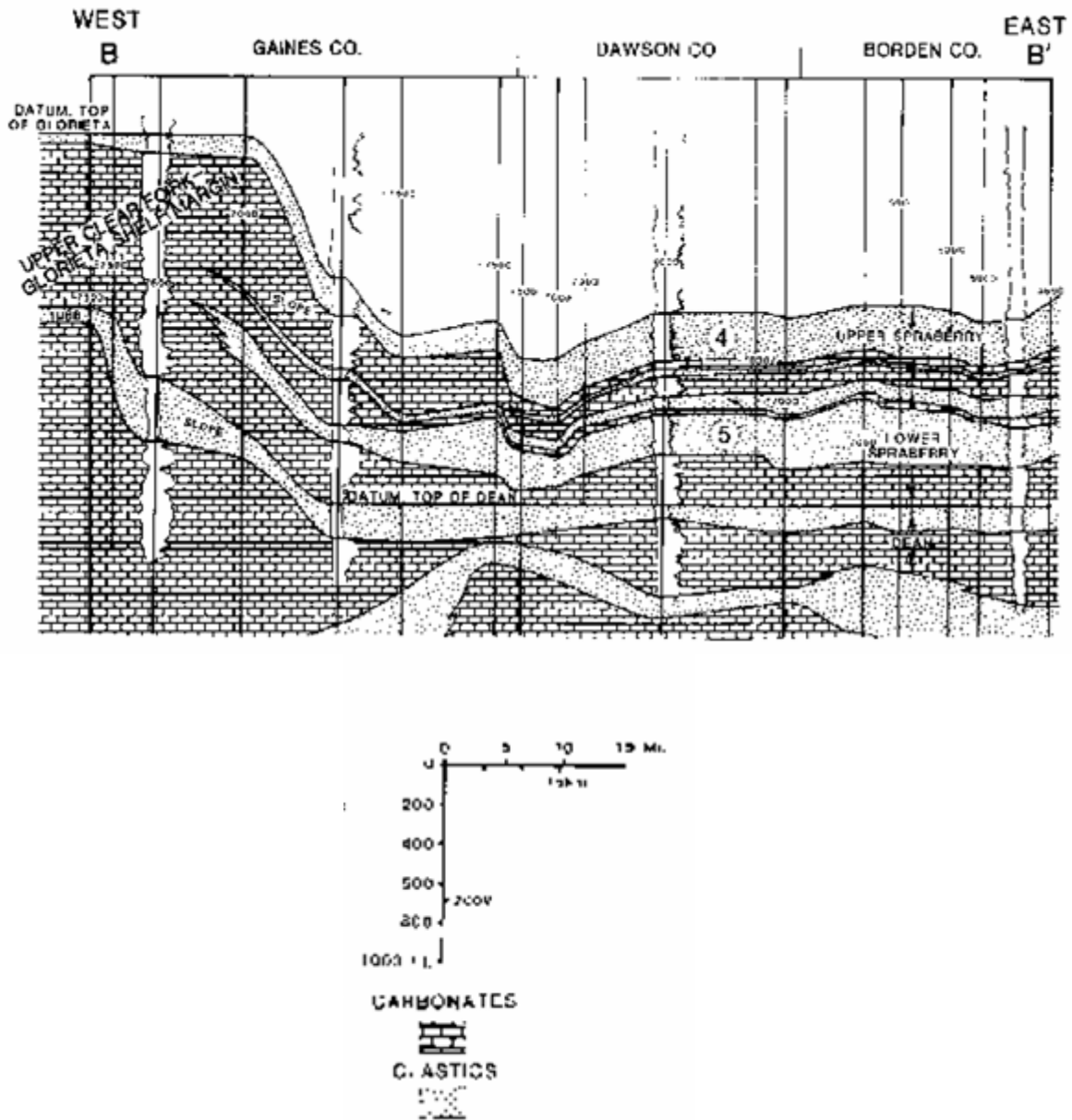


Fig. A3 - West – east stratigraphic cross section BB'<sup>2</sup>.

(Note shelf-to-Basin correlations and informally identified stratigraphic units 4 and 5. See Fig. A2 for location).

Characteristics of the lithofacies are found to be areally and vertically consistent as observed from all the wells examined. Distinctions can be made from electric logs between the upper, middle, and lower Spraberry, however there is no easily apparent characteristic that differentiates the clastic content in the three units from one another, when observed by petrographic microscope. This provides a useful means of recognizing three sandstone-siltstone lithofacies based on bedding characteristics:

- Massive to Parallel and cross laminated sandstone and siltstone.
- Laminated Sandstone and siltstone
- Bioturbated sandstone and siltstone

Gamma-Ray logs can often distinguish lithofacies. Laminated and Bioturbated siltstones having a greater shale content than parallel and cross laminated sandstones and siltstones respond with a more radioactive curve.

A Lithofacies map (Fig. A4) of the four County area (Upton, Reagan, Midland and Glasscock) substantiates the geological features at the close of the Wolfcamp time. The northeast of the Spraberry trend non clastics are dominant with a gradual facies change toward the productive area, where approximately 87% of the Spraberry is shale. West of the producing area a rather abrupt shale to limestone facies change occurs, with several wells on the west side of the present day structural highs containing 85% of non-clastics. The interpretation being that during the time of Spraberry deposition, the west side of the Midland Basin was elevated sufficiently to provide an environment of warm shallow waters, in which carbonates were precipitated and deposited. Superimposed on the lithofacies map are isopach contours representing the thickness of Spraberry type rocks after total deposition and after accounting for all structural movement.

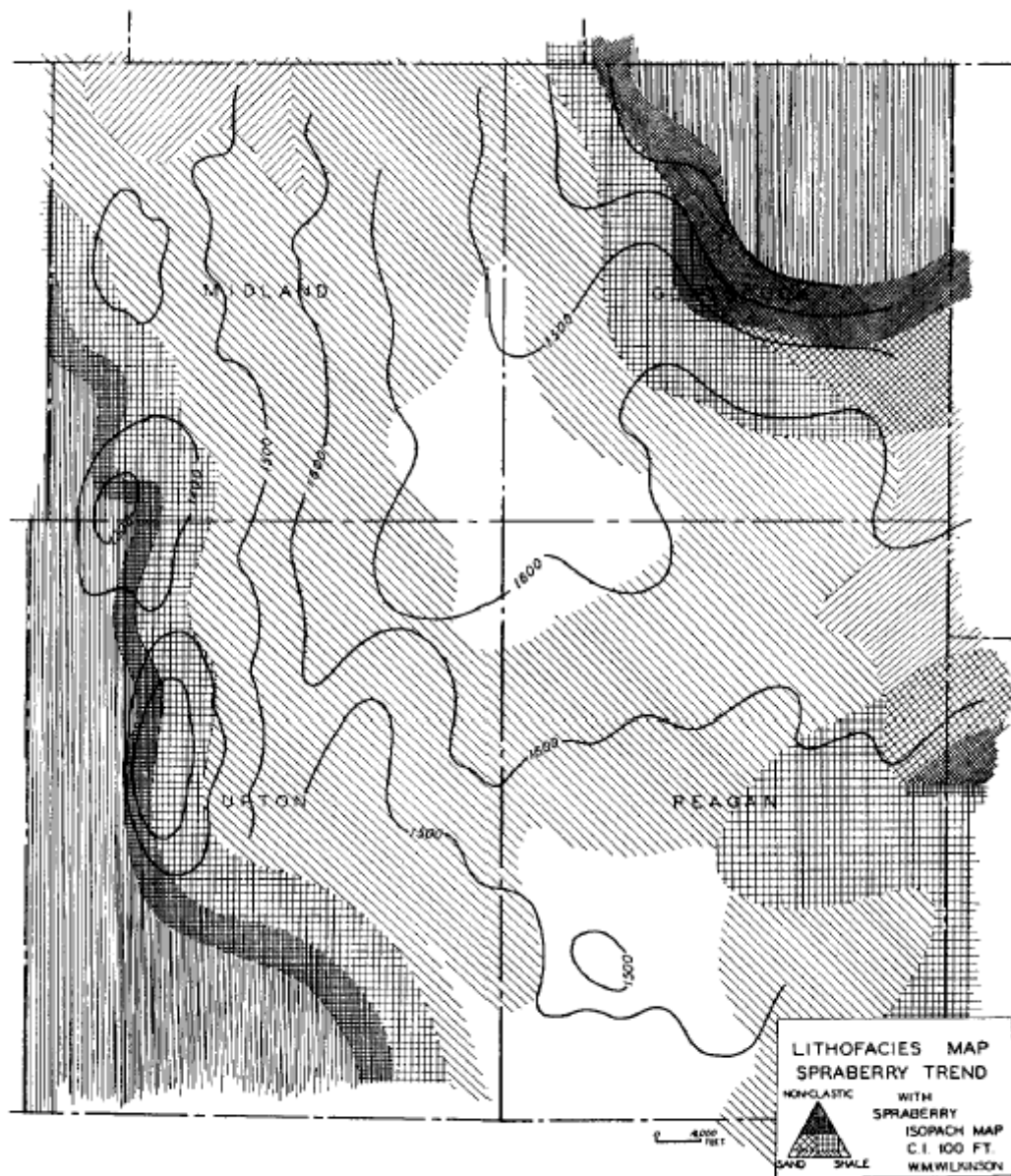


Fig. A4 - Lithofacies map, four County area with Spraberry isopach contours<sup>15</sup>.

### Depositional Model

The Spraberry formation was deposited by debris flow, turbidity currents, saline density currents and suspension settling. Some sediments were later altered by slumping, soft sediment faulting, and fluidization. Deep Basin carbonate members were largely deposited by debris flow, turbidity, saline and density currents, while deposition of terrigenous clastics was dominated by turbidity, saline and density currents, and

suspension settling. Thus clastic and carbonate members shared the same deep-marine setting and most depositional processes. However, the exclusive occurrence of saline density-current deposits within the terrigenous clastic facies indicate that large frequently tapped reservoirs of dense saline waters were stored in shelf lagoons or salt pans near the shelf margin, but only during times of clastic deposition on the shelf.

The fundamental part of any Spraberry model (Figs. A5 – A7) must recognize major alternating periods of carbonate and clastic deposition, incorporate the principal attributes of the carbonate and clastic patterns, and show how styles interacted to form the observed stratigraphic framework<sup>2</sup>.

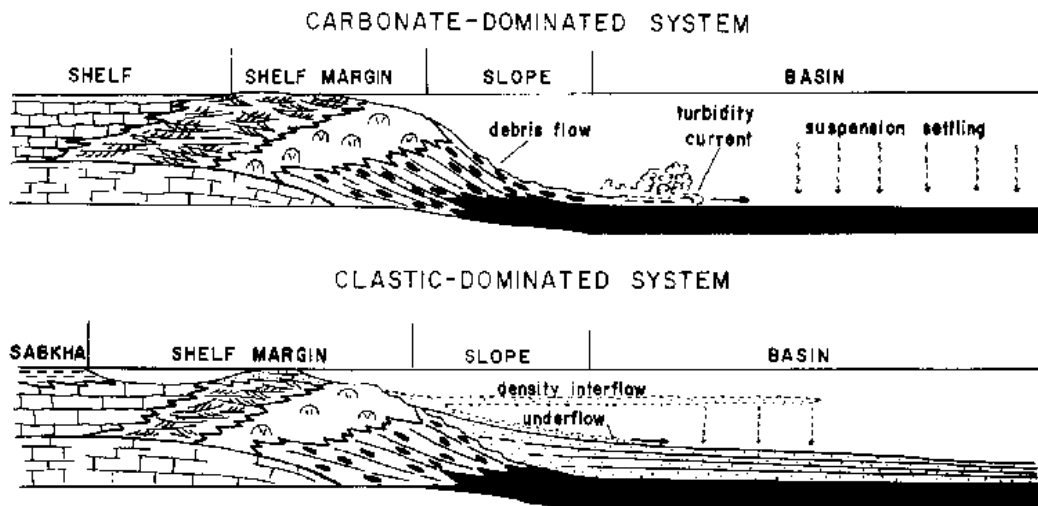


Fig. A5 – Facies model of clastic and carbonate dominated shelf margin systems<sup>2</sup>.

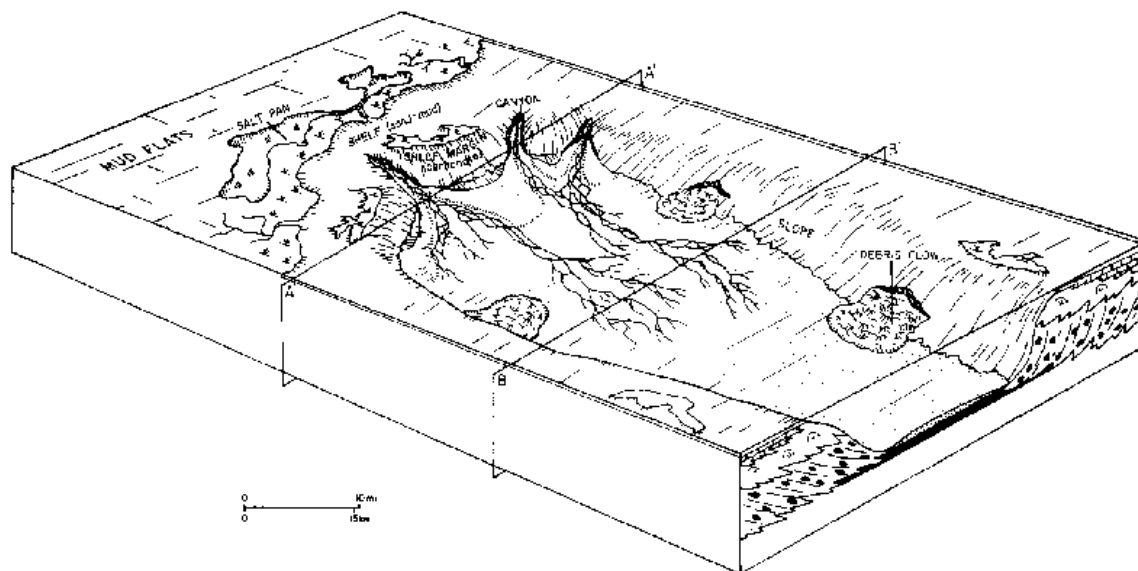


Fig. A6 – Distribution of environments, geometry of deposits, and channel patterns<sup>2</sup>.

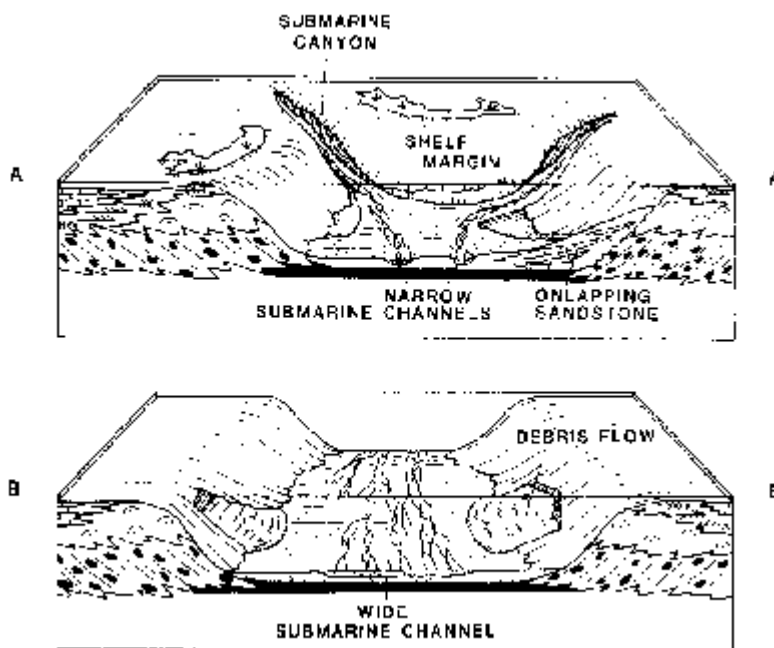


Fig. A7 – Sections of onlapping clastics and downdip widening of channels<sup>2</sup>.

(Sections AA' and BB' from fig. A6)

During carbonate depositional episodes (Fig. A5) which characterized the northern shelf margin in early and late Clear Fork time, calcareous organisms flourished. A massive carbonate shelf margin (1,700 – 2,000 ft) above the floor of the adjacent midland Basin, prograded Basinward over resedimented carbonate debris forming the slope. Slumps debris flow and turbidity currents were the principal mechanisms by which carbonate sediments were moved downslope into the Basin.

During Tubb and Glorieta times, large influx of silt and mud caused mud rich sabkhas and salt pan environments to prograde rapidly across the southern Palo Duro Basin towards the shelf margin of the Midland Basin, giving rise to clastic depositional episodes (Fig. A5). Sub tidal to inter tidal sand sheets accumulated at the shelf margin, from which silt and sand were periodically carried into the Basin by saline density currents that drained hypersaline shelf lagoons and salt pans.

Deposition of terrigenous-clastics sediments formed southward thinning, elongate fan shaped wedges (Fig. A6). Sandstone and siltstone were deposited principally from density underflow and interflow currents. Deposition from bottom hugging currents formed elongate patterns which branch and rejoin in updip regions and bifurcate in downdip regions.

### ***Clastic Patterns***

The total sand and silt found in the upper Spraberry decreases from north to south. During upper Spraberry time, areas in the northeastern part of the Midland Basin subsided more rapidly and received a thicker sequence of sand and silt. Around the edges of the Basin a gradual decrease is noted in the total net thickness of the sand and silt in the direction of the shelf areas. The rate of decrease is more rapid in the northern part of the Basin where there is thicker development of the coarse clastics (Fig. A8). Within the four County area (Midland, Glasscock, Upton and Reagan), the thickness is nearly constant.

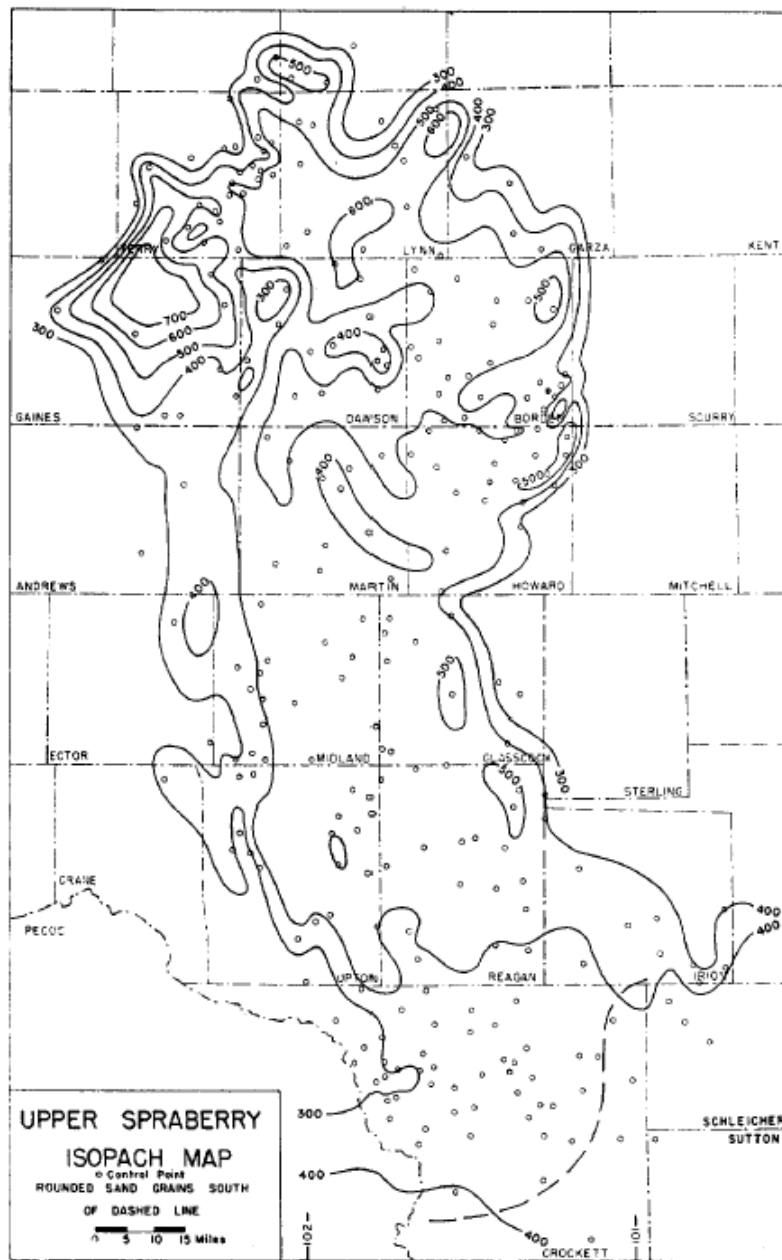


Fig. A8 – Isopach map of upper Spraberry unit in Midland County<sup>16</sup>.

Clastic ratio – Determined by the total thickness of the clastics (sand, shale, silt) at any control point divided by the total thickness of non-clastics (limestone, dolomite). Data is based on sample and electric log study (Fig. A9). Over a wide area in the central part of the Basin, the clastic ratio is greater than 8 (more than 88% of the section is composed of clastics). The width of this zone decreases north and south. Another slight decrease in the



clastic ratio occurs around the edge of the more negative area developed in northeastern Gaines County. Where the section is thinner there may have been a better development of carbonates. Possibly carbonates were deposited as rapidly around the edges as in the central part, but the central part subsided more rapidly and received a thicker sequence of clastics. Along the northeastern edge the decrease in clastics was, in part, due to the thick Pennsylvanian and Wolfcampian reefs<sup>16</sup>.

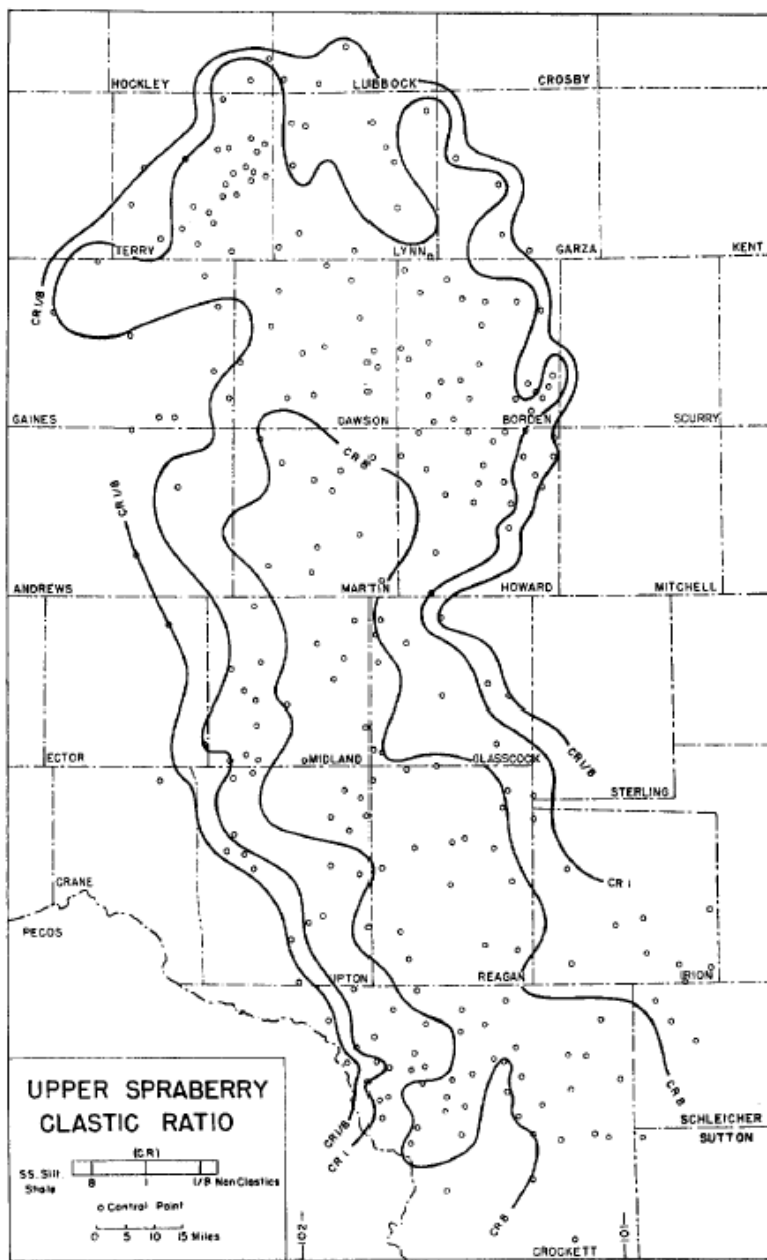


Fig. A9 – Clastic ratio map of upper Spraberry unit in Midland County<sup>16</sup>.

### Flow Units

The Spraberry is divided into 3 main intervals (Upper, Middle and Lower), Tyler & Gholston further sub-divided the Spraberry into distinct episodes or operational units. Of the six units found in the upper Spraberry, only two (1U and 5U) are reservoir quality rock, while in the lower Spraberry only two operational units are identified. Little is known about the lower Spraberry formation, as focus is mostly on the upper Spraberry.

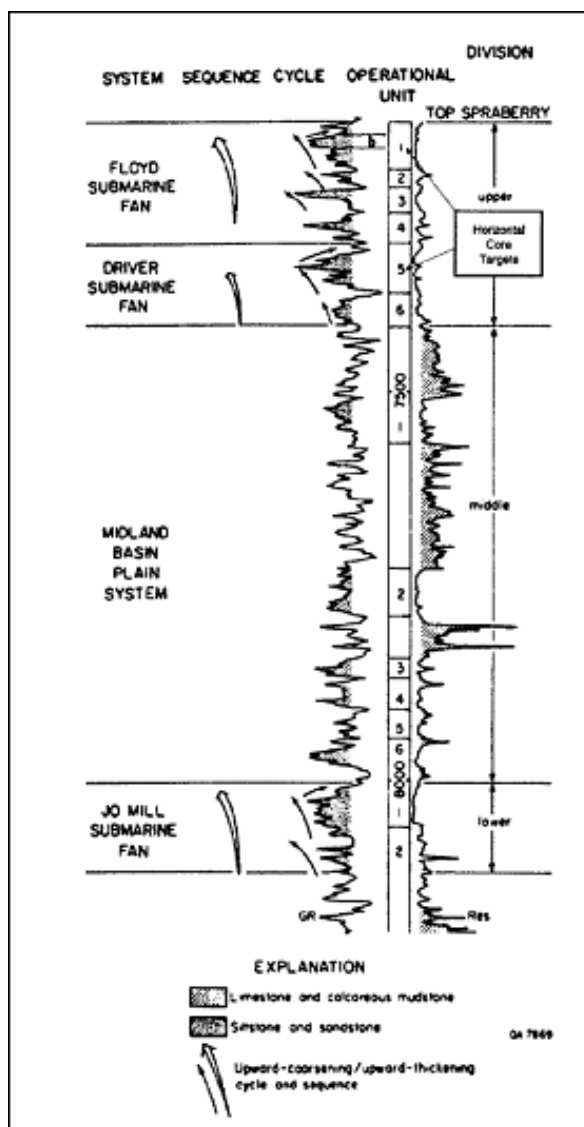


Fig. A10 - Operational units within the upper Spraberry formation.  
(TXL Fee 'B' #1 well located in the central trend area).

In the siltstones the average intergranular siltstone porosity is less than ten percent<sup>38</sup>, and the permeability varies from 0.002 to 2.5 millidarcys<sup>39</sup>.

Fractures constitute the major void space in the reservoir rock. Core evidence shows that vertical fractures are well developed in the intervening shales and argillaceous limestones<sup>4</sup> and apparently less pronounced in the massive siltstone members.

The fracture type reservoirs of the Spraberry can be divided into two classes: a) fields associated with local pre- Leonard structures; b) fields not associated with other than a broad west-dipping monocline. Class 'b' belongs to an almost continuous belt of production from the Pembroke field of Upton County north through the Germania field of Midland County (Fig. A11).

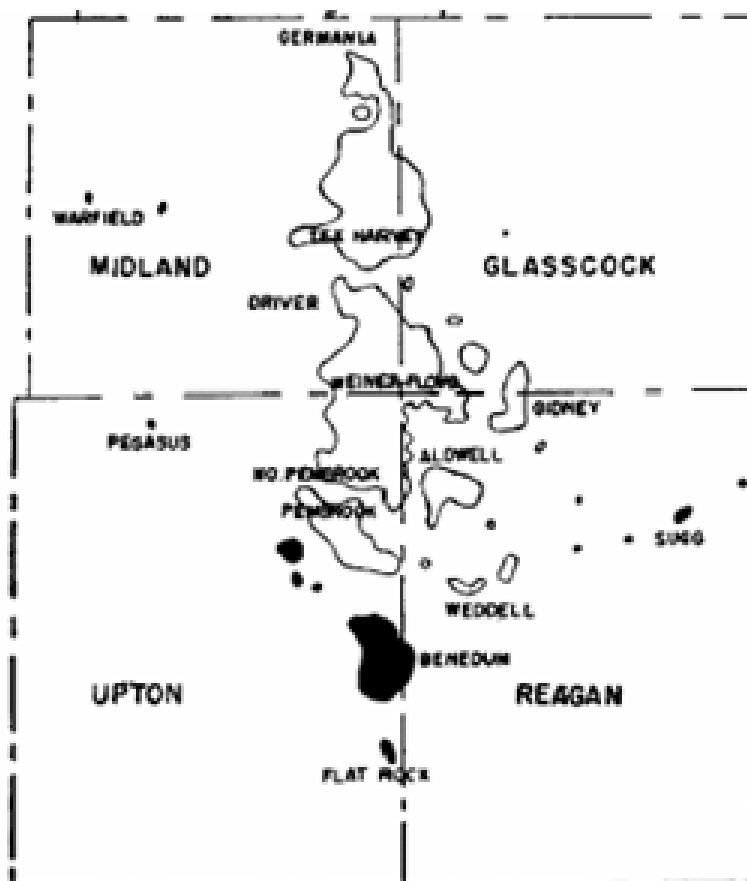


Fig. A11 – Location of class A & B Spraberry reservoirs of west Texas.

(class 'A' reservoirs are shown bold, and class 'B' reservoirs open).

**APPENDIX B**  
**MAPS FOR ET O'DANIEL AND GERMANIA**

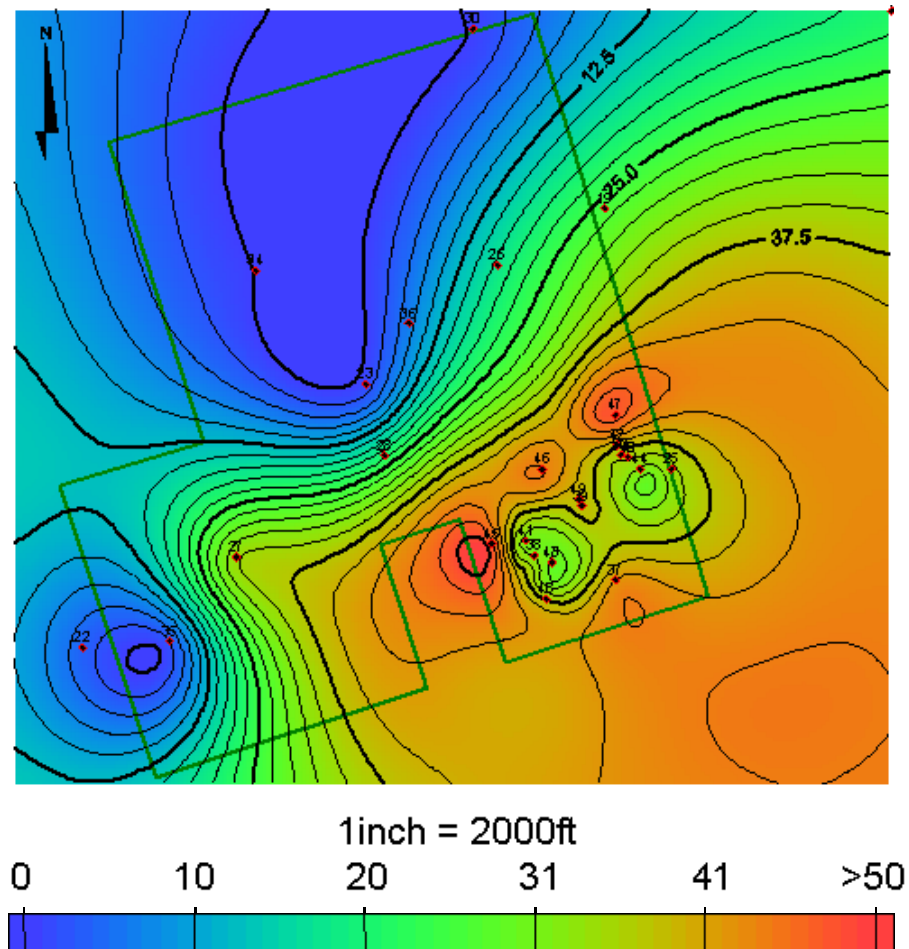


Fig. B1 - Minimum gamma ray map of ET O'Daniel, 5U sand.

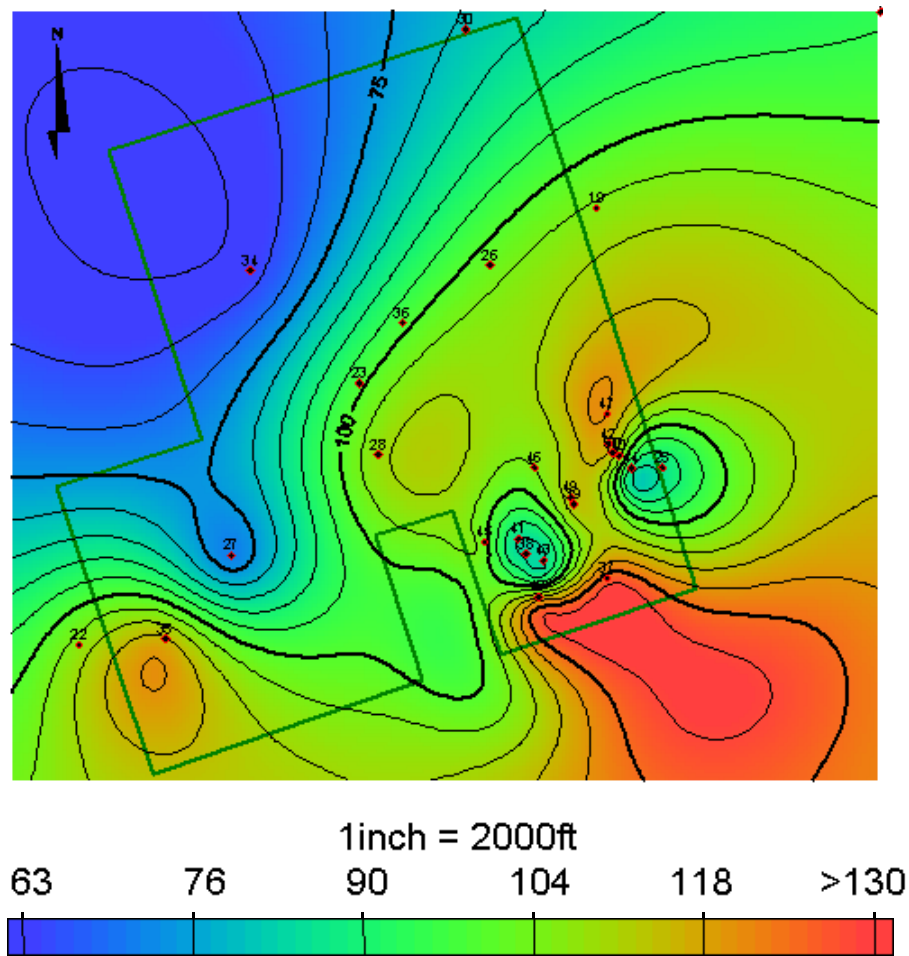


Fig. B2 - Maximum gamma ray map of ET O'Daniel, 5U sand.

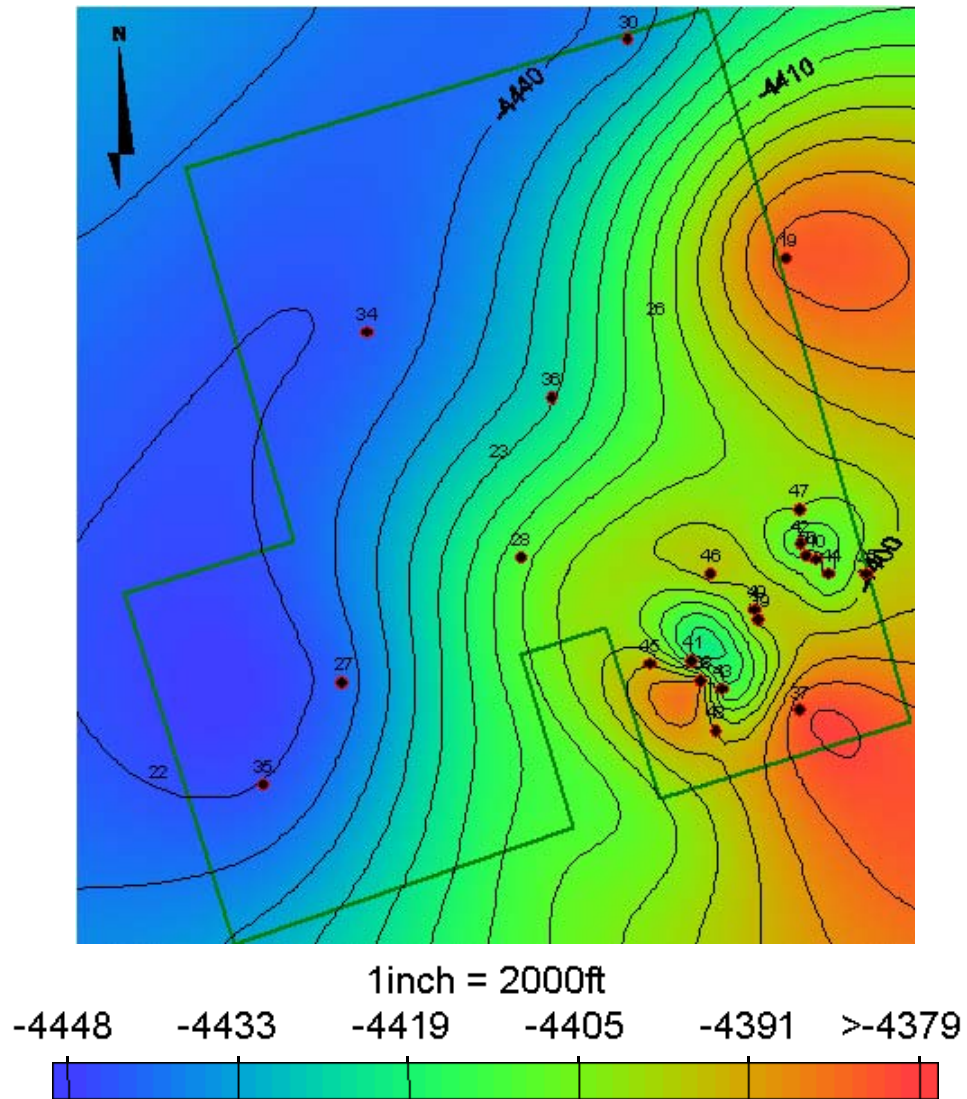


Fig. B3 - Paleo-structure map of ET O'Daniel, 1U sand.

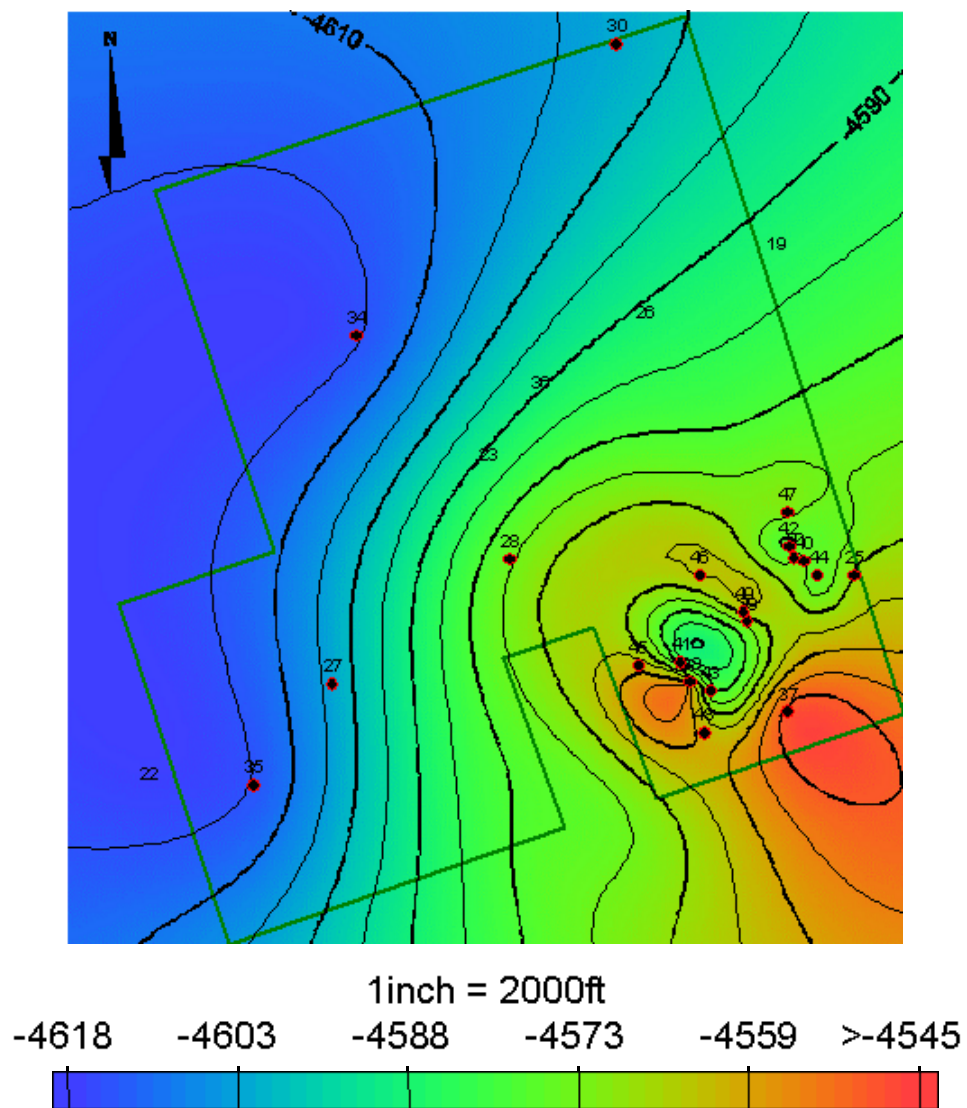


Fig. B4 - Paleo-structure map of ET O'Daniel, 5U sand.

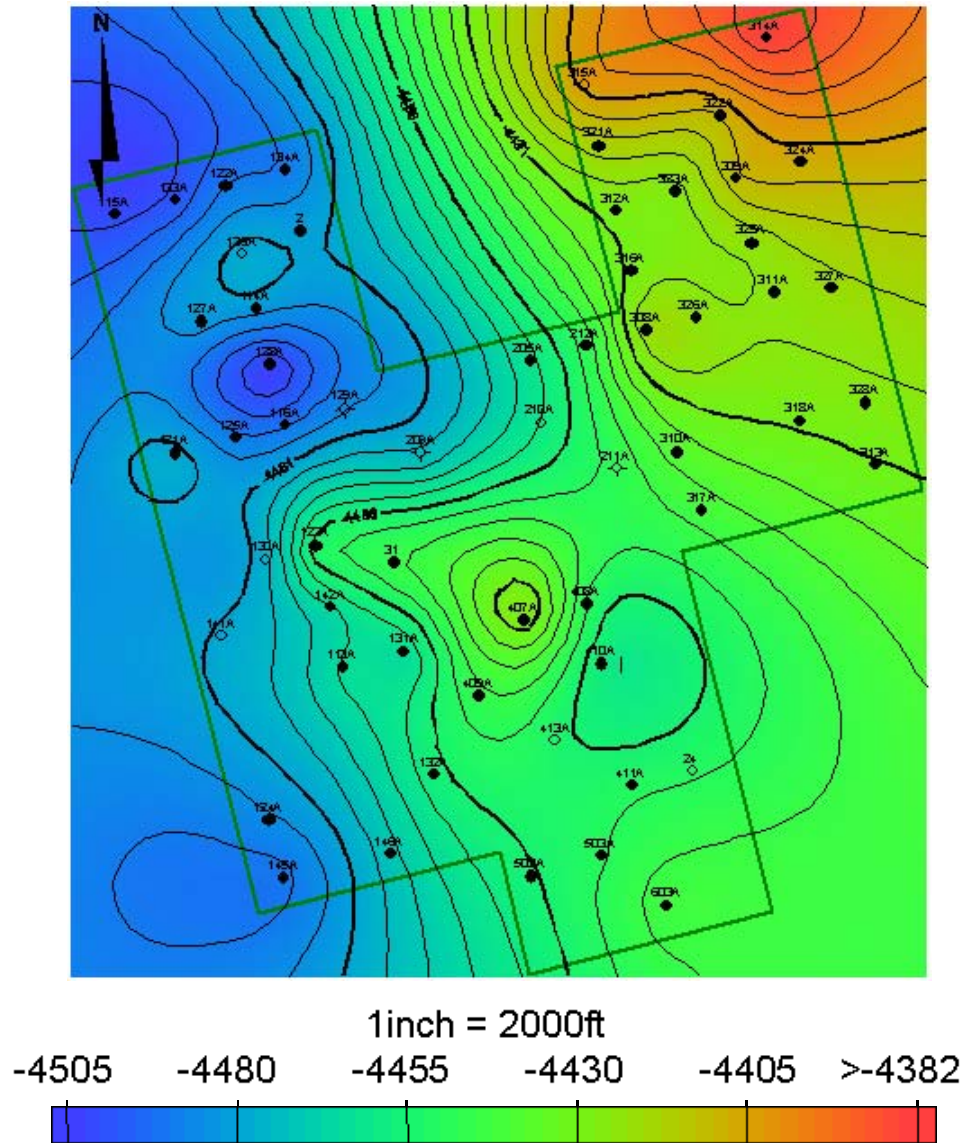


Fig. B5 - Paleo-structure map of Germania, 1U sand.



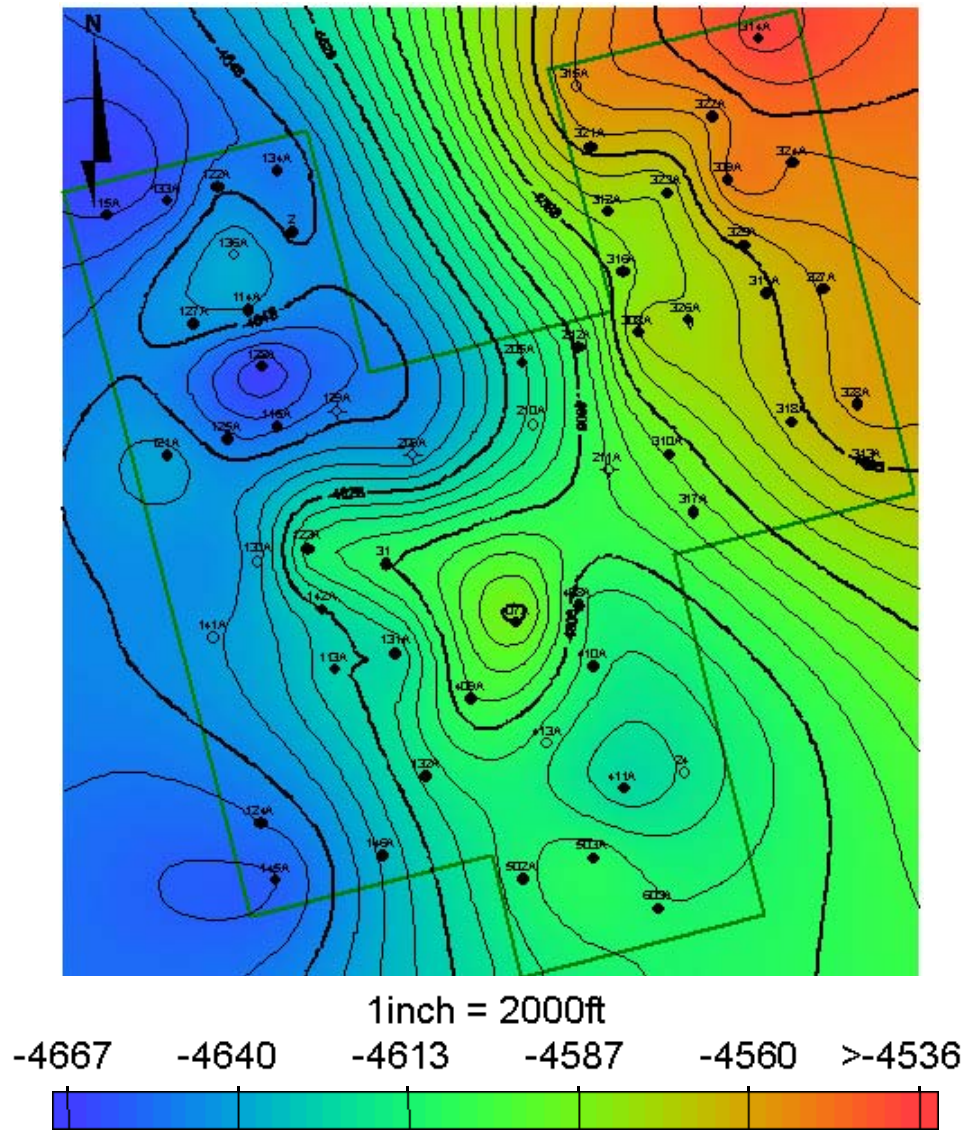
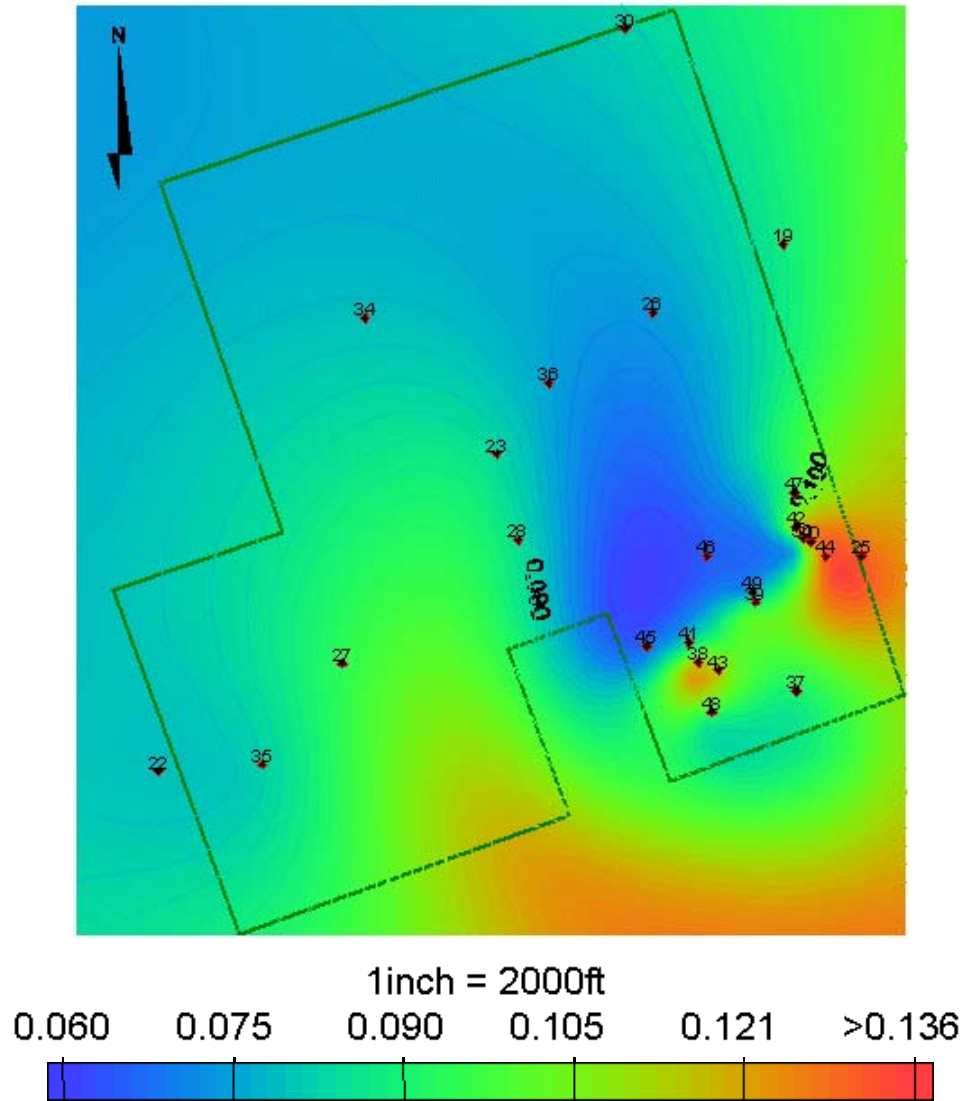


Fig. B6 - Paleo-structure map of Germania, 5U sand.



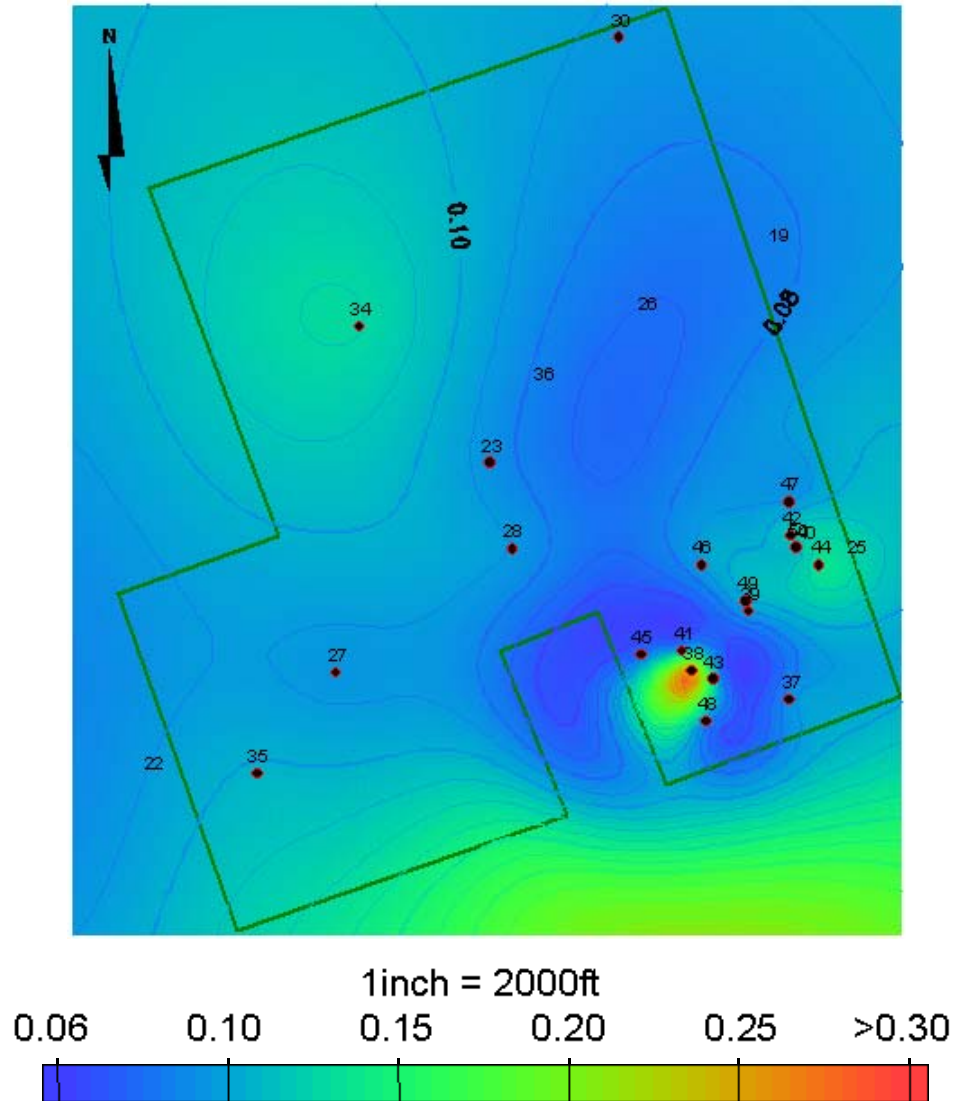


Fig. B8 - Porosity distribution map of ET O'Daniel, 5U sand.

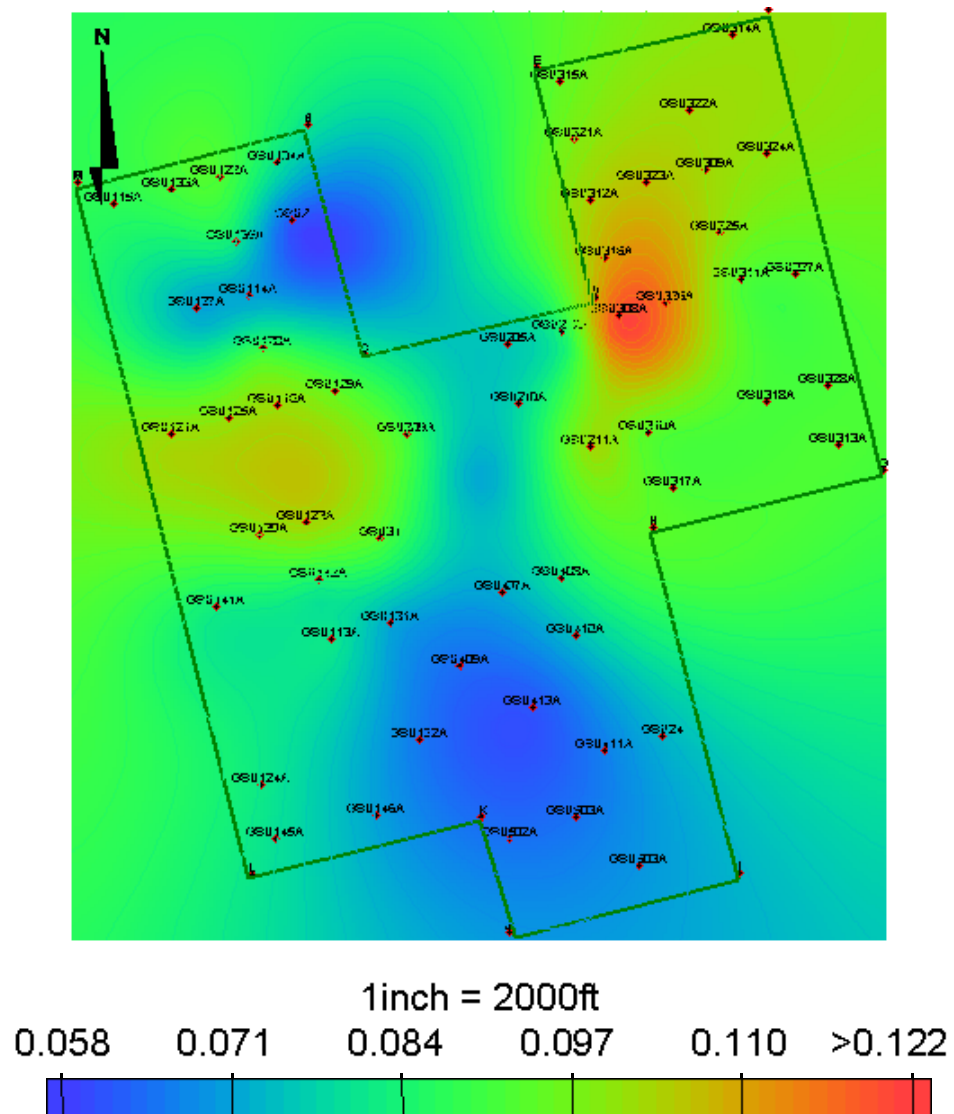


Fig. B9 – Porosity distribution map of Germania, 1U sand.

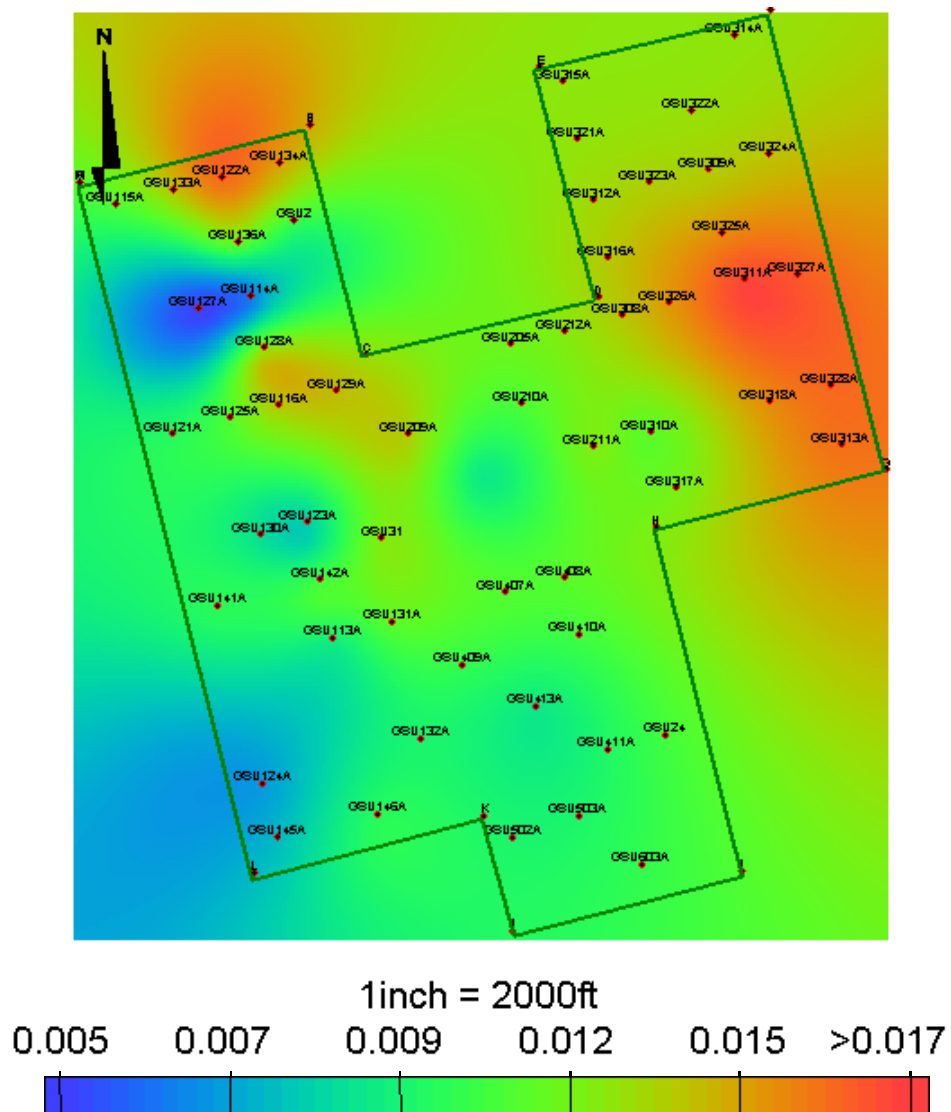


Fig. B10 - Porosity distribution map of Germania, 5U sand.

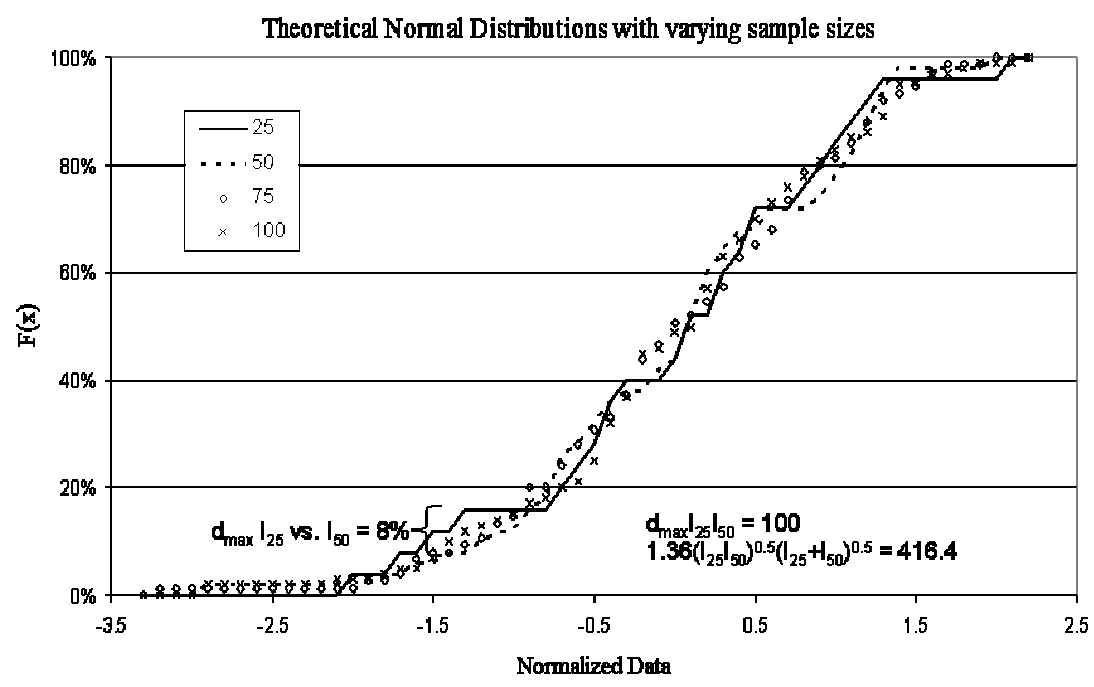


Fig. B11 – Effect of sample sizes on Kolmogorov –Smirnov distribution test.

**VITA**

Babajide Adelekan Olumide

**Education**

B.Sc. Industrial Engineering      U. of Ibadan, Nigeria      Sept. 1993

High School: International School,      U. of Ibadan, Nigeria      Sept. 1987

**Work Experience**

6/99 to 7/01      Texaco Overseas Pet. Co. Nigeria Unlimited

*Responsibilities:*      Senior Drilling Engineer

6/97 to 6/99      Texaco Overseas Pet. Co. Nigeria Unlimited

*Responsibilities:*      Drilling Supervisor

9/94 to 6/97      Texaco Overseas Pet. Co. Nigeria Unlimited

*Responsibilities:*      Drilling Engineer

**Permanent Address**

c/o Joseph Taiwo  
19618 Riverbottom Road  
Katy, TX 77449